Modeling, Control and Real-time Implementation of a Quasi-Z-Source Converter for Variable Speed Micro-Wind Turbines for Residential Applications

By

Hotheyfa OSMAN

THESIS PRESENTED TO ÉCOLE DE TECHNOLOGIE SUPÉRIEURE IN PARTIAL FULFILLMENT FOR A MASTER'S DEGREE WITH THESIS IN ELECTRICAL ENGINEERING
M.A.Sc

MONTREAL, SEPTEMBER 16,2024

ÉCOLE DE TECHNOLOGIE SUPÉRIEURE
UNIVERSITÉ DU QUÉBEC

BOARD OF EXAMINERS (THESIS M.SC. A)

THIS THESIS HAS BEEN EVALUATED

BY THE FOLLOWING BOARD OF EXAMINERS

Mr. Ambrish Chandra, Thesis Supervisor
Department of Electrical Engineering, École de technologie supérieure

Mr. Miloud Rezkallah, Thesis Co-supervisor
Department of Engineering and computer science, Université du Québec en Outaouais

Mr. Adrian Ilinca, President of the Board of Examiners
Department of Mechanical Engineering, École de technologie supérieure

Mr. Qingsong Wang, Member of the jury
Department of Mechanical Engineering, École de technologie supérieure

THIS THESIS WAS PRENSENTED AND DEFENDED

IN THE PRESENCE OF A BOARD OF EXAMINERS AND PUBLIC

MONTREAL, 23 AUGUST 2024

AT ÉCOLE DE TECHNOLOGIE SUPÉRIEURE

ACKNOWLEDGEMENTS

I would like to thank all the members of the Department of Electrical Engineering of the École de technologies supérieure.

I am truly grateful to my thesis supervisor, Prof. Ambrish Chandra, for granting me the opportunity to pursue my research in this area. His invaluable trust, outstanding technical advice, patience, and emotional support were essential to the success of my work.

I'd also like to express my thanks to my co-supervisor, Dr. Miloud Rezkallah for his assistance. Guidance and assistance have been invaluable to me throughout my work.

I express my warm thanks to all my friends that they brought me as well as the invaluable advice that they lavished on me.

I would like to thank my parents very much for their unwavering support and their assistance in carrying out my work in good condition.

Lastly, I extend my deepest thanks to my dear wife for her unwavering support, encouragement, and patience, as well as for shouldering a significant share of our life's responsibilities during the crucial final phases of this thesis.

Modélisation, contrôle et mise en temps réel d'un convertisseur quasi-z-source pour des micro-éoliennes à vitesse variable pour des applications résidentielles

Hotheyfa OSMAN

RÉSUMÉ

Cette étude propose une nouvelle configuration pour intégrer de manière efficace et sécurisée des sources d'énergie renouvelable telles que les éoliennes et les panneaux solaires dans des applications domestiques, notamment les chalets isolés. Cette configuration comprend deux convertisseurs de puissance en cascade : le convertisseur quasi-Z-source et l'onduleur monophasé. Pour garantir une alimentation continue des charges connectées, un système de stockage d'énergie est intégré à la configuration. Pour optimiser la production d'énergie à partir des sources d'énergie renouvelable, la tension de sortie en courant continu du convertisseur quasi-Z-source est augmentée, tandis que l'onduleur monophasé à demi-point est contrôlé à l'aide de deux stratégies de contrôle basées sur l'état de passage (shoot-through state), assurant ainsi une alimentation stable et continue des charges électriques du chalet. La modulation vectorielle spatiale est adoptée pour contrôler les MOSFET de l'onduleur monophasé afin de résoudre les problèmes de non-linéarité de sa sortie. De plus, cette étude présente la conception des paramètres passifs du convertisseur et une modélisation détaillée de la configuration. Un modèle Simulink a été développé sous Matlab Simulink pour tester les performances de la configuration, incluant sa stratégie de contrôle basée sur l'état de passage et la modulation vectorielle spatiale, dans différentes conditions. Un prototype de la configuration de 500W a été réalisé et testé au laboratoire en utilisant le F28379D comme microcontrôleur. Les résultats pratiques et de simulation sont satisfaisants.

Mots-clés : Convertisseurs quasi-z source, convertisseur monophasé à demi-point, contrôle algorithme basé sur l'état de passage (shoot-through), régulation de tension et de la fréquence, maximisation de l'énergie, énergie renouvelable, système autonome, SPWM

Modeling, Control and real time implementation of a quasi-z-source converter for a variable speed micro-wind turbines for residential applications

Hotheyfa OSMAN

ABSTRACT

This study introduces a novel configuration aimed at efficiently and securely incorporating renewable energy sources like wind turbines and solar panels into household settings, including remote chalets. This setup involves two interconnected power converters: the quasi-Z-source converter and the single-phase inverter. To ensure uninterrupted power supply to connected loads, an energy storage system is integrated. To enhance power generation from renewables, the DC output voltage of the quasi-Z-source converter is elevated, while the single-phase half-bridge inverter is controlled using two shoot-through state-based strategies, ensuring a consistent and stable power supply to the chalet's electrical loads. Space vector modulation is employed to regulate the MOSFETs of the single-phase inverter, resolving its output nonlinearity issues. Furthermore, this study details the design of passive parameters for the converter and presents a comprehensive configuration model. A Simulink model was developed using MATLAB Simulink to assess the setup's performance, encompassing its control strategies and space vector modulation, across various conditions. A prototype of the 500W setup was constructed and evaluated in the laboratory, utilizing the F28379D as a microcontroller. Both practical and simulation results demonstrate satisfactory performance.

Keywords: Cascade quasi-z source inverter, shoot-through state, enhanced closed-loop control, maximum power tracking, wind turbine, standalone system, SPWM

TABLE OF CONTENTS

Page

LIST OF TABLES

LIST OF FIGURES

Page

LIST OF ABREVIATIONS

kW	Kilowatt
GW	Gigawatt
TWh	Terra Watt-hour
kHz	Kilohertz
WT	Wind Turbine
DC	Direct Current
AC	Alternating Current
ZSC	Z-Source Converter
ZSI	Z-Source Inverter
QZSI	Quasi-Z-Source Inverter
SoC	State of Charge
WECS	Wind Energy Conversion System
SS	Storage System
SWECS	Standalone Wind Energy Conversion System
PMSG	Permanent Magnet Synchronous Generator
DFIG	Doubly Fed Inductor Generator
MPPT	Maximum Power Point Tracking
CanREA	The Renewable Association in Canada
CSWT	Constant Speed Wind Turbine
VSWT	Variable Speed Wind Turbine
PSF	Power Signal Feedback

TSR	Constant Tip Speed Ratio
P&O	Perturbation and Observation
OT	Optimum Torque
INC	Incremental Conductance
CSI	Current Source Inverter
VSI	Voltage Source Inverter
SiC	Silicon Carbide
GaN	Gallium Nitride
DSP	Digital Signal Processing
CO2	Carbon Dioxide
RE	Renewable Energy
N_2O	Nitrate Oxide

LIST OF SYMBOLS

ρ_{air}	Air Density
$\dot{m}$	Mass flow
β	Pitch Angle of the blade
λ	Blade tip ratio
C_p	Coefficient power
ω_m	Mechanical angular speed
T_m	Mechanical torque
Ω	Angular speed of the wind turbine.
r	Rotor of the turbine
k_t	The torque coefficients
K_e	Machine's voltage constant
ω_r	Rotor speed
B	Boost factor
D_{sh}	Duty cycle of the shoot through state
D_A	Duty cycle of the active state
D_z	Duty cycle of the zero state
V_{DC}	Output voltage of diode rectifier
Ls	Synchronous inductance
v	Wind speed
T	Torque of the generator
η	Generator efficiency

I_a	Stator current
f_s	Switching Frequency
Ts	Switching Period
D	Duty cycle
ΔI_L	Inductance current ripple
ΔV_C	Capacitor voltage ripple
C_r	Current ripple coefficient
P_n	Nominal Power
V_{in}	Input voltage of the QZSI
I_{in}	Input voltage of the QZSI
L_{min}	The minimum inductance needed in the QZSI
I_{C1}	Current passing through C_1
C_{min}	The minimum capacitance needed in the QZSI
f_c	Cut-off frequency
I_{L1}	Input current inductance of L_1
P_{load}	Power of the load
L_f	Inductance filter
C_f	Capacitance filter
Z_{load}	Load impedance
R_{load}	Load resistance
V_b	Battery voltage
I_b	Battery current
P_b	Battery power

P_b^*	Battery power reference
V_{oc}	Voltage open circuit
P_w	Power of the wind
P_L	Power of the load
V_{ref}	Reference voltage
$Vmpp$	Maximum power point voltage
V_{DC1}	Rectified DC link voltage
I_{cap}	Current entering the capacitor filter
I_{invref}	Current reference of the output of the inverter

INTRODUCTION

The reflection of global warming has been exacerbated by the escalated consumption of fossil fuels in recent times (Shamouei-Milan, Asgarniya, Marangalu, Islam, & Mehrizi-Sani, 2023). And with the depletion of conventional energy source, the global demand for energy increased (Shrivastava, Karkar, & Singh, 2016).

To drive primarily by the desire for clean energy and environmental sustainability, to mitigate the impact of global warming, and to cover the demand of the energy increase, the utilization of renewable energy sources has been proposed as a solution.

Among the renewable technologies, wind power generation stands out as one of the most promising. Its efficacy, however, is also highly contingent on climatic conditions (Shrivastava et al., 2016).

In the context of supplying energy to rural areas, the growth of wind power, particularly between 5 kW and 100 kW range, is on the rise. Wind power offers the potential to independently provide electricity to individual facilities (Sonar & Maity, 2013).

Presently, wind turbines (WTs) can adopt various configurations for their power converters. However, during low-speed rotation of the WT, the uncontrolled rectifier may fail to supply the required DC voltage at the grid-side converter input. Nevertheless, these sources often exhibit a low output voltage amplitude. As a solution, high-gain inverters are deemed essential to achieve the necessary voltage amplitude (Shamouei-Milan et al., 2023).

DC-DC converter can be used to elevate the voltage to levels suitable for it. Also this approach is simple, cost-effective, and facilitates maximum power extraction from the WT, it introduces challenges such as increasing the harmonic distortion current inside the windings of the generator, torque oscillations, and overheating (Soares-Ramos et al., 2021).

ZSCs had been suggested as an enhancement compared to conventional converters. ZSCs feature a unique architecture that efficiently reaches a substantial voltage buck-boost characteristic in a single stage, facilitating effective power transfer between a source and a load. Furthermore, they can operate in a shoot-through state without damaging the components. The Z-source converter shows better performance on the traditional converters, due to the capability of the shoot-through of ZSC (Soares-Ramos et al., 2021).

Among the suggested configurations within the ZSI family, the QZSI stands out for its high efficiency. Apart from inheriting all the benefits of the conventional ZSI, the QZSI boasts additional notable advantages. These include a straightforward structure, a continuous direct current (DC) input, minimized stress on passive components, establishment of a shared ground between the inverter and the input source, and to reduce in the switching ripples observed by the source DC (Bajestan, Madadi, & Shamsinejad, 2019).

These characteristics render the QZSI is a suitable choice for acting as an interface converter in systems that convert renewable energy, including photovoltaic systems, wind energy conversion systems (WECSs), and fuel cell systems (Anderson & Peng, 2008).

The implementation of the QZSI network offers a dependable, highly effective, and cost-efficient framework for both buck-boost conversion. Consequently, due to these factors, the QZSI is well-suited for integration into wind energy systems (Shrivastava et al., 2016).

Conventional storage systems typically need an extra DC-DC bidirectional converter to manage the charging and discharging operations of the battery. This leads to additional expenses, increases in the system's volume, and adds complexity to the control algorithm. However, by adding a battery directly in parallel to the capacitor of the QZSI, and with no need for an extra converter, the proposed system can effectively adjust the output voltage to the wanted level, in addition to managing the state of charge of the battery (SOC), and the output power (Bajestan et al., 2019).

Up until now, numerous researchers have directed their efforts toward advancing the applications of both traditional (ZSI)and (QZSI) within grid-tied renewable power generation systems (Jegatheeswaran & Rajesh, 2015)&(Liu, Ge, Abu-Rub, & Peng, 2013).

On grid system share a common control strategy aimed at injecting maximum wind power to the grid. However, the absence of a storage system (SS) may pose challenges to the functioning of the WECSs in scenarios of under-generation and over-generation. This research will introduces a stand-alone WT variable speed PMSG system with a QZSI (Bajestan et al., 2019).

The control system effectively creates a shoot-through state and adjusts the modulation index of the QZSI. This adjustment serves to control the state of charge (SoC) of the battery while ensuring the frequency and the output voltage remain within acquired values, accommodating different conditions of WECS power generation and load changes.

Despite the extensive research on the application of Z-source inverters (ZSIs) in Wind Energy Conversion Systems (WECSs), there is a no literature regarding a thorough investigation into controlling ZSI in conjunction with a battery-based WECS in standalone mode (Bajestan et al., 2019).

This research addresses this gap by providing a precise model of the QZSI with a battery and proposing a control strategy for the Standalone Wind Energy Conversion System, where it’s approved by simulation, and supported by hardware application.

CHAPTER 1

LITERATURE REVIEW

1.1 Introduction

This introduction sets the stage for the literature review by providing context on the importance of the integration of renewable energy sources, such as wind turbines, into standalone power systems presents challenges related to power fluctuations and system stability, it provide analyzing the application of the MPPT technique for optimization the energy extraction from the WT, it discuss about types of generators, DC-DC converter, then it aims to the contribute the aim of QZSI and mentioning the advantages and the disadvantages. This chapter will give a background of the types of the QZSI, in addition, it outlines the mathematical model for the inverter and for the mode of operation of this kind of converter, this chapter also cover the SS used with the QZSI.

1.2 Renewable Energy

Due to quick growth of the population and the increase of the number of people in the world, there will be an increase of the demand of the energy worldwide, and due to the relying mainly on fossil fuel in most of the generation factory, this led to increase in emission of gas such as CO_2, N_2O and methane, in the process of the consumption of the fossil fuel, all these emissions cause change of weather and puts human health at risk. To avoid these dangerous effects, governments are taking into consideration changing laws to limit using fossil fuels, and replacing it with renewable energy sources (Olabi & Abdelkareem, 2022).

The decarbonizing of the energy sector has been taken into consideration for numerous years, it is widely recognized that the most apparent approach to attain decarbonization involves utilization of renewable energy (RE). Consequently, numerous nations have been

increasingly integrating an expanding share of their renewable energy resources, encompassing solar, wind, hydro, geothermal, and biomass energy to produce electricity.

Remarkably, specific countries have already achieved notably elevated proportions of renewable energy in their electricity production, predominantly propelled by hydropower. Instances of such achievements are evident in Paraguay (99%), Norway (97%), Costa Rica (93%) and in Canada about (62%) (Kroposki et al., 2017), in 2023 (71.2%) (« 2023 - Canada's Energy Future 2023 Energy Supply and Dem.pdf », s.d.).

According to the renewable association in Canada (CanREA), the data shows an increase in the solar, wind and storage system by 11.2% in the year 2023 by an increase about 21.9 GW of production(« Canadian Renewable Energy Association », s.d.).

Coming to the Quebec province, its ranked 3rd in Canada for the highest installation capacity of the solar, wind and energy storages, almost about 4 GW are wind energy generation, about 12 MW are solar energy generation and about 2 MW of energy storage has been installed in the year 2023.

The estimated need to cover the demand in the 2050 we need to produce about 150 TWh (« Canadian Renewable Energy Association », s.d.).

By increasing the utilize of the resources of the renewable energy will be the key to sustain the generation of electricity, where solar and wind will act as the most two resources, it expected to reach 56% of the electricity generation in the year 2050 (Sánchez, Zhang, Martín, & Vega, 2022).

1.3 Renewable Energy Sources

There are various types of renewable energy sources, deriving from naturally replenishable or regenerative origins. The primary categories include are the hydropower, wind, solar,

biomass, geothermal, all these renewable energy sources play a role in electricity generation. Geothermal steam is also directly utilized for heating and cooking purposes. Biomass and solar sources find applications in space and water heating, while ethanol, biodiesel, and to a lesser extent, gaseous biomethane are utilized in transportation (« Renewable Energy », s.d.).

The energy sector focuses primary on many factors, it revolves affordability, accessibility and environmentally friendly. The generation of electricity relying on renewable sources is considered an essential and a feasible solution to substitute fossil fuel.

The sights towards the generation of renewable energy are garnering a significant attention to address the limitations of fossil fuels. Renewable energy sources include wind, solar, tidal, hydro, wave, and biomass. Relying on the widespread and abundant availability, wind and solar energies are important for utilizing power generation. But, the credibility of the wind and solar energy are significantly influenced by the changes of climate and by the nature of them of unpredictable, which creates a substantial challenge in terms of energy storage and integration these sources to the grid (Tiwari & Babu, 2016).

Wind power is the most rapidly expanding form between the renewable energy sources, crossing over different engineering challenges. In the last years, there has been a significant rise in building wind-based electricity generation. Nowadays the challenge is to integrate the wind power into the grid, to deal with the unpredictable nature of the wind, and to identify a suitable location for the turbine. To address these challenges, we need to necessary advanced generators, power converters, and controllers to seamless integration of wind turbines into the power grid, or to use it as a standalone system in isolated areas (Tiwari & Babu, 2016).

1.4 Wind Energy

The amount of generated wind power is influenced by many factors such as air density, rotor swept area, and upwind free wind speed. Wind Energy can be captured through the volumetric volume of the mass flow of an air passing through section area (A) of the turbine. This section corresponds to the area swept by the moving rotor as shown in figure 1.1 and it can be illustrated into equation 1.1 (Sonar & Maity, 2013).

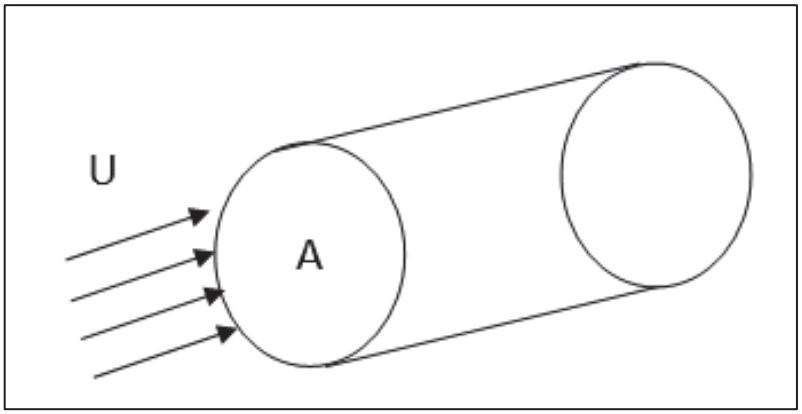

Figure 1.1 Mass flow

$$\dot{m} = \frac{dm}{dt} = \rho_{air} \times A_{rotor} \times v \left[\frac{kg}{s}\right] \tag{1.1}$$

Where $\dot{m}$ is the mass flow (kg/s), ρ_{air} is the density of air (kg/m^3), A_{rotor} is the area of the rotor (m^2), and v is the average speed of air in (m/s).

The output power from a Wind Energy Conversion System (WECS) varies directly with wind speed, meaning any slight changes in wind speed can significantly affect the amount of power generated. This variability makes the power from WECS incompatible with the electricity grid, which requires power of a constant amplitude and frequency. To address this, control strategies are implemented to maximize power output and to ensure the voltage to remain constant from WECS (Tiwari & Babu, 2016).

1.5 Wind Turbine

From deriving the principal of the kinetic energy for the flowing of the air, the power that will pass a sectional area A with a specific velocity υ will be as in equation 1.2:

$$P = \frac{1}{2} \times \rho_{air} \times A \times \upsilon^3 \tag{1.2}$$

Where the $\rho_{air} \cong 1.2$ kg/m^3 is the air density will use in calculation, not all the power converted to mechanical power, the useful power that converted is multiply by the coefficient power C_p (Stiebler, 2008), and is shown be as in equation 1.3:

$$P_m = \frac{1}{2} \times C_p(\beta, \lambda) \times \rho_{air} \times A \times \upsilon^3 \tag{1.3}$$

P_m is the mechanical power generated by the wind, and according to Betz the maximum power coefficient, we can deduce the mechanical torque T_m of the WT as follow:

$$T_m = \frac{P_m}{\omega_m} \tag{1.4}$$

Where the ω_m is the mechanical angular velocity.

Where C_p is the rotor power coefficient of the wind turbine, which is defined by two parameters, the first one is the β the pitch angle of the blades and the λ the blade tip ratio, C_p can be determined by equation 1.5 (Tiwari & Babu, 2016):

$$C_p = 0.22\left(\frac{116}{\gamma} - 0.4\beta - 5\right)e^{\left(-\frac{12.5}{\gamma}\right)} \tag{1.5}$$

Where:

$$\gamma = \frac{1}{\frac{1}{\lambda + 0.08\beta} - \frac{0.035}{\beta^3 + 1}} \tag{1.6}$$

By taking in consideration the pitch angle β is zero, C_p will be a with relation of the blade tip ratio λ (Hussien, Taha, & Mahgoub, 2015).

Theoretically, the power coefficient C_p can be calculated as $C_p = \frac{16}{27} = 0.59$. but, due to real-world inefficiencies and losses in wind turbines, the maximum practical power coefficient is typically in the range of $C_{p-max} = 0.4 \sim 0.5$ (Kosky, Balmer, Keat, & Wise, 2013).

To set the power of the generator we must multiply the power of the wind turbine with efficiency, considering the different losses. Another additional parameter for the wind rotor which is the tip-speed ratio λ, this speed shows the relation between the peripheral speed of the blades and wind energy (Stiebler, 2008), according to the following equation:

$$\lambda = \frac{r\Omega}{\upsilon} \tag{1.7}$$

Where Ω is the angular speed of the wind turbine, the rotor of the turbine is denoted by r.

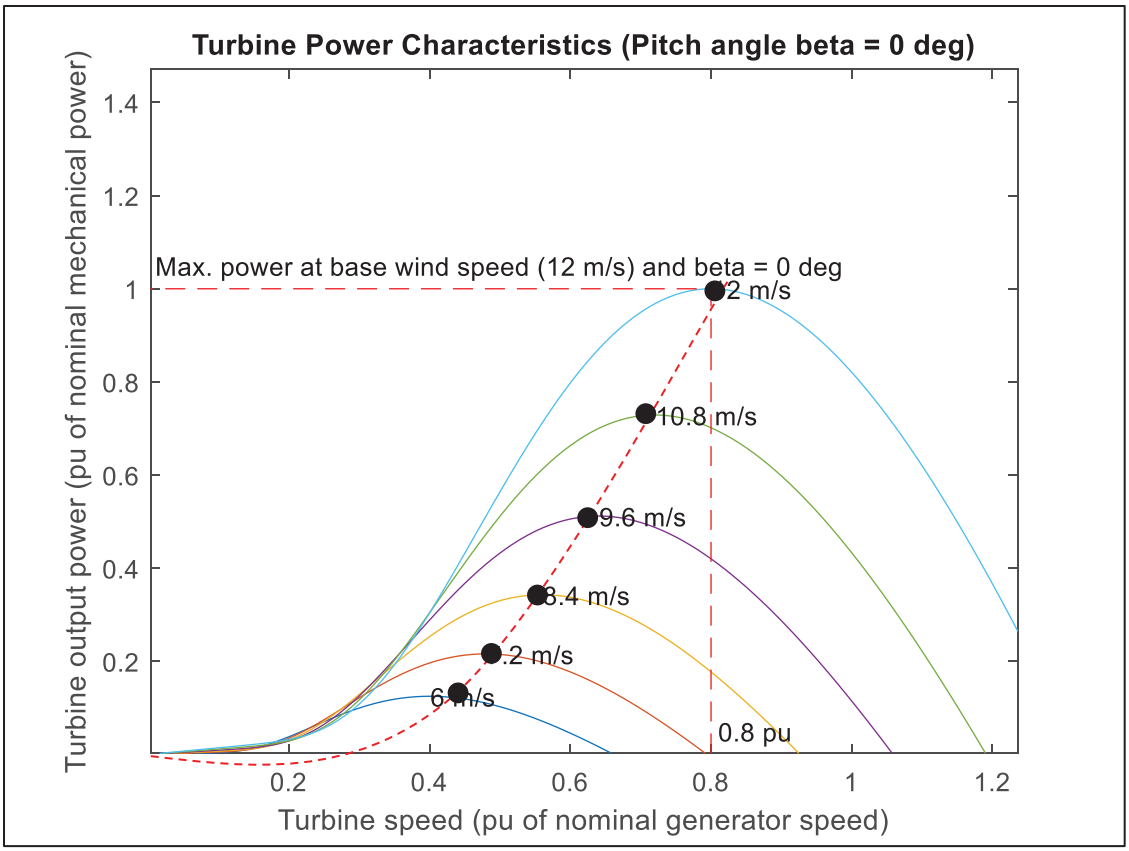

Figure 1.2 Graph shows the power of VSWT with respect to rotational speed at different wind speeds

In figure 1.2, it shows the maximal power that we can catch up from the wind turbine and especially for a variable wind speed type, in the per unit system.

1.5.1 Wind Turbine Types

Wind turbines can be classified into two main types, the first type is the constant speed wind turbines, and the second type is the variable speed wind turbines. Constant speed wind turbines are used much more than the variable speed wind turbine (VSWT). Furthermore, (CSWT) has major disadvantages like increased mechanical stress, low in the power quality, and effect stability of reactive power. While VSWT generators are required to extract the greatest power with varying wind velocities. This is mainly true for stand-alone operations, where they can offer a better voltage and frequency regulation than generators with constant

speeds. VWST proposed to connect a PMSG permanent synchronous generator, particularly at lower to medium power ranges (Bajestan et al., 2019).

Frequently, the wind turbine rotates slowly because in sometimes there will be an absence of the wind, the diode rectifier in this case can't reach the desired voltage level at the output of the inverter, here a DC-DC boost voltage can be implemented between the diode rectifier and the desired output load to step up the voltage to the required level. By depending on this solution comparing to other solutions, this one is simple, low cost, and have the ability to extract the maximum power tracking of the wind turbine, on other hands, this module can overheat, cause a high harmonic in the current distortion, and also cause torque oscillation (Soares-Ramos et al., 2021).

1.5.2 MPPT Control Algorithms for Wind Turbine

In the present wind turbine systems, it is imperative to add Maximum Power Point Tracking (MPPT) control schemes to fully mock the advantages of varying the wind speeds. A various exhibit of MPPT techniques is employed in wind turbines to synchronize the generator speed with the optimal speed (« A Fuzzy Logic-based MPPT Technique for PMSG Wind Generation System », 2019).

These include hill climbing search, power signal feedback (PSF), constant tip speed ratio (TSR), incremental conductance (INC), optimum torque (OT), perturbation and observation (P&O), as well as artificial intelligent techniques. Each technique boasts distinct advantages and drawbacks in driving the MPPT scheme.

For example, while TSR exhibits high efficiency, it requires a precise anemometer measurement for measuring the wind speed, consequently elevating system costs. Therefore, PSF and OT do not enforce anemometers, but the wind turbine parameters are necessary for obtaining the maximum power curve, which differs among different wind turbines.

In the case of INC and P&O, the algorithms do not depend on turbine specifications or sensors, promote system reliability. However, these techniques tend to exhibit slower responses and oscillate around the maximum power point.

Furthermore, they strive to track quick fluctuations in wind speed, thereby impacting system efficiency. To overcome the limitations of classic techniques, soft computing techniques based on artificial intelligence are increasingly utilized due to their high performance and adaptability (« A Fuzzy Logic-based MPPT Technique for PMSG Wind Generation System », 2019).

1.5.2.1 The TSR Control Algorithm

Focusing on (TSR) and (PSF) as traditional approaches. TSR focuses on maintaining the tip speed ratio (λ) at its optimum level ($\lambda_{opt} = 8.1$) regardless of wind speed, requiring an anemometer for wind speed measurement. The comparison between the measured generator

$$\omega_{ref} = \frac{\lambda_{opt} V_w}{R} \tag{1.8}$$

speed (ω_m) and the reference generator speed (ω_{ref}), with any disparities leading to adjustments in the generator speed. Equation 1.8 details the computation of ω_{ref} .On the other hand, PSF does not mandate an anemometer, but a comprehensive understanding of wind turbine parameters remains essential. This technique depends on grasping the wind turbine's maximum power curve (MPP locus in Fig. 1.2), which can be obtained through simulation or experimental trials(« A Fuzzy Logic-based MPPT Technique for PMSG Wind Generation System », 2019).

As depicted in figure 1.3, it is essential to measure both the wind speed and turbine rotor speed for Tip Speed Ratio (TSR) calculation. The controller then compares the predefined optimal TSR with the measured TSR to establish the demand for generator power. Nevertheless, using TSR regulation for MPPT in (WECS) poses two challenges. Firstly, the

inclusion of wind speed measurement increases system costs and poses implementation challenges. Secondly, this technique lacks adaptability to parameter changes, primarily stemming from uncertainties in the power curve(Abdallah, Elshafei, & Arafa, 2015).

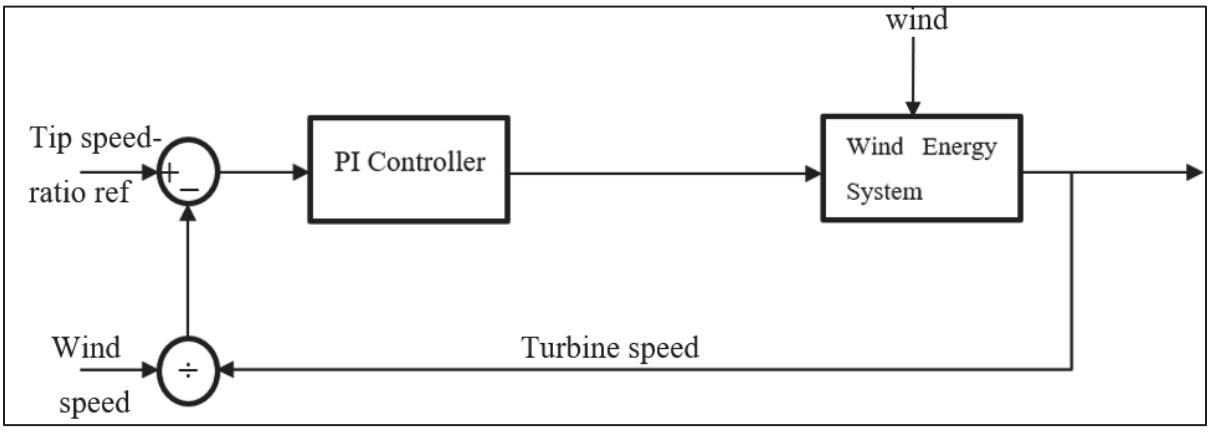

Figure 1.3 Block diagram of the TSR control
Taken from Abdallah et al., (2015)

1.5.2.2 The PFS Control Algorithm

Power signal feedback is often referred to as the standard control law in academic texts. This approach hinges on the premise that the rotor must operate at a speed that ensures the optimal Tip Speed Ratio (TSR) to maximize the power extracted from the wind turbine.

To effectively harness the maximum power from the wind in region 2 of figure 1.5, with an assumed reliable power curve, the generator's power output must adhere to a pre-established lookup table. This table denotes the peak power available from the wind at each rotor speed, which is described as the tracking characteristic. Figure 1.4 shows a block diagram of the power signal feedback control system. In PSF control, only the turbine speed is required for calculations. Additionally, to analyze the system dynamics, a simple rigid body model of the wind turbine is used (Abdallah et al., 2015).

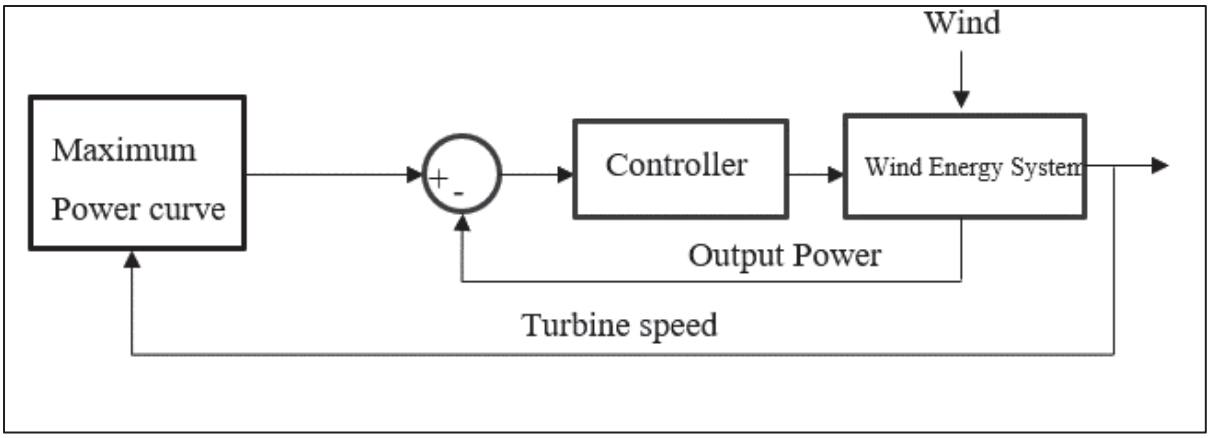

Figure 1.4 Block diagram of the PFS
Taken from Abdallah et al., (2015)

1.6 Electrical Generators

To convert mechanical energy, which comes from the rotation of the wind turbine, into electrical form, one must utilize a specific type of generator. There are three main classifications of generators: the asynchronous generator, commonly referred to as an induction motor, the synchronous generator, and the DC machines (Stiebler, 2008).

Various generators can be employed for generating wind power energy, like, permanent generators, PMSG, induction generator, doubly fed inductor generator (DFIG) (Sue, 2011). Among these, the PMSG stands out as one of the most effective options, given its superior power density and efficiency (Hussien et al., 2015).

1.6.1 Permanent Magnet Synchronous Generator (PMSG)

With all various technologies available of the variable speed wind turbine (VSWT), from the (DFIG) doubly fed inductor generator, and PMSG are frequently used in implementing with wind turbines due to their high efficiency.

Proffering PMSG on DFIG due to the advantages of the PMSG, they can summarize by their high performance, low cost in maintaining compared to DFIG, in addition to the direct drive (self-excitation) of the generator (Soares-Ramos et al., 2021). In addition to these advantages, PMSG include its low weight and small volume space, brushless operation, and a high efficiency because of not using a gearbox, and a high power factor (Bajestan et al., 2019) and (Lai & Chan, 2007).

In a wind turbine based on a PMSG, the power extracted from the wind turbine generator can be adjusted by modulating the voltage output of the PMSG. The equations governing the induced voltage in the stator windings of a PMSG and the generated output torque under steady-state conditions can be formulated in the following equations (Bajestan et al., 2019):

$$E_a = K_e \times \omega_r \tag{1.9}$$

$$T = K_t \times I_a \tag{1.10}$$

Where K_e is the machine's voltage constant, K_t is the torque coefficients, and I_a is the stator current. Coming to the equivalent circuit of the PMSG in the steady state, the equation for the induced voltage can be derived as follows:

$$E_a = V_t + j\omega_r L_s L_a \tag{1.11}$$

$$E_a = \sqrt{V_t^2 + (\omega_r L_s L_a)^2} \tag{1.12}$$

Where V_t represents the output terminal voltage of the PMSG, and L_s denotes by its synchronous inductance.

Alternatively, the output DC1 voltage from the 3-phase diode rectifier can be determined by the following equations:

$$V_{DC1} = \frac{3\sqrt{6}}{\pi} V_t \tag{1.13}$$

Therefore, from equation 1.11, 1.12, and 1.13, the rectified DC1 link voltage can be expressed as:

$$V_{DC1} = \frac{3\sqrt{6}}{\pi} \omega_r \sqrt{K_e^2 - \left(\frac{TL_s}{K_t}\right)^2} \tag{1.14}$$

It is shown that the rectified DC-link voltage is directly influenced by the wind speed and, consequently, by the generator speed. In essence, by regulating the optimal DC1-link voltage derived from equation, it becomes feasible to manage the generator speed to its optimal level and thereby harness the maximum energy from the wind (Bajestan et al., 2019).

$$V_{DC1(mpp)} = \frac{3\sqrt{6}}{\pi} \omega_{r(mpp)} \sqrt{K_e^2 - \left(\frac{TL_s}{K_t}\right)^2} \tag{1.15}$$

1.6.2 Passive Filter Between Stator Terminals and Diode Bridge

The passive filter added between the stator terminals of the Permanent Magnet Synchronous Generator (PMSG) and the diode bridge rectifier serves multiple critical functions in the system. Primarily, its purpose is to smooth out the voltage and current waveforms by filtering out high-frequency components generated by the switching actions in the rectifier. This filtering is essential to reduce the total harmonic distortion (THD) in the output, ensuring that the DC voltage fed into the quasi-Z source inverter (QZSI) is as stable and clean as possible.

By minimizing these harmonics, the filter improves the overall efficiency of the power conversion process and reduces electromagnetic interference (EMI) that could potentially affect the operation of other electronic components in the system. Additionally, the filter protects the rectifier and downstream components from voltage spikes and surges that could lead to premature failure or operational instability.

Design of the Filter Parameters (R and C)

The design of the passive filter involves selecting appropriate values for the resistance (R) and capacitance (C) to achieve the desired filtering effect without introducing significant power losses or affecting the system's dynamic performance. The resistance is chosen to provide damping, preventing oscillations and ensuring system stability. The capacitance is selected based on the cutoff frequency, which is determined by the specific harmonic frequencies that need to be attenuated.

- **Resistance (R):** The resistor value is typically small, chosen to provide just enough damping to prevent resonant oscillations without causing significant power dissipation. A typical range might be between 0.1 to 1 ohm, depending on the specific system requirements.
- **Capacitance (C):** The capacitor is selected to create a low-pass filter with a cutoff frequency below the switching frequency of the rectifier. The capacitance value is calculated based on the desired cutoff frequency f_c using the formula:$C = \frac{1}{2\times\pi\times R\times f_c}$.

1.6.3 Mode of Operation of a WT Coupled with PMSG

The operation of the PMSG based on a variable speed wind turbine can be classified into three modes: the first mode is the silent mode, the second mode is the variable speed operation mode, and the last mode the constant speed mode.

The turbine enters silent mode in two cases: In the first case the wind speed falls below the cut-in level or exceeds the cut-off speed. In the case of wind speed under the cut-in level, the turbine cannot produce sufficient torque to initiate the movement of the turbine. Conversely, wind speeds exceeding the cut-off level pose a risk of turbine damage, requiring shutdown under such circumstances. Typically, turbines commence operation at wind speeds around 3 m/s and are shut down when winds exceed 25 m/s (L Bisenieks, Vinnikov, & Galkin, s.d.).

During variable speed operation mode, the turbine adjusts its speed within the wind velocity range spanning from the cut-in speed to the rated wind speed, which typically stands at 12

m/s, though this value may vary depending on the turbine model. In constant speed mode, occurring above the rated wind speed, the turbine maintains a consistent output power level, refer to figure 1.5, we can see the output power in kW with respect to the speed of wind in m/s as shown with the three modes for a 2 KW VSWT in the following figure.

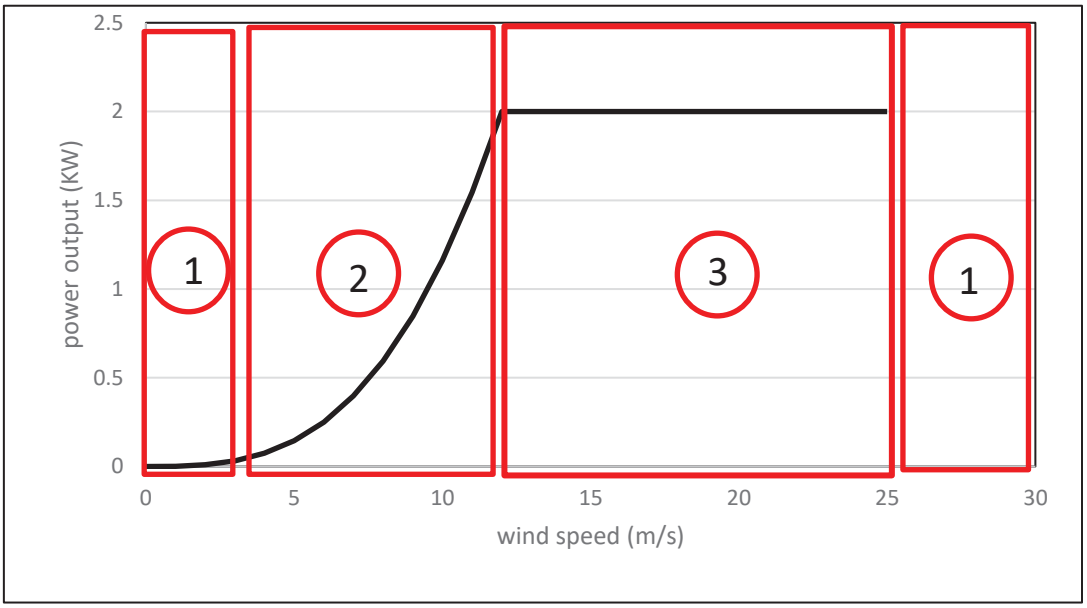

Figure 1.5 The output power of a variable speed wind turbine as a function of wind speed

Based on the analysis that mentioned in (L Bisenieks et al., s.d.), the operation of the PMSG can be categorized into three distinct processes: the inactive mode, the variable speed mode, and the constant speed process.

And based on the PMSG we have three processes as mentioned in (Lauris Bisenieks, Vinnikov, & Galkin, 2013), the inactive mode, the variable speed mode and the last the constant speed process.

when the generator in the inactive mode, the winds speed is beneath the cut in level, or the wind speed is over than the cut off level, at the cut in level there will be no produce for enough torque in order to let the turbine move, and for the cut off level the wind turbine will

be damaged, it must be stopped preventing it from scratching. Most of time, the turbine start working at a speed 3 m/s, and at 25 m/s the turbine must be stopped (Stiebler, 2008). In the range between the cut in and the rated wind speed the turbine will operate according to the wind speed, and above the rated wind speed, the turbine will operate and remains constant from the rated speed (12 m/s) to the cut off speed (25 m/s), as it's shown in in figure 1.5. In the variable speed mode, and to achieve the desired voltage at the output, during this mode we need a power electronic converter.

1.7 Power Electronics Converters

To address the variable and intermittent output power of wind turbines and to optimize the energy captured, an interfacing power electronic converter is required between the wind turbine generator and the grid/load. In traditional two-stage inverters, a PMSG is connected to a three-phase diode bridge rectifier. A DC/DC boost converter is then placed between the rectifier and the voltage-source inverter bridge to regulate the rectifier's wide range of output voltages to a constant desired level. Although this configuration is commonly used, it adds weight, volume, cost, and complexity to the system while also reducing overall efficiency.

1.7.1 DC-DC Power Converters

DC-DC converters simply is combination of elements that can transfer the DC voltage from one stage into another stage, it can be step up or step down the voltage, and it can convert the variable voltage into a constant DC voltage (Nguyen, Lim, Choi, & Cho, 2016a).

Usually, variable speed wind turbines in the variable speed mode will generate a low voltage, in this case, a high step-up DC-DC converter with a high gain voltage must be implemented, to interface between the wind turbine and the load of the residential application that we have. Between all kinds of DC–DC converters, a new topology started in the 21 centuries, which is the Z-source converter, Z-source converter is designed to generate high voltage gain with a lower duty cycle (Fang, Member, & Peng, 2003).

1.7.2 Z-Source Converter

Power electronics research now has a new way to explore because of the concept of the Z-source converters. It is anticipated that novel Z-source topologies would be consistently suggested to satisfy and improve converter efficiency in various applications. Z-source converters have potential uses in RE generation, including PV and wind power, as well as motor drives, due to their unique voltage buck-boost capabilities, low component, and possibly affordable prices. New power electronic technologies, like SiC and GaN, will enhance the efficiency of ZSIs (Siwakoti, Peng, Blaabjerg, Loh, & Town, 2015).

The idea of using ZSIs is to defeat the problems of a traditional VSI and CSI, so by using this kind of inverters it can increase the whole efficiency, reduce the cost and also to do buck-boost for the voltage (Yang, Peng, Lei, Inoshita, & Qian, 2011).

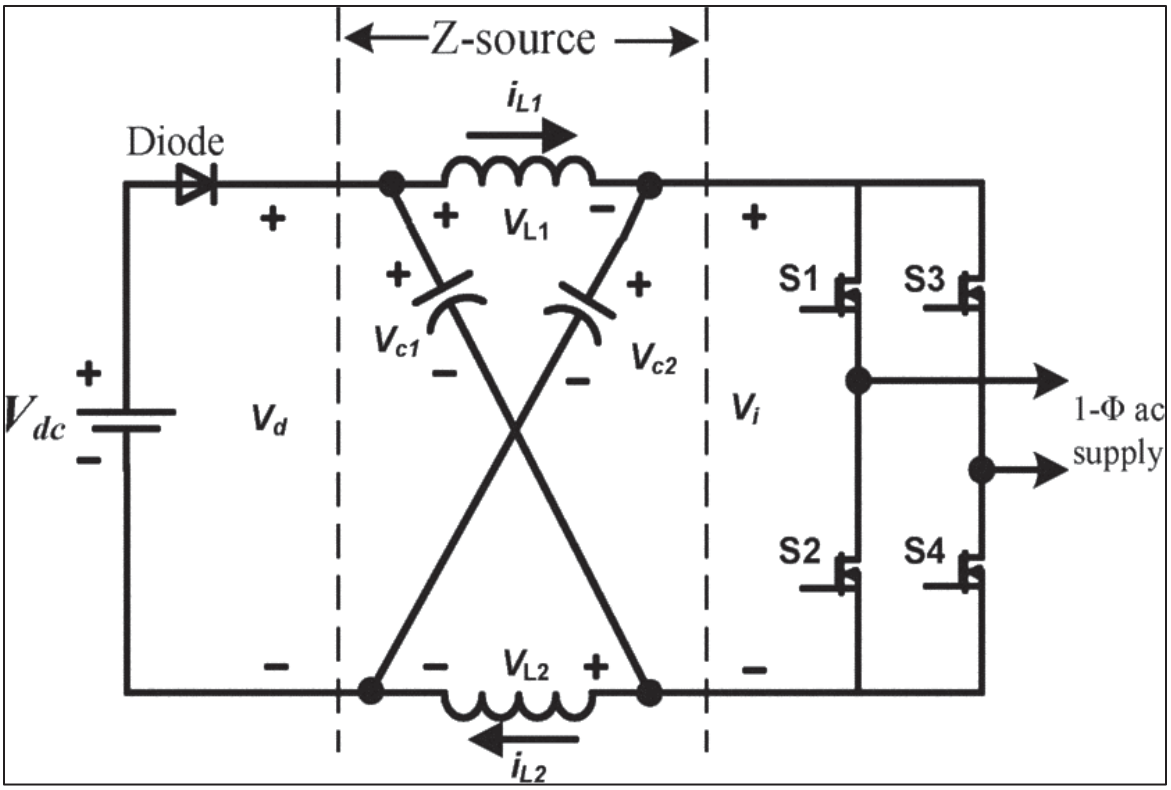

Figure 1.6 The network of a Z-source converter
Taken from Shekar & Veerachary,(2009)

The Z-source converter, as illustrated in Figure 1.6, consists of two inductors and two capacitors linked in an X-shape configuration. This setup is used to create an impedance source that connects the inverter to the source or load (Fang Zheng Peng, 2003), it has disadvantage concerning high-voltage stresses, and reduction of the common between the input source and the load, and finally a discontinuous-current (Samadian, Hosseini, Sabahi, & Maalandish, 2020a).

To explain the operation of the Z-source inverter operates. A three-phase Z-source inverter bridge has nine allowable switching states, unlike the traditional three-phase V-source inverter, which has eight. However, the three-phase Z-source inverter bridge has an additional state when the load terminals are connected through both the upper and lower

devices of any one phase leg (that's mean that both devices are activated) (Fang Zheng Peng, 2003).

The shoot-through zero state, which is prohibited in the traditional V-source inverter due to the risk of a short circuit, and it is enabled in the ZSI. The Z-source network enables this shoot-through zero state, providing the inverter with its buck-boost feature (Fang Zheng Peng, 2003).

For modifying the disadvantages of the ZSI, and to benefit from the shoot through state, a new model is suggested which is called the QZSI that has more advantages than the regular ZSI.

1.8 Quasi Z-Source Power Converter

Over the advantages of ZSIs, and to overcome over the disadvantages, a QZSI is more efficient and have more reliable, low in the cost of the components, and the ability of the buck-boost conversion, these advantages make the quasi-Z-source inverter best choice for wind energy system (Shrivastava et al., 2016).

The advantages of the QZSI include lower ratings for passive components, a continuous DC input current leading to a single DC break between the source and the inverter, in addition to less voltage stress throughout the capacitor. By comparison to the traditional inverters and Z source inverters, QZSI has less voltage stress on the inverter.

QZSIs that have different structures has the aim first to improve the voltage gain, decrease the voltage stress on the elements, and decreasing the overall cost of the system by using less components (Samadian et al., 2020a).

The impedance network of the QZSI, consists of two capacitors and two inductors, links the converter with a DC source, establishing a shared connection between the source and load (Shrivastava et al., 2016).

In the QZSI, the current at the input of the QZSI is continuous, unlike ZSI, and the voltage at the output of the quasi-Z source is the total voltage of the C1 and C2 of the QZSI (Vinnikov & Roasto, 2011a).

With all the configuration of the QZSI, Figure 1.7 below shows the proposed of the network of the QZSI.

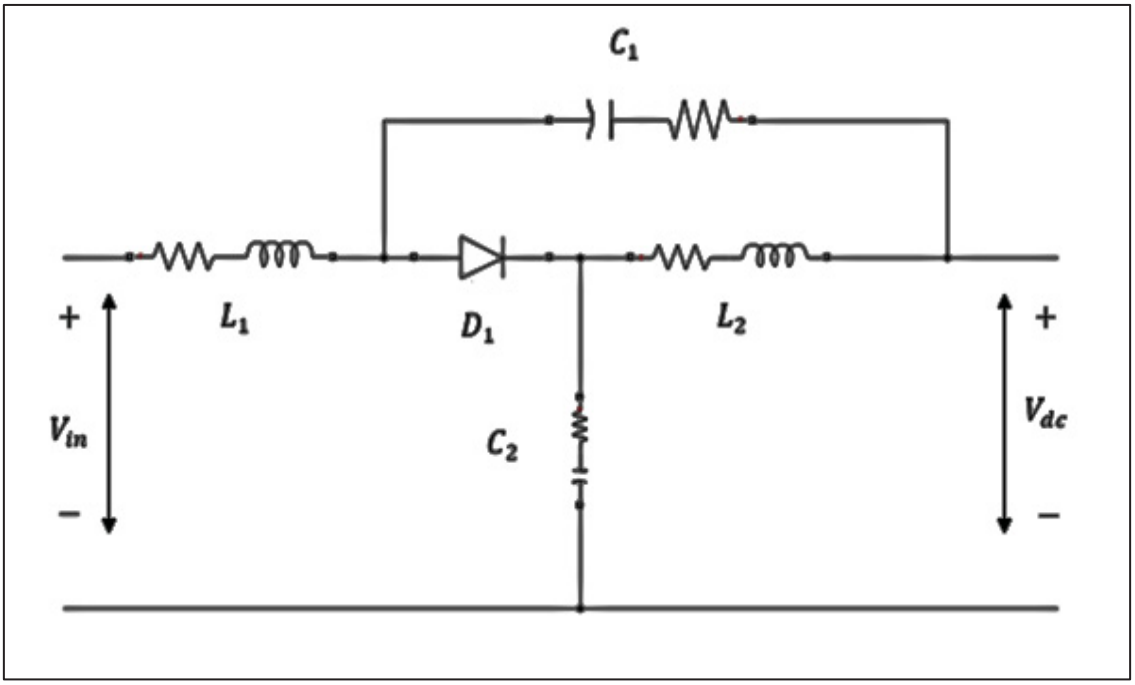

Figure 1.7 The network of the quasi z-source

Consequently, the QZSI proposes, like the ZSI, an extra state over the actual states that are found in the traditional VSI, which is the shoot through state, which works on boosting the voltage.

1.8.1 Voltage-Fed vs Current-Fed QZSI Configurations

1.8.1.1 Voltage-Fed Quasi-Z source

The voltage-fed QZSI as shown in figure 1.7 above, works on boosting the input voltage of the quasi-Z source inverter, this boost of the voltage can be achieved by adding a state called the shoot through state (Vinnikov & Roasto, 2011b).

As mentioned with the Z – source inverter, the use of this state with a traditional inverter can cause a short circuit to the DC capacitors.

The disadvantage linked with the voltage fed Z-source inverter is taken in consideration, were during the boost mode a discontinuous of the input current which effect the DC-input, from here a voltage-fed quasi-Z source inverter was a reformation of the known voltage-fed Z-source inverter, which characterized by continuous input current (Vinnikov & Roasto, 2011b).

1.8.1.2 Current Fed Quasi-Z Source

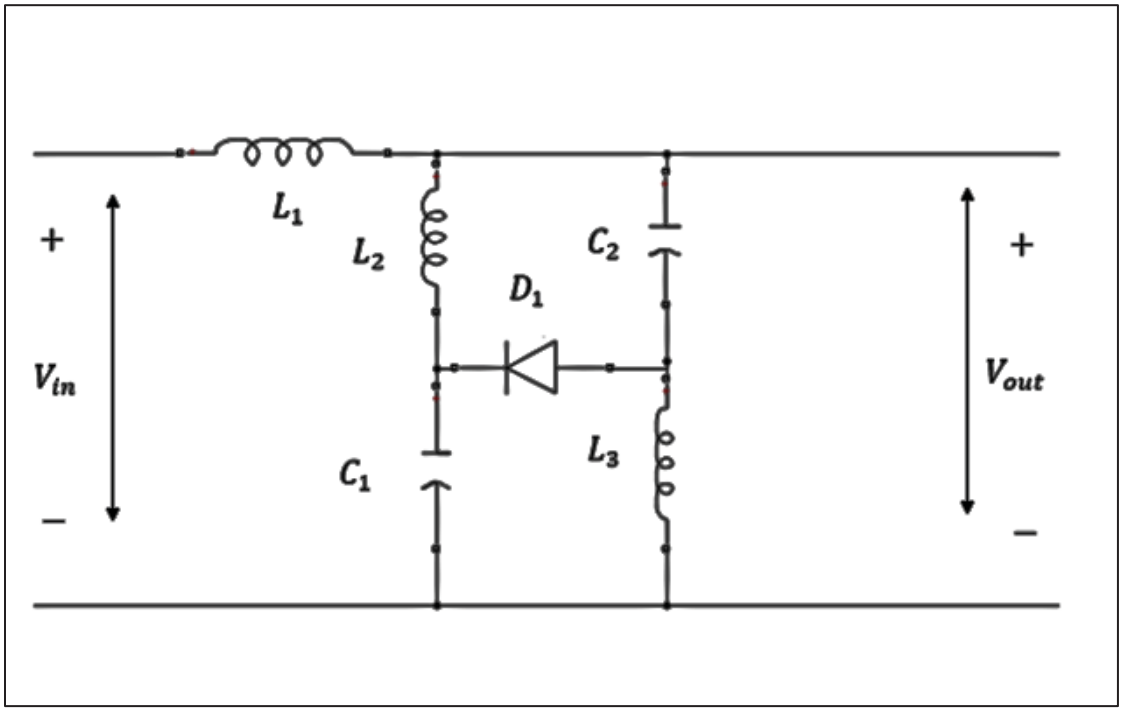

Figure 1.8 The network of the current fed quasi-Z-source

In figure 1.8 above, the network shows a current fed quasi -Z source, this kind can be work as a bidirectional inverter due to the Diode in the network, unlike the voltage fed quasi-Z source, it can't preserve a bidirectional power flow.

The weakness of the current-fed ZSI is a high current must keep inside the inductors. In the traditional CSI that can work on the boost voltage and also allow the power to flow in a unidirectional, whereas we need an IGBT/MOSFET switches instead of the diode in the voltage fed ZSI/QZSI needs to achieve the bidirectional flow of power (Yang et al., 2011).

1.8.2 Types of QZSI

We can classify QZSI into two types based on (Vinnikov & Roasto, 2011b), (Samadian, Hosseini, Sabahi, & Maalandish, 2020b) and ((Nguyen, Lim, Choi, & Cho, 2016b) QZSI with an isolation, and a QZSI without isolation.

Recently, there has been a surge in the development of high step-up DC-DC converters to achieve significant voltage amplification in both isolated and non-isolated configurations.

1.8.2.1 QZSI with Isolation

The provided galvanic isolation (between the input and output phases of the power converters) falls short of complying with safety regulations. To remedy this issue, several isolated converters designed for high step-up functions have been introduced. These converters utilize boost-type mechanisms combined with transformers like in (Raghavendra et al., 2019) and voltage lift strategies as mentioned in (Wong, Chen, Liu, & Hsieh, 2017) to achieve significant voltage amplification (Nguyen et al., 2016b).

This kind usually represent two cascaded stages, we have first stage from DC to AC and from AC to DC power conversion, this have a boost voltage that may be implemented before the bridge of the inverter or it can be integrated in the second part (AC-DC) power conversion, while the transformer that contain a high turn ratio it can do the main boost for the voltage. A soft-switch technique is preferred to improve the efficiency of the converter for a high step-up isolated DC to DC converters (Nguyen et al., 2016b).

Figure 1.9 shows one topology of the QZSI with isolation, mostly this kind is used for on grid system.

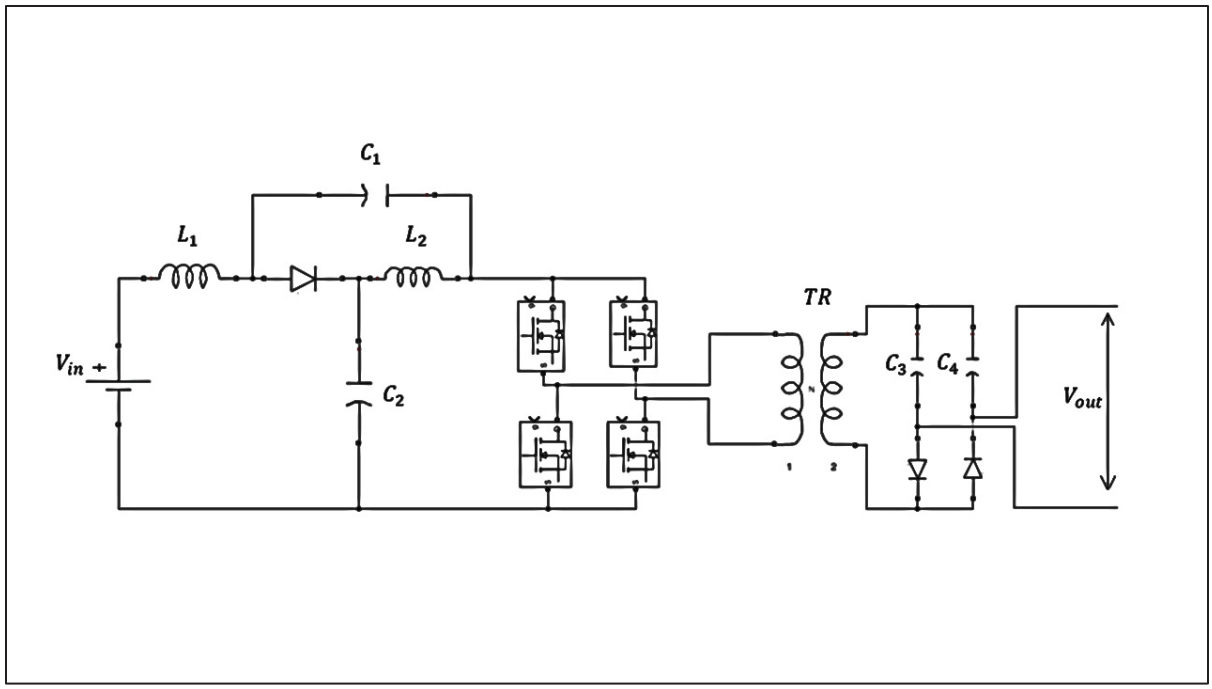

Figure 1.9 QZSI Isolated DC-DC Converter

1.8.2.2 QZSI without Isolation

In non-isolated configurations, where galvanic isolation is not provided, several methods have been proposed, including the use of a coupled inductor, cascaded techniques, switched capacitors, switched inductors, and voltage multiplier cells. These approaches aim to enhance the DC-DC conversion process, resulting in substantial voltage amplification in both cascade and transformer less setups, achieving high efficiency and power density (Nguyen et al., 2016b).

This can be illustrated in figure 1.10 where no isolation is used in the configuration. But, in non-isolated converters, the galvanic isolation between the input and output stages does not meet safety standards. To overcome this limitation, various isolated converters tailored for high step-up applications have been introduced. These isolated converters typically

incorporate boost-type converters integrated with transformers and voltage-lift to achieve significant voltage gain (Nguyen et al., 2016b).

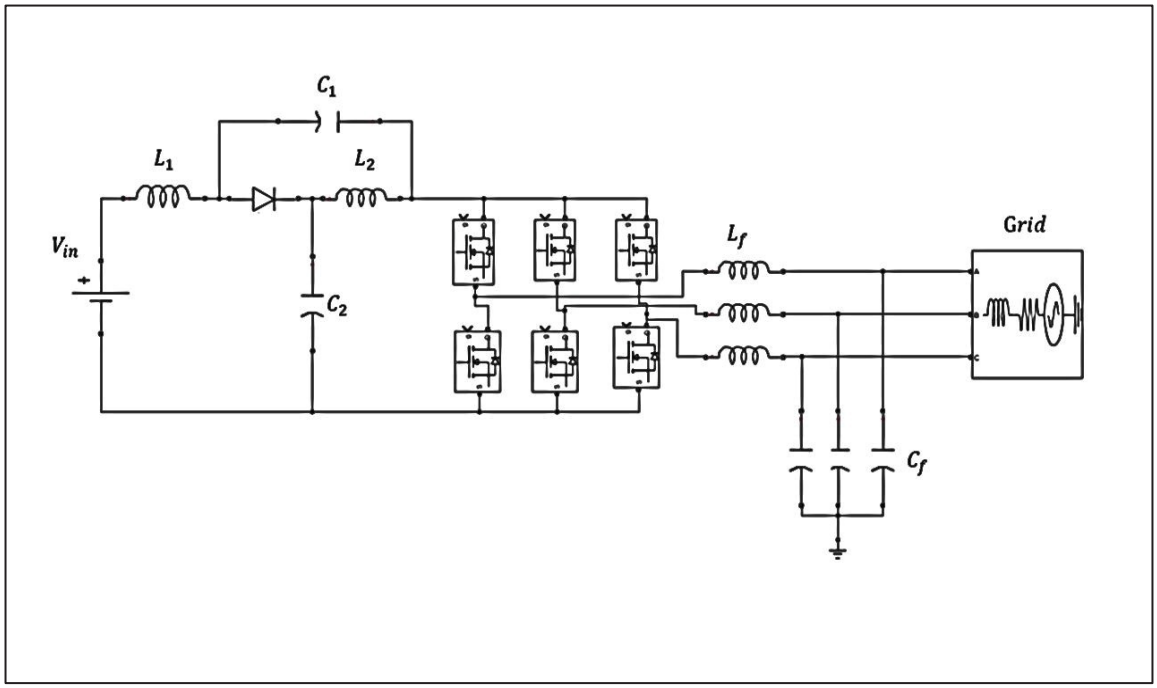

Figure 1.10 Configuration of Isolated QZSI

1.8.3 Modes of Operation of QZSI

The key design features of the QZSI are represented in figure 1.7, showcasing arrangements of two capacitors and inductors as illustrated. The QZSI operates in two distinct modes: the active mode and the shoot through mode.

1.8.3.1 Active mode

The switching scheme of the QZSI, whether in active or passive mode, represents that of the VSI, in other words, it's the same as of the traditional inverter. Here, the input DC voltage serves as an intermediate circuit potential feeding into the inverter, thus making the QZSI

function similarly to a standard VSI (Raja Nayak, Tulasi, Divya Teja, Koushic, & Suresh Naik, 2023).

The equivalent circuit for the QZSI in the active mode is as shown in figure 1.11 below.

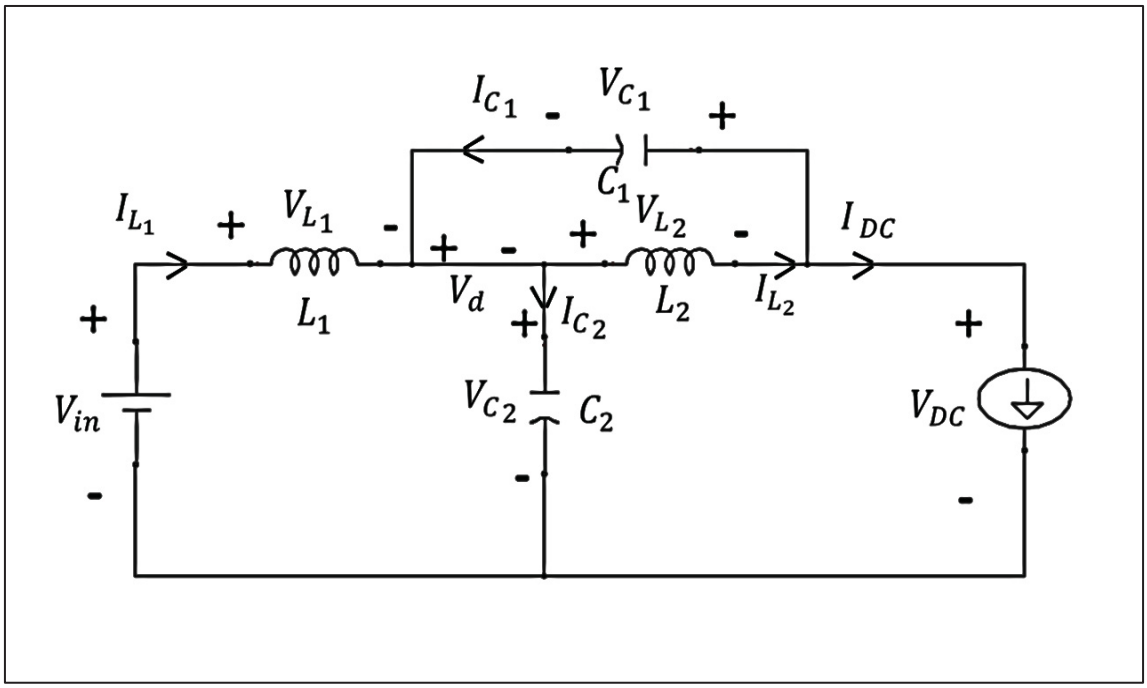

Figure 1.11 Equivalent circuit of QZSI in active mode

In this mode the diode D of the QZSI, act as a short circuit, and the output voltage at the output is equal to V_{DC}, the polarities voltage of the component of the QZSI and the direction of the current is shown in figure 1.11.

1.8.3.2 Shoot through mode

As mentioned before, the shoot through state is an additional state to the regular traditional inverter states. This state involves the same leg phase of the inverter bridge to trigger the switching operations simultaneously for a very short duration.

The LC system inside the QZSI protects any effect on the input voltage and eliminating the risk of doing short circuit on the H bridge converter and results in increasing the output voltage (Raja Nayak et al., 2023).

In this state the switches on the same leg of the inverter are turned on. The period of the shoot through can be denoted by (T_{sh}) overall the period that denoted by T. Also in this state, the diode D will work as a reversed biased (it can be acted as an open circuit) like in figure 1.12 (Bajestan et al., 2019).

The duty cycle of the shoot through can be denoted by $D_{sh} = \frac{T_{sh}}{T}$, and by controlling the modulation index and the duty cycle, it can provide a capability of the buck and boost of the voltage, reduce the cost and the line harmonics (Bajestan et al., 2019).

The quasi-Z source inverter throughout the shoot-through and active state are shown with the polarities of the voltages in figure 1.12.

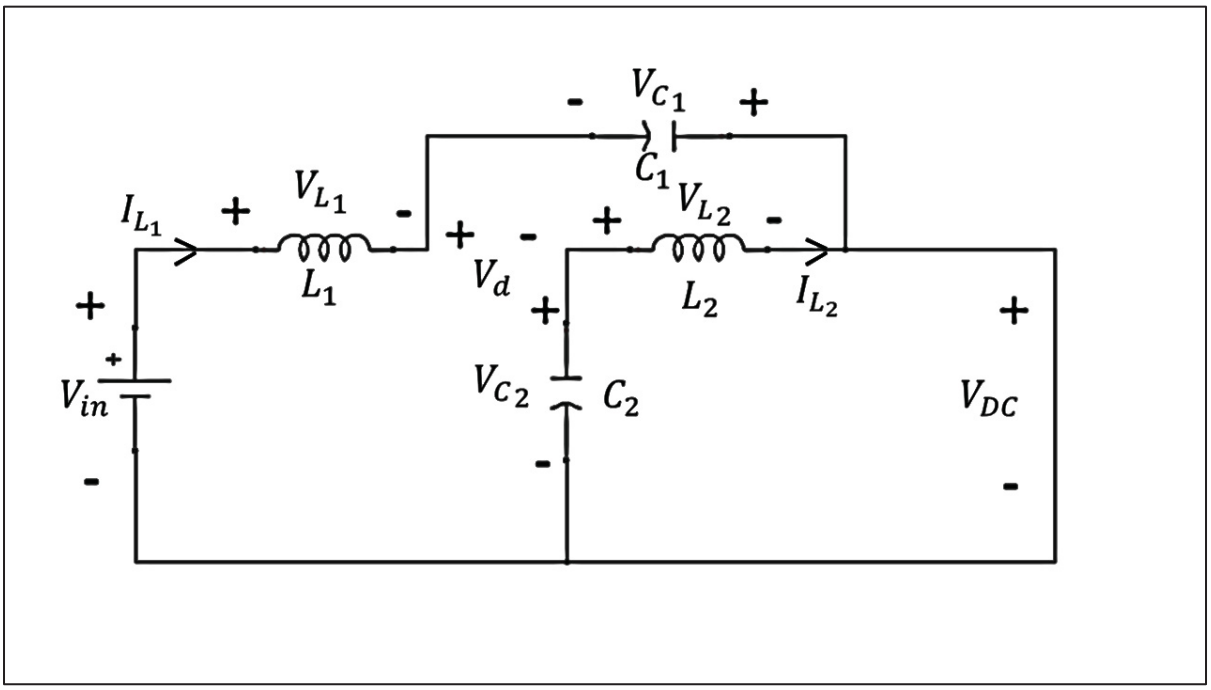

Figure 1.12 Equivalent of QZSI in the shoot through state mode

When the voltage produced by the wind turbine is sufficiently high, the need for the shoot-through state is eliminated, allowing the QZSI to function like a standard VSI. Consequently, the QZSI is capable of both increasing and decreasing voltage levels without the requirement for additional switching mechanisms, with just controlling the duty cycle of the shoot-through (Vinnikov & Roasto, 2011).

By adjusting the duty cycle of the shoot-through in the inverter's bridge, which includes switches S1, S2, S3, and S4, the DC voltage V_{DC} can be controlled to achieve the targeted voltage. This adjustment accounts for changes in V_{DC} and variations in wind speed ranging, as detailed by (Lauris Bisenieks, Vinnikov, & Zakis, 2011).

In the shoot-through phase, the quasi-Z-source's impedance network offers both isolation and protection. When the shoot-through occurs (meaning the switches are engaged), it facilitates the storage of magnetic energy in the two inductors within the quasi-Z-source network without causing a short circuit across capacitors C1 and C2. Subsequently, during the inverter's active phases, an increase in magnetic energy within these inductors occurs, thereby enhancing the voltage (Vinnikov & Roasto, 2011).

In this mode, Diode D act as an open circuit, and the V_{DC} at the output of the QZSI is a short circuit, the voltage polarities of the QZSI components, and the direction of the current are shown in figure 1.12.

To illustrate and to understand the states of the quasi-Z source figure 1.13 explains the switching pattern of the four switches, showing the shoot-through state and the active state.

T1, T2, T3, and T4 corresponds to the switches S1, S2, S3, S4 of the single phase inverter, S1 and S4 are ON, S2 and S3 are OFF from time 0 to 90°, while from 90° to 180°(zero state), there is no active state, a shoot through state happen in this time, its created by two signals, V_p and V_n, form 180° to 270°, S2 and S3 are ON, S1 and S4 are OFF.

When the shoot through occurs, $V_{DC} = 0$, it can be shown clearly in graph (c), where the shoot through state occurs V_{DC} is equal to zero, while in active and zero state the output voltage is equal to V_{DC}. In graph (d) it shows the output of the voltage of the QZSI.

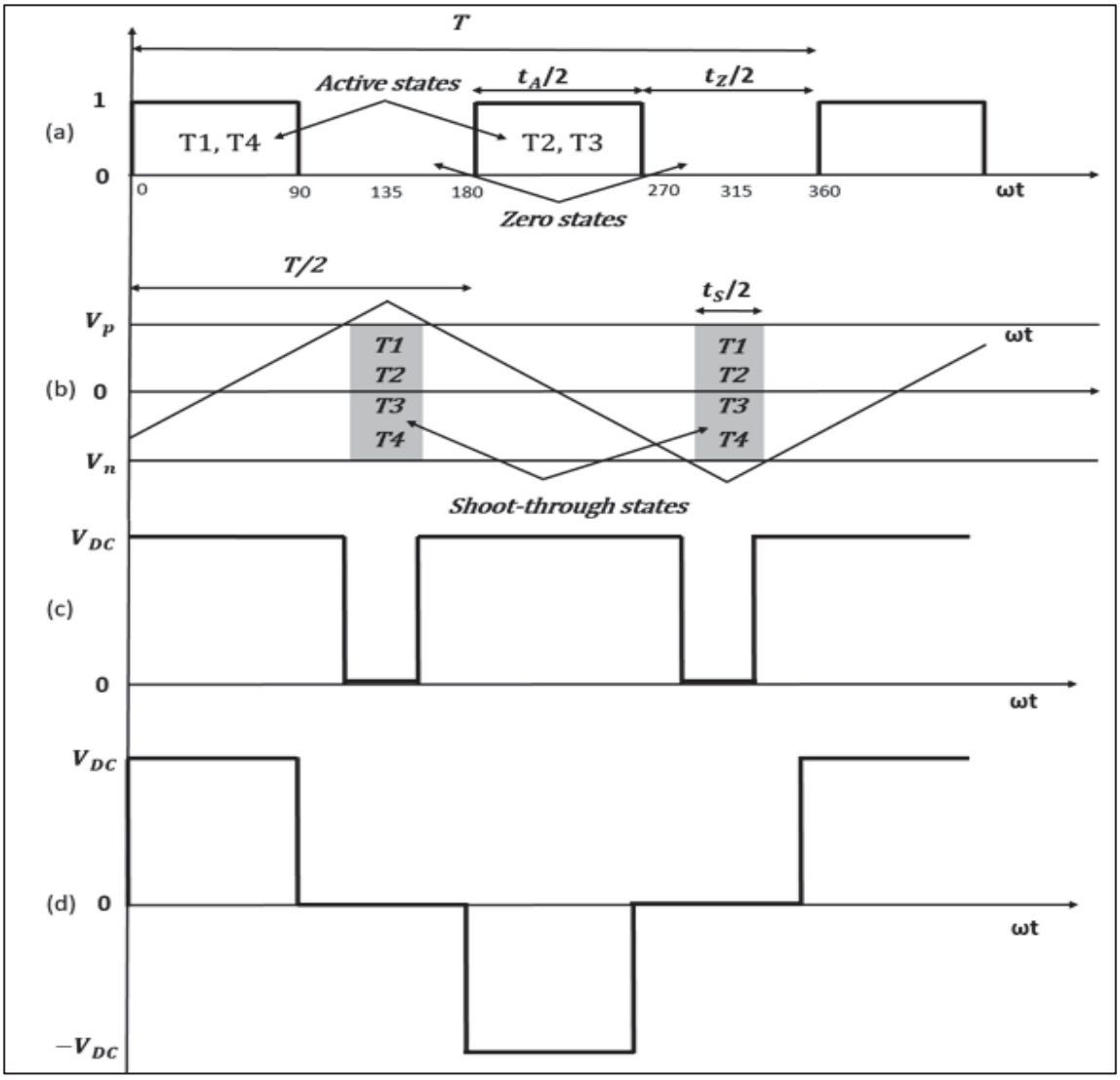

Figure 1.13 Switching pattern of the QZSI

Taken from Vinnikov & Roasto (2011)

1.8.4 Mathematical Analysis of QZSI

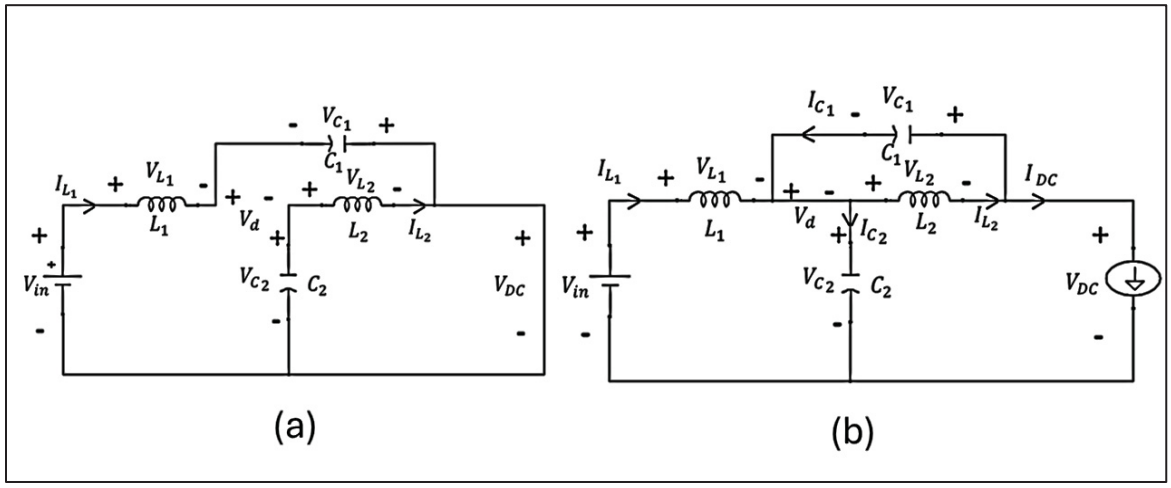

Figure 1.14 Equivalent circuit of the QZS a) in shoot-through mode b) in active mode

From figure 1.14.a, it shows the equivalent circuit at the shoot-through state of the QZSI for a duration T_{sh}, we can obtain the following equations:

$$\begin{cases} V_{L1} = V_{C1} + V_{in} \\ V_{L2} = V_{C2} \\ V_{DC} = 0 \\ V_d = V_{C2} + V_{C1} \end{cases} \tag{1.16}$$

From figure 1.14.b which shown the equivalent circuit at the active state of the QZS inverter with the duration of $(T - T_{sh})$, we can obtain the following equations:

$$\begin{cases} V_{L1} = V_{in} - V_{c2} \\ V_{L2} = -V_{c1} \\ V_{DC} = V_{c2} - V_{L2} = V_{c2} + V_{c1} \\ V_d = 0 \end{cases} \tag{1.17}$$

At the steady state, the average voltage of V_{L1} and V_{L2} is zero for one switch period:

$$\bar{V}_{L1} = \frac{(V_{c1}+V_{in})(T_{sh})+(V_{in}-V_{c2})(T-T_{sh})}{T} = 0 \quad (1.18)$$

$$\bar{V}_{L2} = \frac{(V_{c2})(T_{sh})+(-V_{c1})(T-T_{sh})}{T} = 0 \quad (1.19)$$

And from the above equations we can derive a relation between the V_{c2}, V_{c1} and the voltage V_{in} and we get the following relations:

$$V_{c1} = \frac{(T_{sh})}{(T-T_{sh})} V_{c2} \quad (1.20)$$

$$V_{c2} = \frac{1-\frac{T_{sh}}{T}}{1-\frac{2T_{sh}}{T}} V_{in} \quad (1.21)$$

Substitute in 1.18:

$$V_{c1} = \frac{\frac{T_{sh}}{T}}{1-\frac{2T_{sh}}{T}} V_{in} \quad (1.22)$$

By supposing that $\frac{T_s}{T} = D_{sh}$, the duty cycle of the shootout through period, and by calculating the peak DC link voltage of the bridge of the inverter:

$$\hat{V}_{DC} = V_{c1} + V_{c2} = \frac{1}{1-2\frac{T_{sh}}{T}} V_{in} = \frac{1}{1-2D_{sh}} V_{in} \quad (1.23)$$

$$\hat{V}_{DC} = B.V_{DC} \quad (1.24)$$

Where B is the boast factor which is derived by the shoot through duty cycle D_{sh}.

During the following process mode, the current over the switches of the desired inverter will reach its maximum. And relying on the control algorithm used, the current of the shoot-through can be divided between one or two of the legs of the inverter.

Taking to the account the following control methodology for generating the shoot through, the shootout state will be made during the zero states of the full bridge converter, in this case where the primary winding of the transformer is be shorted by the upper leg (S1 and S3) or by the lower leg (S2 and S4) (Vinnikov & Roasto, 2011).

To provide a suitable organizing margin, the zero-state time T_Z must always exceed the maximum duration of the shootout states T_{sh-max} for each switching period.

$$T_Z > T_{sh-max} \tag{1.25}$$

Thus, each processing period of the QZSI during the shoot through always contain of an active state T_A, shoot-through state T_{Sh}, and a zero state T_Z, where the overall period is the sum of the three periods.

$$T = T_A + T_{Sh} + T_Z \tag{1.26}$$

and we can represent it by:

$$\frac{T_A}{T} + \frac{T_{Sh}}{T} + \frac{T_Z}{T} = D_A + D_{Sh} + D_Z = 1 \tag{1.27}$$

Where D_A is the duty cycle of the active state, D_{Sh} is the duty cycle of the shootout through state, and D_Z is the duty cycle of the zero state. It must be taken into consideration that the duty cycle of the shoot-through state will not exceed 0.5.

In the proposed design, we have two cases, first case the shoot-through state must be used for boosting the voltage at the input of the proposed quasi-Z source to the DC voltage level needed, the second case, when the input voltage is equal to the QZSI DC voltage level, then

there is no shoot through state and the proposed design will act as traditional voltage source inverter (Vinnikov & Roasto, 2011).

The battery is connected to the capacitor C_2, we can have the following equations:

$$\begin{cases} L_1 \dot{i_{L1}}(t) = V_{c1}(t) + V_{in} \\ L_2 \dot{i_{L2}}(t) = V_{c2}(t) \\ C_2 \dot{V_{c2}}(t) = i_{L2}(t) - I_b \\ C_1 \dot{V_{c1}}(t) = -i_{L1}(t) \end{cases} \tag{1.28}$$

Where V_{in} is the input voltage of the QZSI, L_1, L_2, C_2, C_1 are the inductance and the capacitance impedance of the converter, I_b is the current generated by the battery. It can represent this equation in a state space equation as follow:

$$\begin{bmatrix} L_1 & 0 & 0 & 0 \\ 0 & L_2 & 0 & 0 \\ 0 & 0 & C_2 & 0 \\ 0 & 0 & 0 & C_1 \end{bmatrix} \begin{bmatrix} \dot{i_{L1}}(t) \\ \dot{i_{L2}}(t) \\ \dot{V_{c2}}(t) \\ \dot{V_{c1}}(t) \end{bmatrix} = \begin{bmatrix} 0 & 0 & 0 & 1 \\ 0 & 0 & 1 & 0 \\ 0 & 1 & 0 & 0 \\ -1 & 0 & 0 & 0 \end{bmatrix} \begin{bmatrix} i_{L1}(t) \\ i_{L2}(t) \\ V_{c2}(t) \\ V_{c1}(t) \end{bmatrix} + \begin{bmatrix} 1 & 0 & 0 \\ 0 & 0 & 0 \\ 0 & 0 & -1 \\ 0 & 0 & 0 \end{bmatrix} \begin{bmatrix} V_{in} \\ I_{DC} \\ I_b \end{bmatrix} \tag{1.29}$$

For the non-shoot through state, we can get the following equations:

$$\begin{cases} L_1 \dot{i_{L1}}(t) = -V_{c2}(t) + V_{in} \\ L_2 \dot{i_{L2}}(t) = -V_{c1}(t) \\ C_2 \dot{V_{c2}}(t) = i_{L1}(t) - I_{DC} - I_b \\ C_1 \dot{V}_{c1}(t) = i_{L2}(t) - I_{DC} \end{cases} \tag{1.30}$$

Where I_{DC} is the current at the output of the quasi-Z-source. We can represent them these equation in a state space equation as following:

$$\begin{bmatrix} L_1 & 0 & 0 & 0 \\ 0 & L_2 & 0 & 0 \\ 0 & 0 & C_2 & 0 \\ 0 & 0 & 0 & C_1 \end{bmatrix} \begin{bmatrix} \dot{i_{L1}}(t) \\ \dot{i_{L2}}(t) \\ \dot{V_{c2}}(t) \\ \dot{V_{c1}}(t) \end{bmatrix} = \begin{bmatrix} 0 & 0 & -1 & 0 \\ 0 & 0 & 0 & -1 \\ 1 & 0 & 0 & 0 \\ 0 & 1 & 0 & 0 \end{bmatrix} \begin{bmatrix} i_{L1}(t) \\ i_{L2}(t) \\ V_{c2}(t) \\ V_{c1}(t) \end{bmatrix} + \begin{bmatrix} 1 & 0 & 0 \\ 0 & 0 & 0 \\ 0 & -1 & -1 \\ 0 & -1 & 0 \end{bmatrix} \begin{bmatrix} V_{in} \\ I_{DC} \\ I_b \end{bmatrix} \tag{1.31}$$

For simplify the calculation we suppose that:

$$\begin{cases} V_{c2} = V_b = V_{oc} - R_b I_b \\ \dot{V}_{c2}(t) = -R_b \dot{I}_b \\ -C_2 R_b \dot{I}_b = i_{L1}(t) - I_{DC} - I_b \\ L_1 \dot{i_{L1}}(t) = -V_{oc} + R_b I_b + V_{in} \end{cases} \tag{1.32}$$

Where R_b is the internal resistance for the battery.

$$\begin{bmatrix} L_1 & 0 & 0 & 0 \\ 0 & L_2 & 0 & 0 \\ 0 & 0 & -R_b C_2 & 0 \\ 0 & 0 & 0 & C_1 \end{bmatrix} \begin{bmatrix} \dot{i_{L1}}(t) \\ \dot{i_{L2}}(t) \\ \dot{I_b}(t) \\ \dot{V_{C1}}(t) \end{bmatrix} = \begin{bmatrix} 0 & 0 & R_b & 0 \\ 0 & 0 & 0 & -1 \\ 1 & 0 & -1 & 0 \\ 0 & 1 & 0 & 0 \end{bmatrix} \begin{bmatrix} i_{L1}(t) \\ i_{L2}(t) \\ I_b(t) \\ V_{C1}(t) \end{bmatrix} + \begin{bmatrix} 1 & 0 & -1 \\ 0 & 0 & 0 \\ 0 & -1 & 0 \\ 0 & -1 & 0 \end{bmatrix} \begin{bmatrix} V_{in} \\ I_{DC} \\ V_{oc} \end{bmatrix} \tag{1.33}$$

For the shoot through mode:

$$\begin{bmatrix} L_1 & 0 & 0 & 0 \\ 0 & L_2 & 0 & 0 \\ 0 & 0 & -R_b C_2 & 0 \\ 0 & 0 & 0 & C_1 \end{bmatrix} \begin{bmatrix} \dot{i_{L1}}(t) \\ \dot{i_{L2}}(t) \\ \dot{I_b}(t) \\ \dot{V_{C1}}(t) \end{bmatrix} = \begin{bmatrix} 0 & 0 & 0 & 1 \\ 0 & 0 & -R_b & 0 \\ 0 & 1 & -1 & 0 \\ -1 & 0 & 0 & 0 \end{bmatrix} \begin{bmatrix} i_{L1}(t) \\ i_{L2}(t) \\ I_b(t) \\ V_{C1}(t) \end{bmatrix} + \begin{bmatrix} 1 & 0 & 0 \\ 1 & 0 & 0 \\ 0 & 0 & 0 \\ 0 & 0 & 0 \end{bmatrix} \begin{bmatrix} V_{in} \\ I_{DC} \\ V_{oc} \end{bmatrix} \tag{1.34}$$

Then the overall state space equation as follows:

$$\begin{bmatrix} L_1 & 0 & 0 & 0 \\ 0 & L_2 & 0 & 0 \\ 0 & 0 & -R_b C_2 & 0 \\ 0 & 0 & 0 & C_1 \end{bmatrix} \begin{bmatrix} \dot{i_{L1}}(t) \\ \dot{i_{L2}}(t) \\ \dot{I_b}(t) \\ \dot{V_{C1}}(t) \end{bmatrix} = \begin{bmatrix} 0 & 0 & R_b(D_{sh}-1) & D_{sh} \\ 0 & 0 & -R_b D_{sh} & D_{sh}-1 \\ 1-D_{sh} & D_{sh} & -1 & 0 \\ -D_{sh} & 1-D_{sh} & 0 & 0 \end{bmatrix} \begin{bmatrix} i_{L1}(t) \\ i_{L2}(t) \\ I_b(t) \\ V_{C1} \end{bmatrix} + \begin{bmatrix} 1 & 0 & D_{sh}-1 \\ D_{sh} & 0 & 0 \\ 0 & D_{sh}-1 & 0 \\ 0 & D_{sh}-1 & 0 \end{bmatrix} \begin{bmatrix} V_{in} \\ I_{DC} \\ V_{oc} \end{bmatrix} \quad (1.35)$$

Where $D_{sh} = \frac{t_{sh}}{T}$ is the duty ratio of the shoot out through.

Doing for the following state space a Laplace transformation we can deduce the following:

$$\begin{cases} L_1 s\, i_{L1}(s) = D_{sh} V_{c1}(s) - R_b(D_{sh}-1) I_b(s) + V_{in} + (D_{sh}-1) V_{oc}(s) + d(V_{c1} + R_b I_b - V_{oc}) \\ L_2 s \times i_{L2}(s) = (D_{sh}-1) V_{c1}(s) - R_b(D_{sh}) I_b(s) + D_{sh} V_{in} + d(-V_{c1} - R_b I_b + V_{in}) \\ -R_b C_2 s \times I_b = (1-D_{sh}) i_{L1}(s) + D_{sh}\, i_{L2}(s) - I_b + (D_{sh}-1)\, I_{DC} + d(-i_{L1} + i_{L2} - I_{DC}) \\ C_1 s V_{C1} = -D_{sh} i_{L1}(s) + (1-D_{sh}) i_{L2}(s) + (D_{sh}-1)\, I_{DC} + d(-i_{L1} - i_{L2} + I_{DC}) \end{cases} \quad (1.36)$$

And from these equations we can derive the transfer function of the system; by choosing the input and the outputs of different equations, it can assist more to study the stability and control of the system.

The table below will classify the voltage and current of the different components of the QZSI, it shows the different indication and the calculated value in both states, in the active state and in the shoot through state:

Table 1.1 The value of different voltage and current through shoot through and active state

	Indication	Active state	Shoot-through state
Inductor voltage	V_{L1}	$-\frac{1}{1-2D_{sh}}\,V_{DC}$	$\frac{1-D_{sh}}{1-2D_{sh}}\,V_{DC}$
Peak DC link voltage	V_{DC}	$\frac{1}{1-2D_{sh}}\,V_{DC}$	0
DC link current	I_{DC}	$\frac{P(1-2D_{sh})}{V_{DC}}$	$\frac{2P}{V_{DC}}D_{sh}$
Diode D1 voltage	V_{D1}	0	$\frac{1}{1-2D_{sh}}\,V_{DC}$
Capacitor C2 voltage	V_{C2}	$\frac{1-D_s}{1-2D_{sh}}\,V_{DC}$	
Capacitor C1 voltage	V_{C1}	$\frac{D_{sh}}{1-2D_{sh}}\,V_{DC}$	
Input current	I_{DC1}	$\frac{P}{V_{DC}}$	
Capacitor current	I_{C1}	$I_{DC,av}-I_{L1,av}$	
Inductor current	I_{L_1}	$\frac{P}{V_{DC}}$	
Diode current	I_D	$2I_{L1,av}-I_{DC,av}$	

1.9 Voltage Boosting and Speed Control in QZSI

The QZSI is designed to step up the voltage output from the PMSG, which is particularly important when operating under variable wind speeds that result in fluctuating rotor speeds. The boost in voltage is achieved through the unique impedance network of the QZSI, which allows for both buck and boost operations without the need for additional converters. This enables the system to maintain a stable and higher voltage at the inverter's output, even when the input from the generator is inconsistent due to changes in wind speed.

To control the speed and maximize power extraction, a maximum power point tracking (MPPT) algorithm is employed. The MPPT algorithm adjusts the inverter's switching patterns to ensure that the rotor speed of the PMSG is aligned with the optimal point where the maximum power can be harnessed from the wind. By continuously adjusting to the varying wind conditions, the system ensures that the generator operates at its peak efficiency, maximizing energy capture.

This approach has its limitations. One of the key challenges is the potential for increased complexity in the control system, particularly under rapidly changing wind conditions. The requirement for precise control of the shoot-through duty cycle in the QZSI can introduce delays and may require high computational power, which could affect the real-time responsiveness of the system.

While the QZSI effectively boosts voltage, the system's overall efficiency may be impacted by the inherent losses in the converter, particularly under low wind speed conditions where the boost requirement is higher. Furthermore, the increased voltage stress on the components of the QZSI, especially the capacitors and switches, can lead to reduced lifespan and reliability of the system, necessitating careful design considerations and possibly higher-rated components, which can increase the overall cost.

1.10 Energy Storage System

Renewable resources possess a natural intermittent, they state a primary challenge for emerging this resource into electricity system. Focusing on these characteristics ensures the resilience and stability of the grid, along with maintaining a balance between electricity production and demand. Thus, incorporating both intermittent and non-intermittent renewable sources combined with energy storage solutions, is more imperative (Sánchez et al., 2022).

Several energy storage technologies have been suggested, each catering to different time scales and power capacities, with varying environmental implications. Currently, compressed-air energy storage and pumped-hydro are the two commercially available options. However, there have been considerable obstacles hindering the widespread adoption of these technologies (Sánchez et al., 2022).

Batteries have emerged as a feasible option for different applications in both standalone system and on-grid system., the primary trade-off arises from balancing the benefits of energy savings enabled by storing low-cost electricity against the costs associated with battery replacement.

The performance and reliability of these technologies are significant considerations. Various electrical storage technologies and methodologies can be categorized into four main groups: mechanical, chemical, electrochemical, and electrical. The subsequent sections provide an overview of many of these categories, with Figure 1.15 illustrating the power ratings and typical discharge times of numerous electrochemical and mechanical electricity storage systems currently in development or practical use. These systems demonstrate a broad spectrum of discharge characteristics and power ratings.

The discharge times and system sizes serve as useful criteria for selecting appropriate storage systems tailored to specific applications. For instance, grid management tasks like frequency

regulation and load leveling often require rapid response times in the order of seconds, making storage solutions like flywheels and supercapacitors suitable. Conversely, bulk power management may necessitate longer response times, typically in the order of hours, where technologies such as pumped hydro and compressed air storage present appealing options (Gür, 2018).

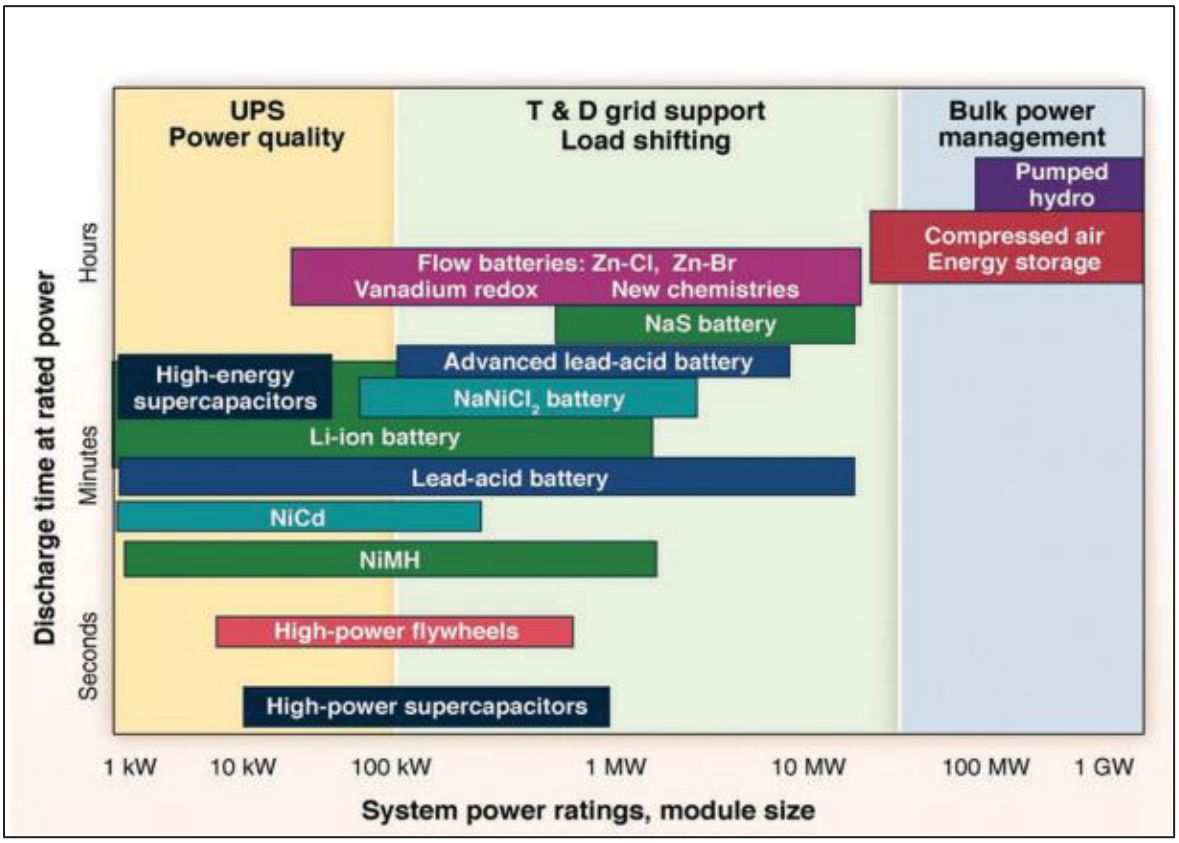

Figure 1.15 Different types of the batteries

Taken from B. Dunn, H. Kamath and J. M. Tarascon (2011, p 334, 928–935)

Many topologies uses battery technology with quasi-Z source network, for example the author in this paper (Liu, Ge, Abu-Rub, & Peng, 2014) he used a battery connected in parallel to the capacitor C_1, and also the author in (Ge, Peng, Abu-Rub, Ferreira, & De Almeida, 2014) the used a battery connected to the leg capacitor (C_2), both topologies are used with the PV system, and used for the on-grid system.

1.11 Conclusion

In this comprehensive literature review, we embarked on an exploration of various aspects related to renewable energy, with a specific focus on wind energy and its integration into the power grid. It examines the fundamental concepts of renewable energy and its significance in the context of global sustainability.

Delving deeper into wind energy, we dissected the anatomy and functionality of wind turbines, shedding light on different types and the critical role of MPPT for optimizing energy extraction. Furthermore, we elucidated the intricate workings of generators, particularly PMSGs, and their mode of operation within wind turbine systems.

The discussion then shifted towards power converters, with a particular emphasis on the QZSI, an innovative solution for enhancing the efficiency and reliability of renewable energy systems. By dissecting its various configurations, modes of operation, and mathematical analysis, we gained valuable insights into the potential of QZSI to revolutionize power conversion in renewable energy applications. It also touched upon the importance of energy storage, particularly batteries, in facilitating the integration of renewable energy into the grid and ensuring grid stability and reliability.

CHAPTER 2

CONFIGURATION ELEMENTS DESIGN

2.1 Introduction

To comprehensively design the entire system, it's imperative to meticulously develop the various components of our network. The whole system is illustrated in figure 2.1. This process begins with the input source, specifically the wind turbine, followed by the design of the QZSI. Additionally, we will focus on designing the storage elements employed within the system. The process also includes the meticulous design of the single-phase inverter, coupled with the LC filter design, and the load configuration.

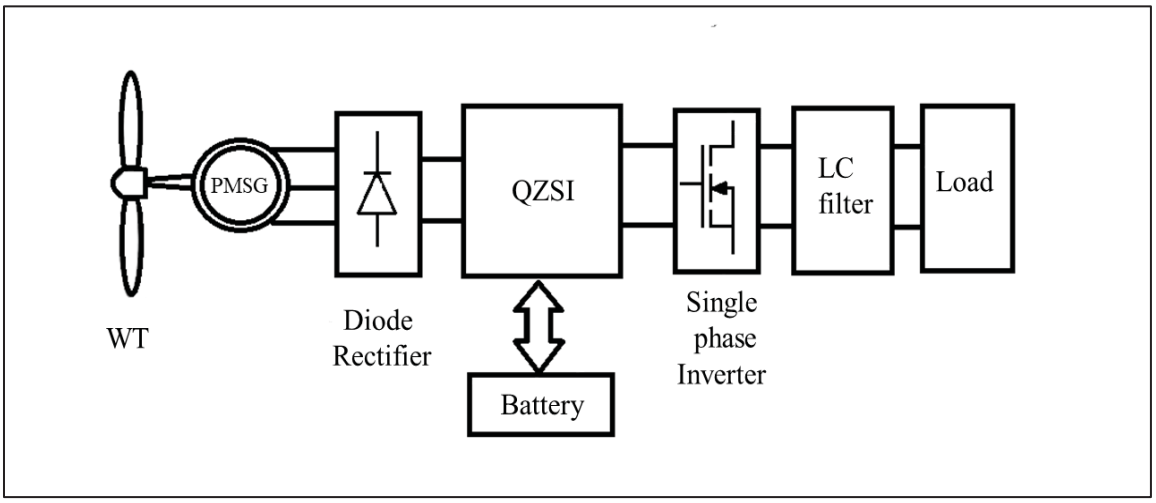

Figure 2.1 Proposed System

2.2 Design of the Wind Turbine and PMSG

In designing the input of our system, we have the wind turbine connected with the PMSG with a diode rectifier as an input for the optimal design. Since the wind turbine that we will use it in design is variable speed and not constant, so we used for the design is the permanent

magnet synchronous generator it has the ability of working at low speed without using a gearbox (Lai & Chan, 2007).

And based on the PMSG, we have three processes as mentioned in (Lauris Bisenieks et al., 2013), the inactive mode, the variable speed mode and the last one which is the constant speed process. when the generator in the inactive mode, the wind speed is beneath the cut in level, or the wind speed is over than the cut off level, at the cut in level there will be no produce for enough torque in order to let the turbine move, and for the cut off level the wind turbine will be damaged, it must be stopped preventing it from scratching.

Most of time, the turbine starts working at a speed of 3 m/s, and at 25 m/s the turbine must be stopped (Stiebler, 2008). In the range between the cut in and the rated wind speed the turbine will operate according to the wind speed, and above the rated wind speed, the turbine will operate and remains constant from the rated speed (12 m/s) to the cut off speed (25 m/s), as it's shown in figure 2.1. The results in this figure are tested in the lab, and the result data are transferred into this diagram, and by using a diode rectifier to convert the AC to DC for simplicity and not for using a control circuit to activate the diode rectifier.

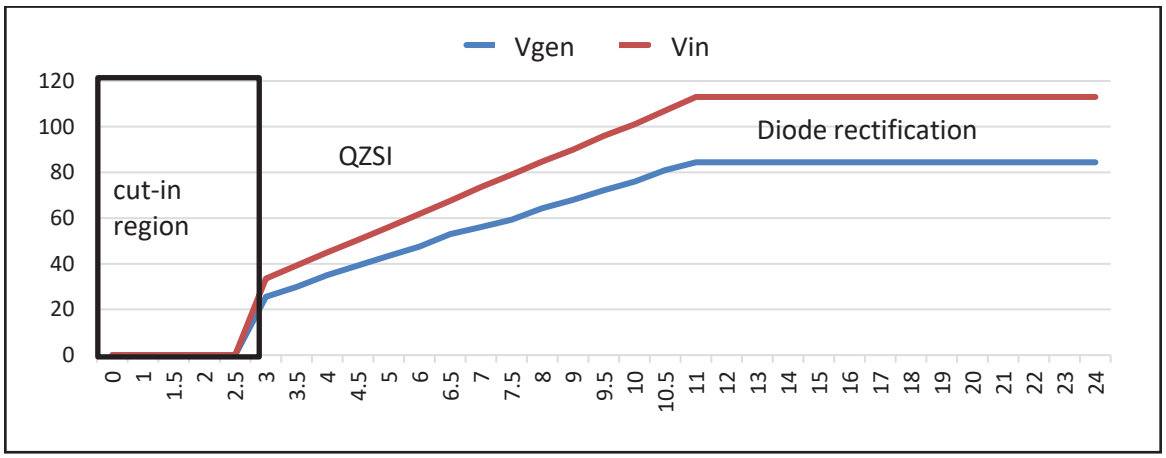

Figure 2.2 Output power of variable speed wind turbine and diode rectifier.

.

Our focus is on the mode where the generator generates in a low voltage, in this case the high step DC-DC converter will act as a high gain voltage, in interface between the wind turbine and the residential load.

From the equation 1.15, we can calculate the estimated output of the DC voltage at the output of the diode rectifier based on the torque and speed of the wind turbine, we will assume our design will be working with a 500W wind turbine power generation.

2.3 Rectified DC Link Voltage (V_{DC1}) in a Variable Wind Speed PMSG

To determine the V_{DC1} range for a 500W variable wind speed PMSG, we want to find the Vdc range across different wind speeds for a proposed 500W PMSG. We cannot provide exact values for the torque coefficient K_t and the induced voltage coefficient (K_e) without the datasheet. But we will estimate them and use the wind turbine power curve to account for the variation of the torque. In addition to the synchronous inductance (Ls) is another vital parameter dependent on the PMSG design. Here, we'll assume a typical value.

Assumptions:

Table 2.1 PMSG Parameters

Parameter	Value	Unit
PMSG Power Rating	500	W
Synchronous Inductance (Ls)	1.5	mH
Reference Ke	1.2	V/rad/s

Wind Turbine Power Curve:

The first step is to obtain the wind turbine power curve (P_{wind} vs v_{wind}) from the manufacturer. This curve relates the captured wind power (proportional to torque) to the wind speed (v_{wind}).

Table 2.2 Power wind vs wind speed

Wind Speed (v_{wind})	Captured Power (P_{wind})
4 m/s	100 W
6 m/s	250 W
8 m/s	400 W
10 m/s	500 W
12 m/s	550 W

2.4 Calculating the Torque (T) for Different Wind Speeds:

Knowing the captured power (P_{wind}) from the power curve, we can estimate the torque (T) for each wind speed using the following relationship (assuming constant generator efficiency):

$$T = \frac{P_{wind}}{\omega_r * \eta} \tag{2.1}$$

Here, ω_r is the rotor speed (rad/s) and η is the generator efficiency (typically between 80% and 90%). We need to estimate ω_r for each wind speed. By assuming a constant generator efficiency of 85% we can have the following table:

Table 2.3 Torque (T) for Different Wind Speeds

Wind Speed (v_{wind})	Captured Power (P_{wind})	Estimated ω_r (rad/s)	Torque (T)
4 m/s	100 W	20 rad/s	2.9 Nm
6 m/s	250 W	25 rad/s	4.2 Nm
8 m/s	400 W	30 rad/s	5.7 Nm
10 m/s	500 W	35 rad/s	7.1 Nm
12 m/s	550 W	40 rad/s	8.4 Nm

Calculating K_t at Different Wind Speeds:

Since K_t depends on the operating point (speed and magnetic field strength), we can calculate it for each wind speed using the equation:

$$K_t(v_{wind}) = \frac{T(v_{wind})}{Ke * I_a} \quad (2.2)$$

In this case, Ke is the induced voltage coefficient, which is an estimated value, and I_a is the stator current (assumed value based on typical operating ranges for a 500W PMSG). (assuming K_e = 1.2 V/rad/s and I_a = 10 A):

Table 2.4 Kt at Different Wind Speeds

Wind Speed (v_{wind})	Torque (T)	$K_t(v_{wind})$
4 m/s	2.9 Nm	0.24 Nm/A
6 m/s	4.2 Nm	0.35 Nm/A
8 m/s	5.7 Nm	0.47 Nm/A
10 m/s	7.1 Nm	0.59 Nm/A
12 m/s	8.4 Nm	0.70 Nm/A

Calculating the VDC1 for Different Wind Speeds:

Now that we have Kt for each wind speed, we can use the final equation 1.15 to calculate the rectified DC link voltage (Vdc):

From table 2.2, and suggesting that the wind speed of 8 m/s:

$$\omega_r = 30\ rad/s \quad (2.3)$$

$$T(v_{wind}) = 5.7\ Nm \quad (2.4)$$

And from table 2.3 we can get:

$$Kt(v_{wind}) = 0.47\ Nm/A \tag{2.5}$$

And from the equations 2.3, 2.4, 2.5 we can get:

$$V_{DC1} = \frac{3\sqrt{6}}{\pi} * 30 * \sqrt{(1.2)^2 - \left(\frac{5.7 * 1.5}{0.47}\right)^2} \approx 48.2\ volts \tag{2.6}$$

Repeating the calculation for each wind speed in the table to get the Vdc range. By calculating Vdc for each wind speed using the corresponding Kt value, you'll obtain a range of Vdc values that reflect the variations in wind speed. This will help you understand how the DC link voltage fluctuates with the changing operating conditions of the wind turbine.

Absolutely, here's the completed table with VDC1 calculations for each wind speed:

Table 2.5 The output voltage DC1 of different wind speed and Torque

Wind Speed (v_{wind})	Captured Power (P_{wind})	Estimated ω_r (rad/s)	Torque (T)	Kt (v_{wind})	VDC1(volts)
4 m/s	100 W	20	2.9 Nm	0.24 Nm/A	15.4
6 m/s	250 W	25	4.2 Nm	0.35 Nm/A	29.1
8 m/s	400 W	30	5.7 Nm	0.47 Nm/A	48.2
10 m/s	500 W	35	7.1 Nm	0.59 Nm/A	71.8
12 m/s	550 W	40	8.4 Nm	0.70 Nm/A	98.7

As you can see, the VDC1 range falls between approximately 15.4 volts at 4 m/s wind speed and 98.7 volts at 12 m/s wind speed. This demonstrates how the rectified DC link voltage varies with changes in wind speed due to the influence of the torque coefficient (Kt).

To mitigate the challenges posed by the variable and intermittent output from wind power and to ensure maximum energy capture from the wind, employing a power electronic converter between the wind turbine generator and the grid/load is essential. Traditional setups involve PMSGs being linked to a three-phase diode bridge rectifier in a two-stage inverter configuration. In such arrangements, an additional boost DC/DC converter is integrated between the diode bridge rectifier and the voltage-source inverter bridge. This setup aims to normalize the fluctuating DC output voltage from the rectifier to a stable, desired voltage level.

2.5 Design of Elements of the QZSI Converter

The sizing of the quasi-Z source inverter components is determined to restrict the switching frequency of the voltage and current. The minimum component values for the impedance network, including L1, L2, C1, and C2, were derived based on the guidelines provided in (Liu et al., 2016).

2.5.1 Inductor Design

To design the inductors of the quasi-Z-source inverter, and starting from the basics of the equation of the inductance we can deduce the following equation:

$$L = V_L \times \frac{dt}{di_L} \tag{2.7}$$

And by considering that $dt = DT_s = \frac{D}{f_s}$, and $di_L \times \Delta I_L = C_r i_L\%$, where f_s is the switching frequency, D is duty cycle, and ΔI_L is the inductance current ripple.

So, ΔI_L can be considered as $C_r\%$, of the input current and C_r is current ripple coefficient(Samadian et al., 2020a). By combining the following equations during the ON state of the switches:

$$i_L = \frac{P_n}{V_{in}} \tag{2.8}$$

$$V_L = V_{in} + V_{C3} = V_{in} + \left(\frac{D_{sh}}{1 - 2D_{sh}} V_{in}\right) \tag{2.9}$$

We can deduce by combining the equation (2.7), (2.8), and (2.9) the minimum inductance L_{min}needed to be calculated using the following equation.

$$L_{min} \geq \frac{Vin * D_{sh} * (1 - D_{sh}) * Ts}{k_i * I_{in}} \tag{2.10}$$

Where V_{in} is the input voltage (ranging from 20 V to 80 V in our case), D_{sh} is the duty cycle of the shoot-through cycle, Ts the switching period (1/fs = 1/5 kHz = 200 µs), k_i is the current ripple coefficient (0.2 for 20%), and I_{in} is the input current (varies with V_{in} due to power limitation: $P_n = V_{in} * I_{in}$).

As we talk about the Boost factor in the literature review is equal to $\frac{1}{1-2D_{sh}}$. So, if we need to achieve an output voltage = 100V, the Duty cycle of the shoot through will be equal to 0.4.
Minimum Inductance (for Vi = 20 V and supposing the duty cycle =0.4):

$$I_{in} = \frac{P_n}{V_{in}} = \frac{500}{20} = 25\ A \tag{2.11}$$

Then we will get:

$$L_{min} \geq \frac{20\ V * 0.4 * (1 - 0.4) * 200\ \mu s}{0.2 * 25\ A} \approx 0.19\ mH \tag{2.12}$$

2.5.2 Capacitance Design

Starting from the principal equation of the capacitance:

$$C = i_c \frac{dt}{dV_c} \tag{2.13}$$

And taking into consideration that $dt = DT_s = \frac{D}{f_s}$, and $dV_c = \Delta V_c = 2\% V_c$, where ΔV_C is the capacitor voltage ripple and it is considered as 2% of the voltage across capacitors(Samadian et al., 2020a). By combining the following equations during the ON state of the switches:

$$I_{C1} = I_{DC} - I_{L1} \tag{2.14}$$

$$I_{C1} = \frac{P_n(1 - 2D_{sh})}{V_{in}} - \frac{P_n}{V_{in}} \tag{2.15}$$

By combining the equations (2.13), (2.14), and (2.15) the minimum capacitance C_{min} needed to be calculated using the following equation.

$$C_{min} \geq \frac{D_{sh} * T_s}{\Delta Vc * (1 - D_{sh}) * Vc} \tag{2.16}$$

where: D_{sh} is the shoot-through duty cycle, T_s is the switching period (200 µs), ΔVc is the capacitor voltage ripple (0.02 * Vdc = 0.02 * 100 V = 2 V)
Vc is the voltage across each capacitor (assumed to be half the DC link voltage: (Vc ≈ Vdc / 2).

$$Vc \approx 100\,V / 2 = 50\,V \tag{2.17}$$

$$C_{min} \geq \frac{0.2 * 200\,\mu s}{0.02 * (1 - 0.2)50\,V} \approx 200\,\mu F \tag{2.18}$$

Since the input voltage (V_{in}) varies, the minimum inductance needed (L_{min}) will also change based on the operating voltage and the resulting input current (I_{in}). We will need to consider this variation for inductor selection. This can be done by selecting an inductor with a value greater than the worst-case the L_{min} (lowest V_{in} leads to highest I_{in}).

2.6 Design of the Output Inverter Filter and Load

2.6.1 Design the LC Output Filter Design

Designing an LC filter requires considering the switching frequency ($f_s = 5kHz$) of our qZSI and the desired cut-off frequency (f_c) where we want to significant attenuate the switching harmonics. By assuming that we have a resistive load only and an output voltage =110V-120V, and we need to estimate the cut-off frequency by

$$f_c = \frac{f_s}{15} = \frac{5000}{15} \approx 333.33 \text{ Hz.} \tag{2.19}$$

2.6.2 Inductance (L_f)

We need the DC link voltage (V_{DC}) of our QZSI system for this calculation. Let's assume a sample DC link voltage (V_{DC}) for illustration:

For example, supposing the DC Link Voltage (V_{DC}): 110 V.

$$L_f \approx \frac{(V_{DC}^2)}{f_c * P_{load}} \approx \frac{(110)^2}{333.33\ Hz * 500\ W} \approx 7.2\ mH \quad (2.20)$$

2.6.3 Load Impedance (Z_{load})

Since we're assuming a resistive load, the impedance (Z_{load}) is simply the load resistance (R_{load}) which can be calculated using the voltage and assuming a specific power rating (P_{load}). Let's choose a sample power rating for illustration, for example by taking the load Power (P_{load}): 500 W.

2.6.4 Resistance (R_{load})

$$R_{load} = \frac{V_{load}^2}{P_{load}} = \frac{120^2}{500} = 28.8\ \Omega \quad (2.21)$$

2.6.5 Capacitance (C_f)

$$C_f \approx \frac{1}{2 * pi * f_c * Z_{load}} \approx \frac{1}{2 * pi * 333.33\ Hz * 28.8\ \Omega} \approx 15\ \mu F \quad (2.22)$$

CHAPTER 3

CONTROL ALGORITHM DESIGNFOR THE PROPOSED CONFIGURATIONBASED ON QZSI

3.1 Introduction

The advanced control strategy for the QZSI connected with battery and based on SWECS is designed to meet the following key objectives:

1. Optimize the maximum wind power capture through the variable regulation of the wind turbine generator's velocity.

2. Sustain a steady state of both amplitude and frequency for the output voltage, ensuring a consistent and stable power supply to the stand-alone AC load.

3. Add battery management control to control and protect the battery performance, ensuring efficient energy storage and supply during variable wind conditions.

To achieve these goals, introducing a dynamic and coordinated control approach for SWECS is essential for the effective distribution of active power across various system components under different operational scenarios. These scenarios include periods of over-generation and under-generation, as well as emergency conditions that necessitate a control system-induced shutdown of the SWECS. It is crucial to continuously monitor the state of charge (SoC) of the energy storage system due to its variability.

3.2 Control of the DC Side

3.2.1 Control Duty Cycle of the Shoot-through

To control the duty cycle of the shoot through, we start from the principal shoot through for a single-phase inverter, we can start from the definition of the shoot through state, where one leg of the inverter is turned on, to generate this state, we will add this states to the traditional voltage inverter states, which are the active and zero states, (V_p and V_n) two reference voltages must be added to usual signals. If the triangle wave is greater than V_p or if the triangle wave is lower V_n, these comparison with the reference voltage create an additional state by an OR gate with the signal of the traditional inverter signals, we can show this in the figure below.

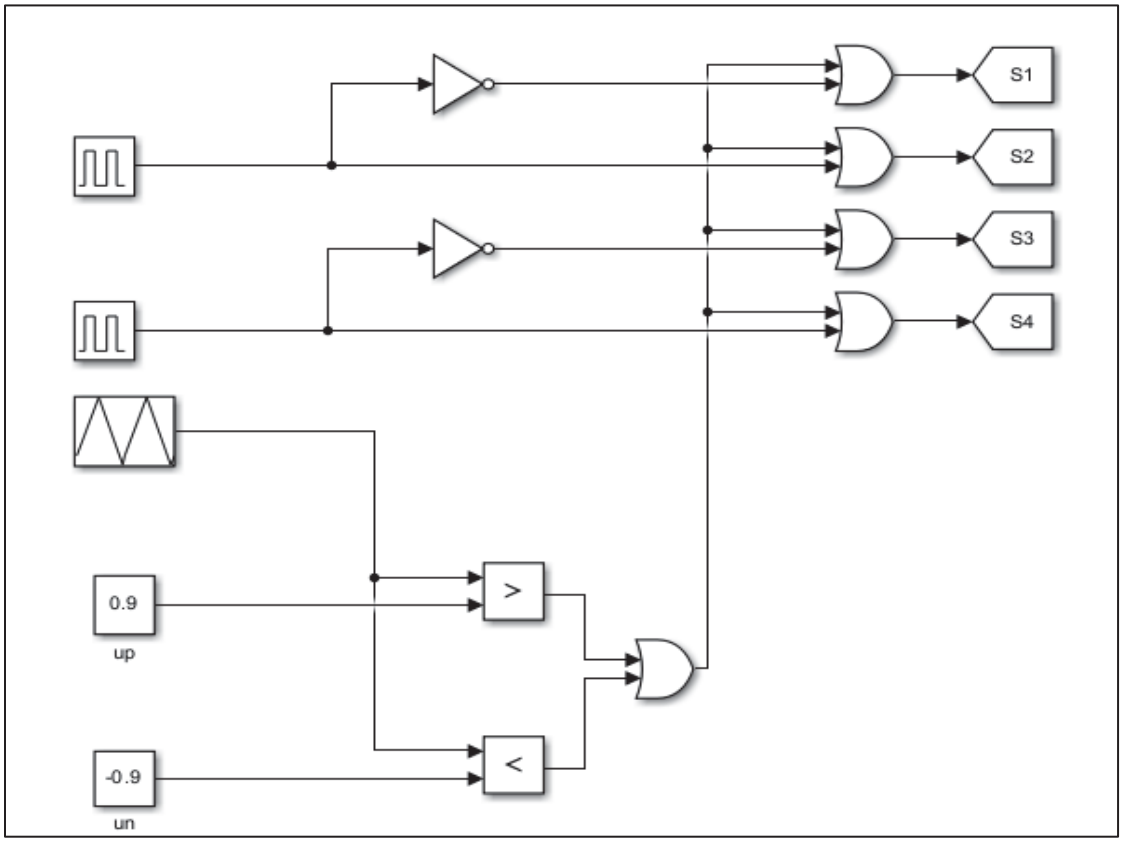

Figure 3.1 Creating the shoot through state

The shoot-through conditions occur must occur during the zero states of the full-bridge inverter.

Going to our control in controlling the duty cycle and in addition to the mathematical model that discussed in the literature review and based on the equations 1.21 and 1.23. We can estimate the duty cycle we need to calculate the voltage of the V_{C2} and from the equations of the shoot through state we have that:

$$V_{in} = V_{C2} + V_{L1} + V_D \tag{3.1}$$

So,

$$V_{C2} = V_{in} - V_D - V_{L1} \tag{3.2}$$

And because we have a wind turbine, and we need to get the maximum voltage of the wind turbine, so we can substitute the V_{in} with the V_{mpp} extracted from the MPPT were discussed in the literature review.

The figure 3.2 shows the control proposed to the duty cycle of the shoot through, where the calculated V_{DC} compared to a reference voltage, a PI controller is added to the error of the difference between the calculated and the reference.

The reason why we didn't put directly is due to the state itself it's hard to regulate a voltage is going between 0 and V_{DC}, with the using the measured V_{DC} we can regulate the V_{DC} at the output of the quasi-Z source network.

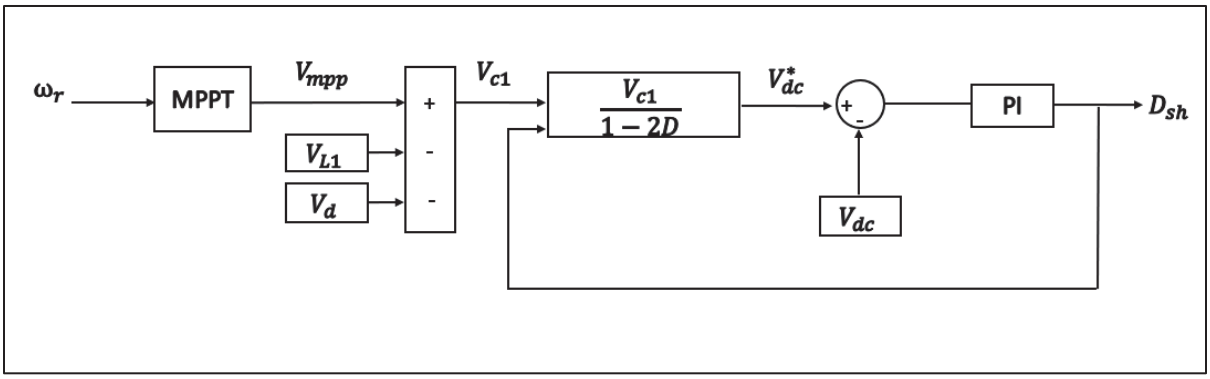

Figure 3.2 Controlling the Duty cycle of the shoot through

3.2.2 Battery Management and Protection

For using a controller for the desired optimum design there is many objectives that the controller can achieve, the principal objective of the controller is to preserve the voltage amplitude and frequency at the output of the design, and in order to include the optimal working of a wind turbine it's important to perform the maximum wind energy captured by the wind turbine even at low-speed wind turbine (maximum power point tracking). We must focus to control the active power that is found in different components with different modes including over and under generation of our design to realize the main objective, so for the over generation we can describe it by the following equation.

$$P_w = P_L + P_b \tag{3.3}$$

And for the under generation, it can be described it by

$$P_w + P_b = P_L \tag{3.4}$$

Where P_w is the output power of the wind turbine, P_L is the power of the load, and the P_b is the power of the battery.

When the wind velocity is between the cut-in speed and cut-out speed, and the power output of the wind turbine P_w is larger than the power of the load P_L the extra power will charge the

battery. The state of charge should be uninterrupted, and limited between the minimum of the state of charge and the maximum ($SoC_{min} \leq SoC \leq SoC_{max}$), when the surplus of the generation ($P_w - P_L$) is more than the SOC_{max}, the charge of the battery will stop.

And for the under-generation of wind turbine, where the power generation of the wind turbine P_w is less than the load demand P_L, the battery will consume energy into the load, and it starts in the mode of discharging. When the state of charge of the battery is less than SOC_{min} the battery will stop discharging to the load, and load will be disconnected from the wind turbine by using this control system (Liu, Ge, Abu-Rub, & Peng, 2014).

For the DC side controller, it will exceed the control of the power output of the wind turbine, it will organize the shootout through duty cycle and the battery management (as we discussed above).

Through a proportional coefficient $P = \frac{1}{VOC}$, the battery current reference is produced by the power reference of the battery Pb*.

While this control strategy is effective under normal operating conditions, it presents a significant issue when V_{oc} approaches zero, as the gain P tends towards infinity. This could lead to instability in the control system, resulting in erratic behavior or even failure of the power converter.

To mitigate this risk, an improved control strategy is proposed by introducing a conditional limit on the proportional coefficient P. Specifically, the control algorithm can be enhanced by implementing a threshold value V_{ocmin}, below which the proportional coefficient is capped at a maximum safe value. This prevents P from becoming excessively large when V_{oc} is low.

The Condition: If $\boldsymbol{V_{oc} < V_{ocmin}}$, then set $\boldsymbol{P = \frac{1}{V_{ocmin}}}$.

Pb* is based on the system power balance $P_b^* = P_{out}^* - P_{in}$

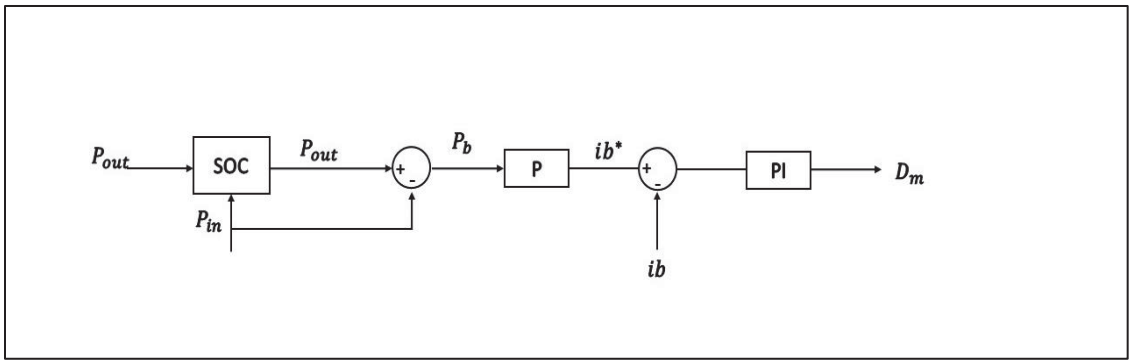

Figure 3.3 Block diagram of battery management

The three power sources are:

$$P_w + P_b = P_L \tag{3.5}$$

$$P_{in} = V_{in} \times I_{DC} \tag{3.6}$$

$$P_b = V_b I_b \tag{3.7}$$

$$P_{out} = V_{DC} I_{DC} = (1 - D) V_{DC} I_{DC} \tag{3.8}$$

We have from calculation before that:

$$\widehat{U}_{DC} = \frac{1}{1 - 2D_{sh}} V_{DC} \tag{3.9}$$

So, we can perform the output power as:

$$P_{out} = \frac{1 - D_{sh}}{1 - 2D_{sh}} V_{DC} I_{DC} \quad (3.10)$$

The third power will be determined if we control two of the powers of the three. The wind turbine is controlled to extract the maximum power, the status of the operating battery is based on the output power, and we can classify it for three cases:

1) the first case: $P_{in} = P_{out}$, then $P_b = 0$, all the power generated by the wind turbine is consumed by the residential load.

2) $P_{in} > P_{out}$, $P_b < 0$, the battery absorbs the excess power generated by wind turbine.

3) $P_{in} < P_{out}$, $P_b > 0$, all the power generated goes to the load and the battery also give energy to make equilibrium with the demand.

   The status of the battery operating refers to the state of charging (SoC) as shown in figure 3.4.

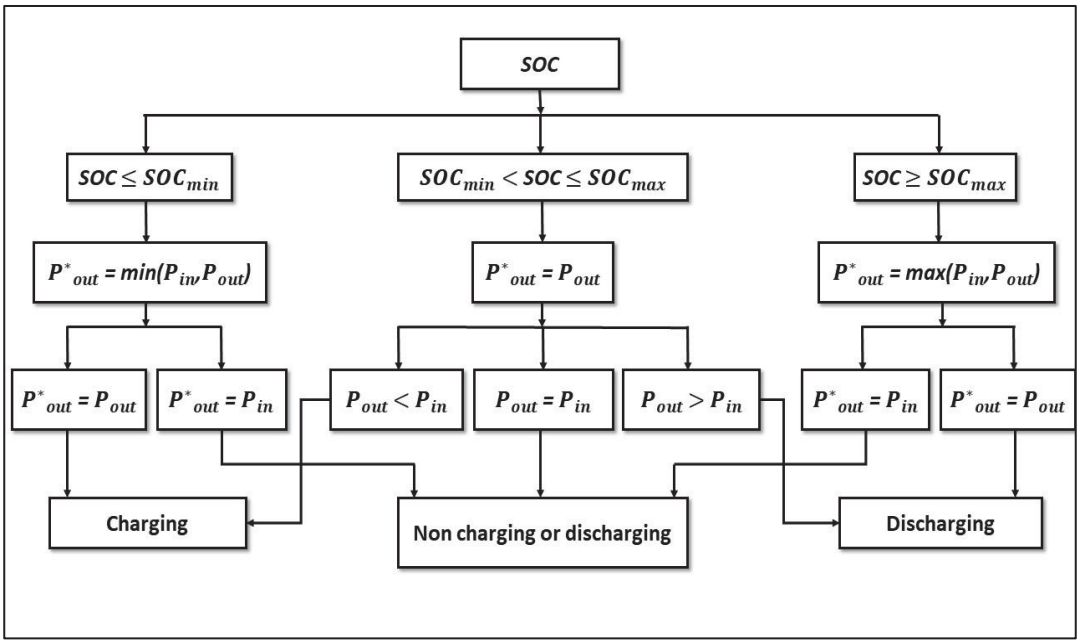

Figure 3.4 Flowchart for sate of charge of battery management
Taken from Liu, Ge, Abu-Rub, et al (2014)

For the battery we have two variables, the minimum state of charge (SoC_{min}) which is the lower limit of the SoC, and the maximum state of charge (SoC_{max}) which is the maximum limit of the SoC.

1. If the state of charge (SoC) is less than of the minimum state of charge (SoC_{min}), $SoC < SoC_{min}$, in this case the battery will no longer discharge, and P^*_{out} is equals to the minimum between the P_{in} and P_{out}. So if the P_{in} is less than P_{out}, the reference output power $P^*_{out} = P_{in}$, and $P^*_b = P_{in} - P_{in} = 0$, and the battery will operate in the no charging state or the no discharging state, while if the P_{out} is smaller than P_{in}, the reference output power will equal to output power $P^*_{out} = P_{out}$, $P^*_b = P_{out} - P_{in} < 0$, the excess of the input power of the wind turbine goes for charging the battery.

2. If the SoC of the battery is exceed the maximum of SoC ($SoC > SoC_{max}$) the battery must not be charged more and the output power reference will be more than the P_{in} and P_{out} if the P_{in} is more than P_{out}, the reference output power $P^*_{out} = P_{in}$, and

$P_b^* = P_{in} - P_{in} = 0$, and the battery will operate in the no charging state nor the no discharging state, while if the P_{out} is greater than P_{in}, the reference output power will equal to output when power $P_{out}^* = P_{out}$, $P_b^* = P_{out} - P_{in} > 0$, the battery will be in the mode of discharging.

3. If the SoC is between SoC_{min} and SoC_{max} ($SoC_{min} < SoC < SoC_{max}$), the battery in this case will charge or discharge, and P_{out}^* is equal to P_{out}, then $P_b^* = P_{out} - P_{in}$. If the input power of wind turbine is in excess, the battery will go in the charging mode. On other hand when it's in less the battery will be in discharge mode(Liu, Ge, Abu-Rub, et al., 2014).

3.2.3 MPPT Control Algorithm for the Wind Turbine

Extracting the maximum power point tracking (MPPT) of a variable speed wind turbine is to get the maximum power at the output during the variation of the wind turbine. To know the maximum power tracking controller, we must go in deep to know the mechanical power generated by the wind turbine:

$$P_{mec} = T_{mec}\omega_r \tag{3.11}$$

Where the ω_r is the angular velocity of the rotor of the wind turbine, and the T_{mec} is the mechanical torque. And as known that the generated power generated by the generator it can be written as:

$$P_{elec} = V \times I \tag{3.12}$$

By considering there's no losses we get:

$$P_{mec} = P_{elec} \rightarrow T_{mec}\omega_r = V \times I \tag{3.13}$$

We also have the electrical and motion equation as known as:

$$T_{elec} = KI \times I_f \tag{3.14}$$

$$I = \frac{V - E_a}{R_a} \tag{3.15}$$

$$E_a = K\omega_e \times I \tag{3.16}$$

Where $\omega_e = p\omega_r$ where p is the number of poles of the generator. To get the maximum power we can derive the electrical power with respect to the dc voltage is equal to zero:

$$\frac{dP_e}{dV_{dc}} = 0 \tag{3.17}$$

By taken in consideration the characteristics of a wind turbine we can notice to extract the maximum power from the wind turbine we must derive the mechanical power with respect to the rotor speed as the following equation:

$$\frac{dP_{mec}}{d\omega_r} = 0 \tag{3.18}$$

Before starting for finding for the maximum power we must determine an inconsistent dc voltage reference we can called V_{ref}. Then the controller will measure the voltage and the current of the DC side and so we can find the electric power initial which is equal to:

$$P_{in} = V_{DC} I_{DC} \tag{3.19}$$

Then the V_{ref} is incremented by ΔV_{dc}, so we can get the following equation:

$$V_{ref}(k) = V_{ref}(k-1) + \Delta V_{dc} \tag{3.20}$$

For the DC power it can be calculated by

$$P(k) = V_{dc}(k) * I_{dc}(k) \tag{3.21}$$

After calculating the $P(k)$ and $P(k-1)$, we compare the two powers, if $P(k)$ is greater than $P(k-1)$, the level of the maximum power will not achieve yet so the reference voltage must be increased by ΔV_{dc}, and the DC power needs to be compared. This operation will repeat until reaching the maximum power (Kesraoui, Korichi, & Belkadi, 2011).And, if $P(k-1)$ is greater than the $P(k)$, then we must decrement the reference voltage by ΔV_{dc}.

To find the maximum power at different wind speed, we have four conditions:

1. If $P(k) < P(k-1)$, and $V(k) < V(k-1)$, in this case, the power is decreasing due to the low speed of the wind turbine, so the V_{ref} must be increased by ΔV_{dc}.

2. If $P(k) < P(k-1)$, and $V(k) \geq V(k-1)$, in this situation, the maximum power point is exceeded, and we must decrease the V_{ref} by ΔV_{dc}, it achieved when wind turbine is working at high speed and power is lowering.

3. If $P(k) \geq P(k-1)$, and $V(k) < V(k-1)$, in this condition the wind turbine is working on a high speed, and we must decrease V_{ref} by ΔV_{dc}.

4. If $P(k) \geq P(k-1)$, and $V(k) \geq V(k-1)$,in this case the wind turbine is processing at a low speed, we must increase ΔV_{dc} for the reference voltage (Kesraoui et al., 2011).

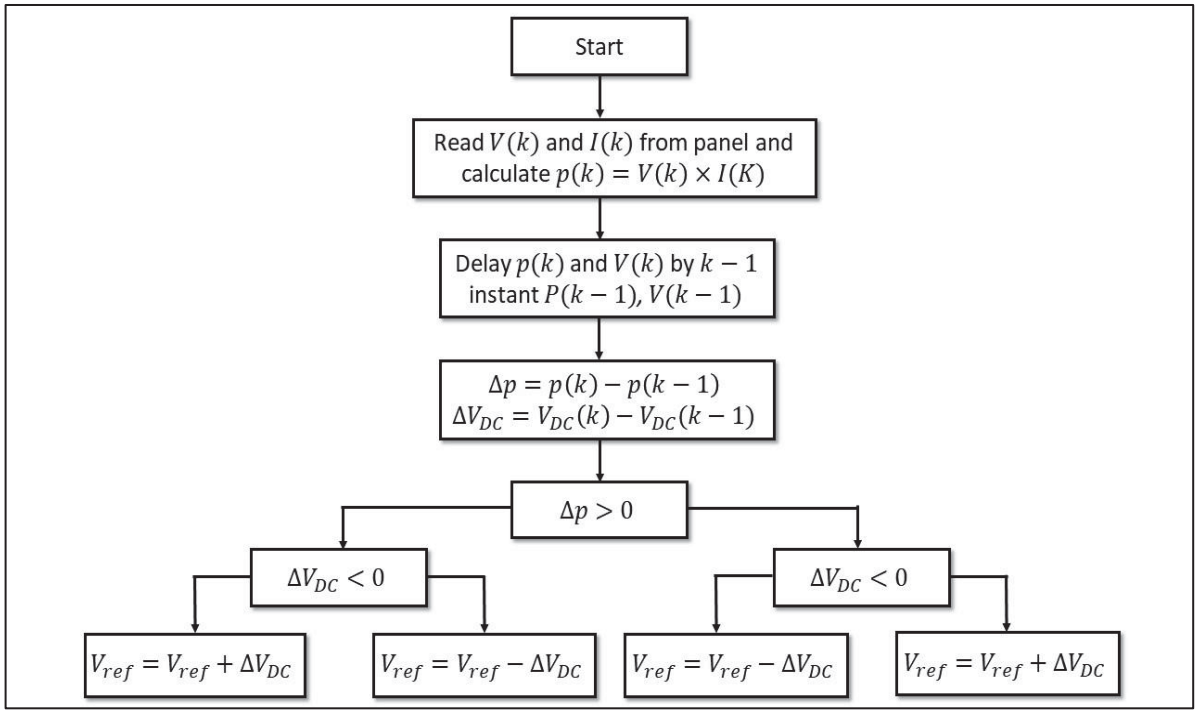

Figure 3.5 Flowchart of the MPPT

Taken from Kesraoui et al (2011)

3.3 Control Algorithm for Voltage and Frequency Regulation

Normally to control the IGBT inverter bridge a voltage reference, where it's compared by a triangle signal to activate the switches of the inverter, this is done for the open loop system, transferring to the closed loop we must control the voltage reference, by comparing a sine wave with the output voltage, and by tunning the K_p and K_i of the PI controller, the first PI controller generate the I_{cap} of the load, add the output load current to it we create I_{invref} subtract to I_{inv} we create an error with a PI controller we create V_L adding it to V_{load}, so we get a voltage reference that can be used to compared to a triangle signal of 5000 Hz , the D_{sh} is added as discussed in the control of duty cycle of the shoot through, is added to the output as seen in the figure below.

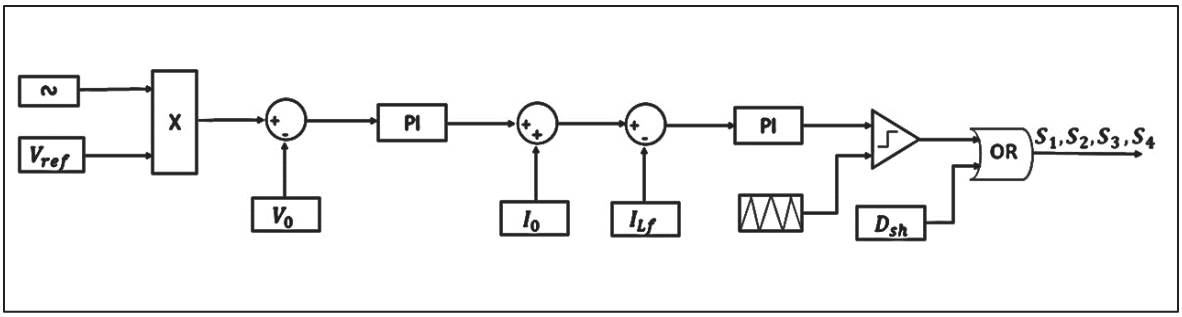

Figure 3.6 Block diagram of desired control

A study is done to control the switching of the inverter using the state vector PWM (SVPWM), but there are no results achieved by this technique, we try to work on the control of a voltage regulation and frequency regulation where I got more precise results, I attached in the annex I.

CHAPTER 4

SIMULATION AND RESULTS

4.1 Simulation

To improve the design of the quasi-Z source and to analyze our desired system and control, we use the MATLAB - Simulink software, tools like this software can create a virtual environment for a hardware module. In figure 4.1 the whole system is done, where the WT connected to the PMSG (without using a gearbox) is then connected to the QZSI then it's connected to a battery and a single-phase inverter, a LC filter and a load is connected to the inverter.

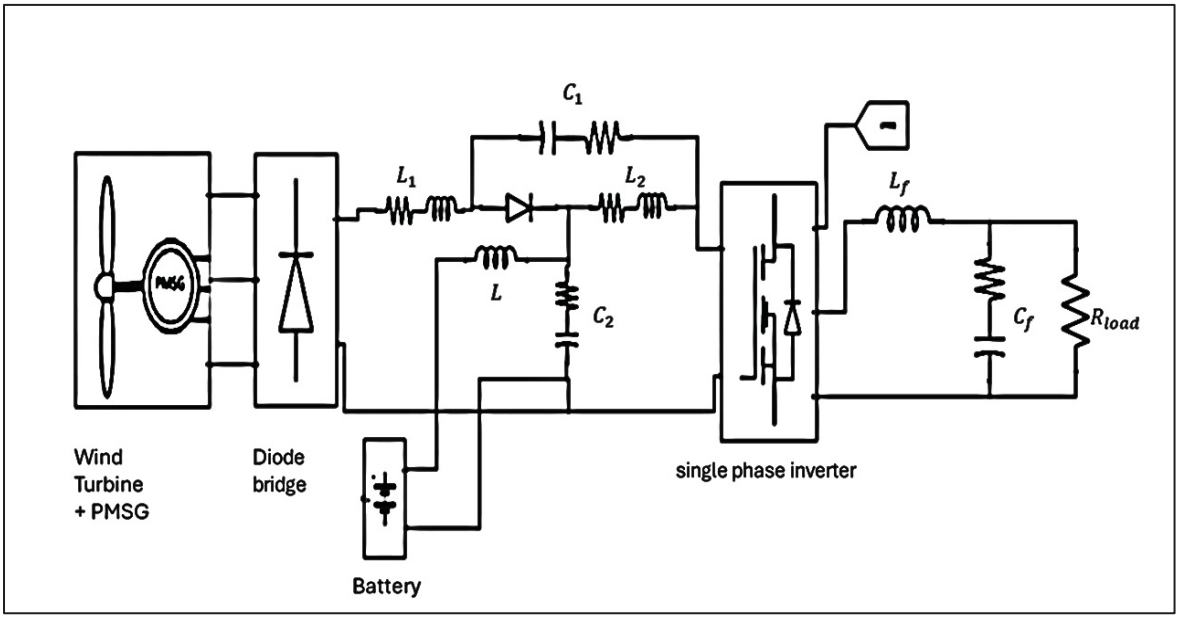

Figure 4.1 The whole system in the MATLAB Simulink

4.1.1 The Wind Module and Diode Rectifier

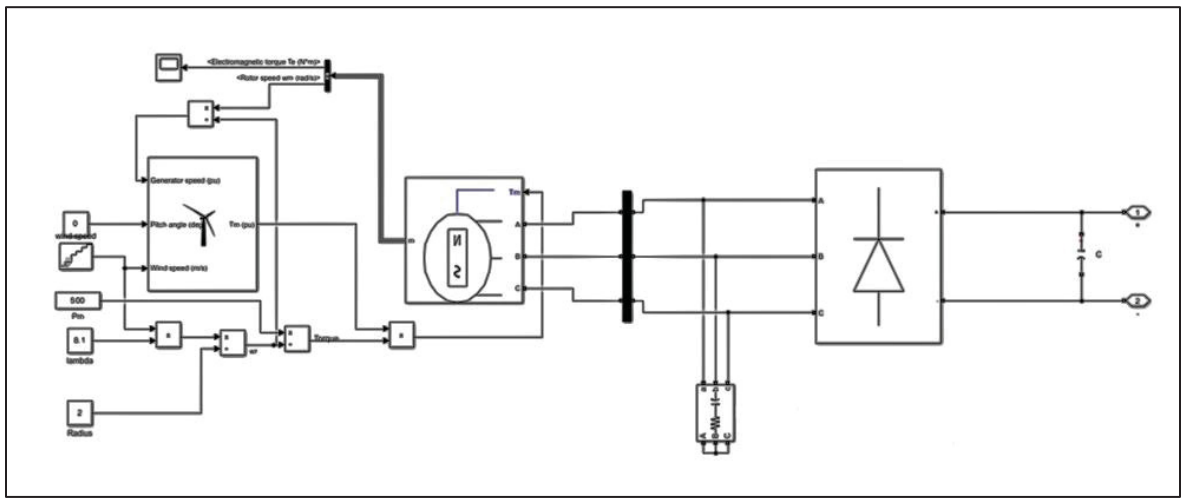

Figure 4.2 The module of the WT

In the figure 4.2 we use the wind turbine module used in MATLAB Simulink, by adjusting the needed parameters for the module to generate the needed power and the voltage, we change the speed of the wind using repeating sequence block, and by adjusting λ=8.1, the radius of the WT is 1 meter length, and with a nominal power of 500w, these parameters can estimated the torque needed to enter the PMSG, by dividing by the torque in PU of the wind turbine torque which is equal to the wind speed times λ divide by the radius , to get the actual torque which is the input of the PMSG, a small filter added after the PMSG to regulate the voltage and frequency, then a diode rectifier to transfer the AC voltage from the WT to a DC voltage.

The characteristic of the wind turbine is shown in figure 4.3, where it shows the nominal power of the wind turbine in per unit system with respect to the wind speed in per unit system and by not affecting the pitch angle and remains zero.

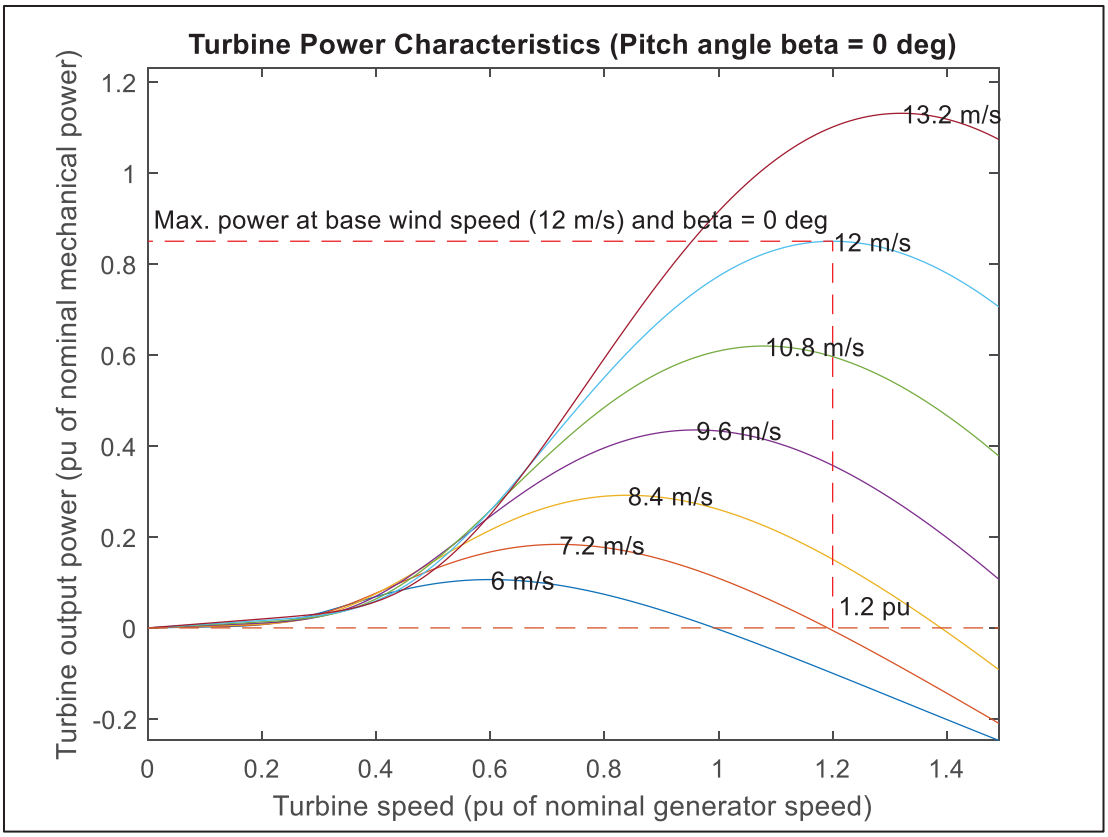

Figure 4.3 The characteristics of the power of wind turbine

4.1.2 QZSI Power Converter with Battery

A lot of quasi-Z sources are designed and are proposed and as we mentioned in the literature and the design the system used is in figure 4.4.

The parameters used for a QZSI are as follow, $L_1 = L_2 = 0.5\,mH$, $C_1 = C_2 = 200\mu F$. The battery that is connected to the C_2 is of 48V with a 50Ah, and the battery is of a lithium-ion kind and initiate to 70% of SoC.

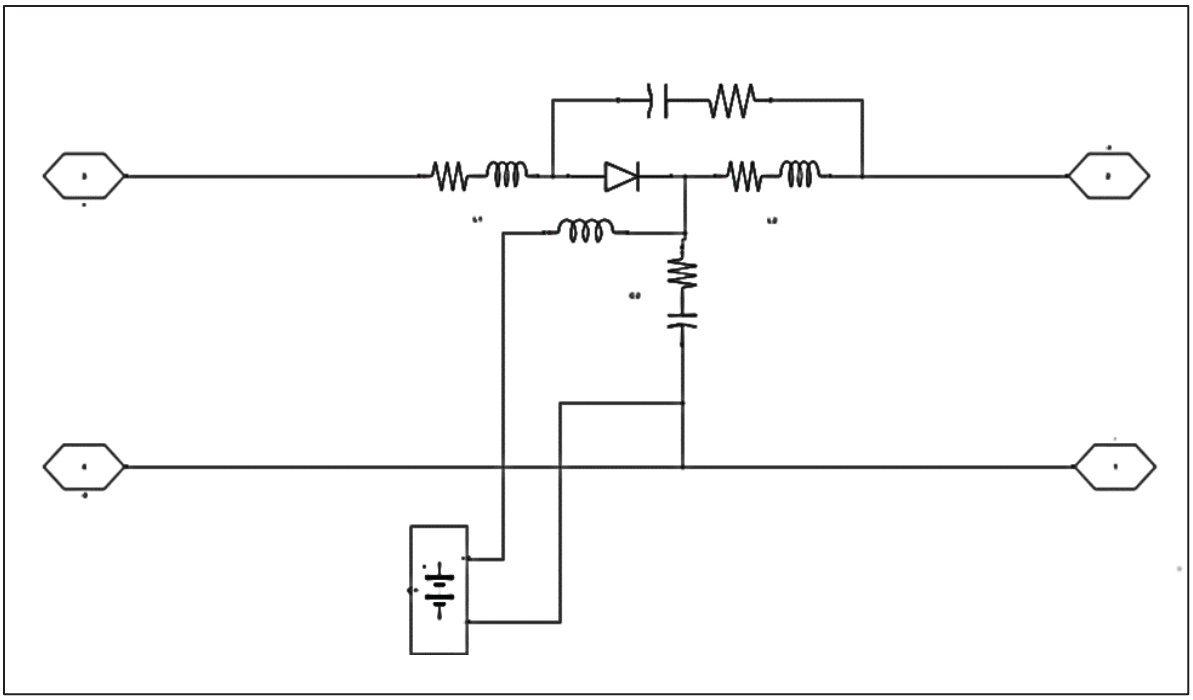

Figure 4.4 Quasi-Z source network with battery

4.1.3 Control System Proposed

The control system used in our system is illustrated in the figure 4.5, a step response is added to regulate the voltage we need, we can regulate different voltage to test the functioning of the control, the duty cycle input is generated and compared to the modulation signal, four signal switches are send to the gates of the half bridge converter

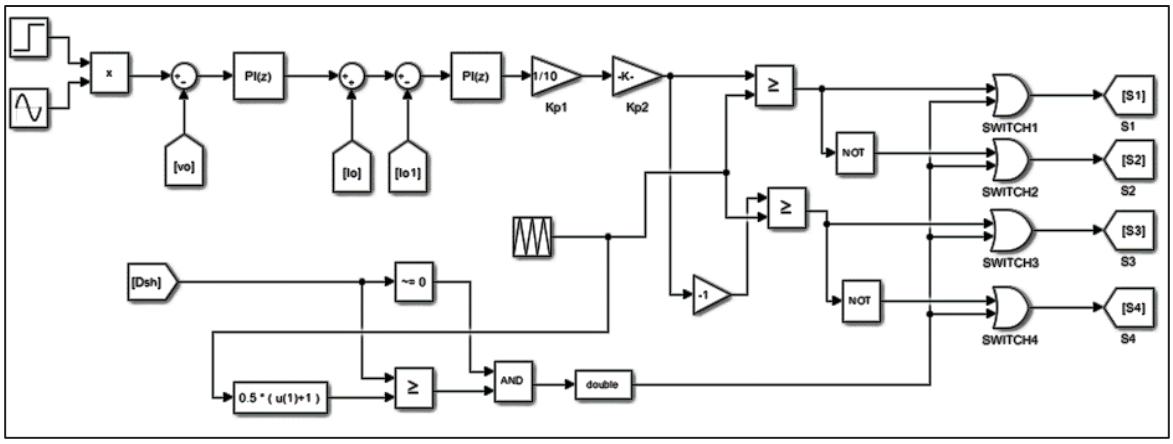

Figure 4.5 Control of the half-bridge converter

4.1.4 Calculation of Duty Cycle of the Shoot-through

As discussed in 3.2.1 the duty cycle of the shoot through is controlled by the principal equation of the duty cycle and the equations of the QZSI, where we subtract the $Vmpp$ from the V_d and V_{L1}, we get the calculated value of the V_{C2}, by using equation 1.21 we get a calculated V_{DC} its compared with the reference voltage, adding a PI control to generate the duty cycle of the shoot through. It can be shown clearly in figure 4.6.

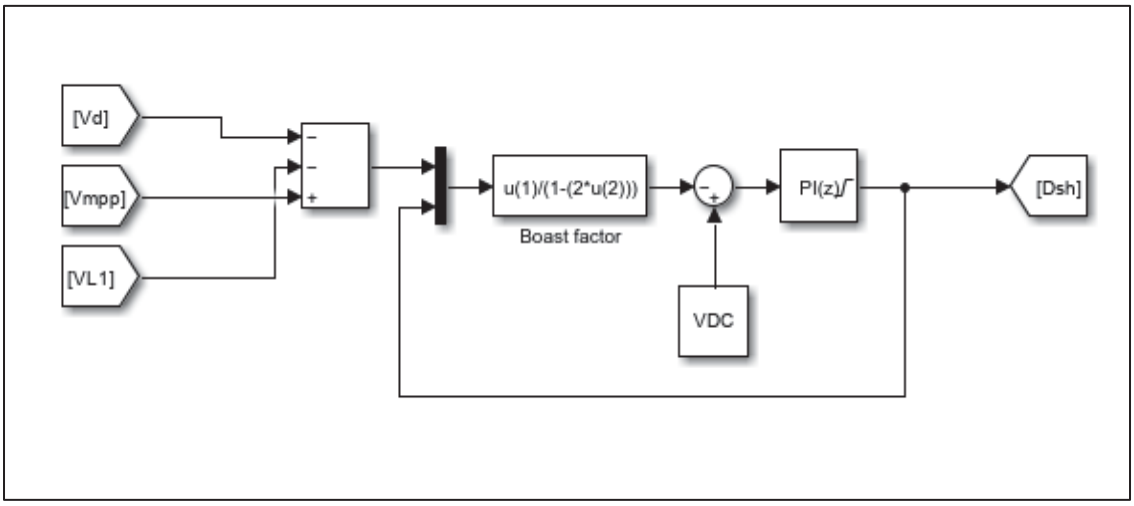

Figure 4.6 Controlling the duty cycle of the shoot through

4.1.5 The MPPT Algorithm for Wind Turbine

To simulate the MPPT algorithm for a wind turbine, the control scheme integrates both rotor speed and electrical power measurements to dynamically adjust the maximum voltage and ensure optimal power extraction. The simulation starts by measuring the optimal rotor speed, and compare it to the actual rotor speed, compared to a PI controller. The change in electrical power (ΔP) is calculated by comparing the current power to the previous measurement. The PI controller generates a control signal to adjust $Vref$, which is then used to derive the maximum power point voltage $Vmpp$. This $Vmpp$ is added to generate the duty cycle of the shoot-through electronics and to regulate the DC voltage reference, ensuring the turbine operates at its maximum power point despite varying wind conditions.

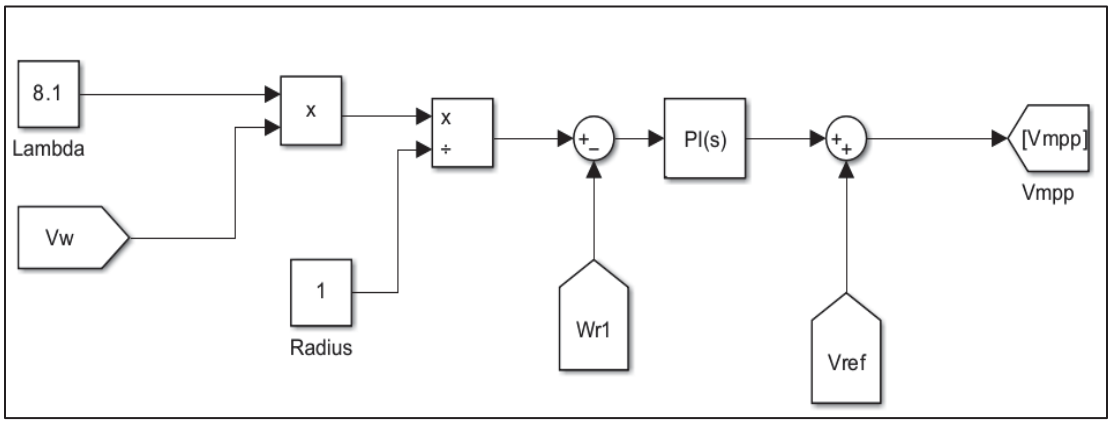

Figure 4.7 Generating Vmpp

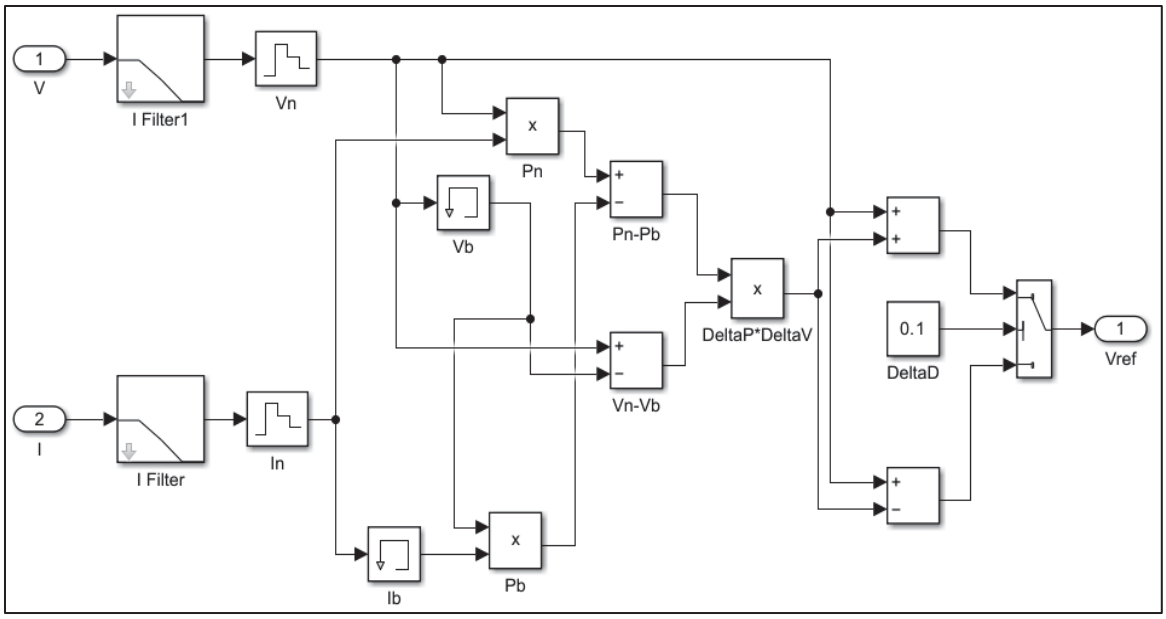

Figure 4.8 Generating Vref

4.2 Simulation Results

4.2.1 Wind turbine and PMSG Side

Starting from the WT we got the following results, figure 4.9 shows the speed of the generator ω_r, the speed is variable due to the variation of the wind done, to see the effect of the control and the system on the variation of the wind speed, the speed variation is set to zero to check the charging and discharging of the battery.

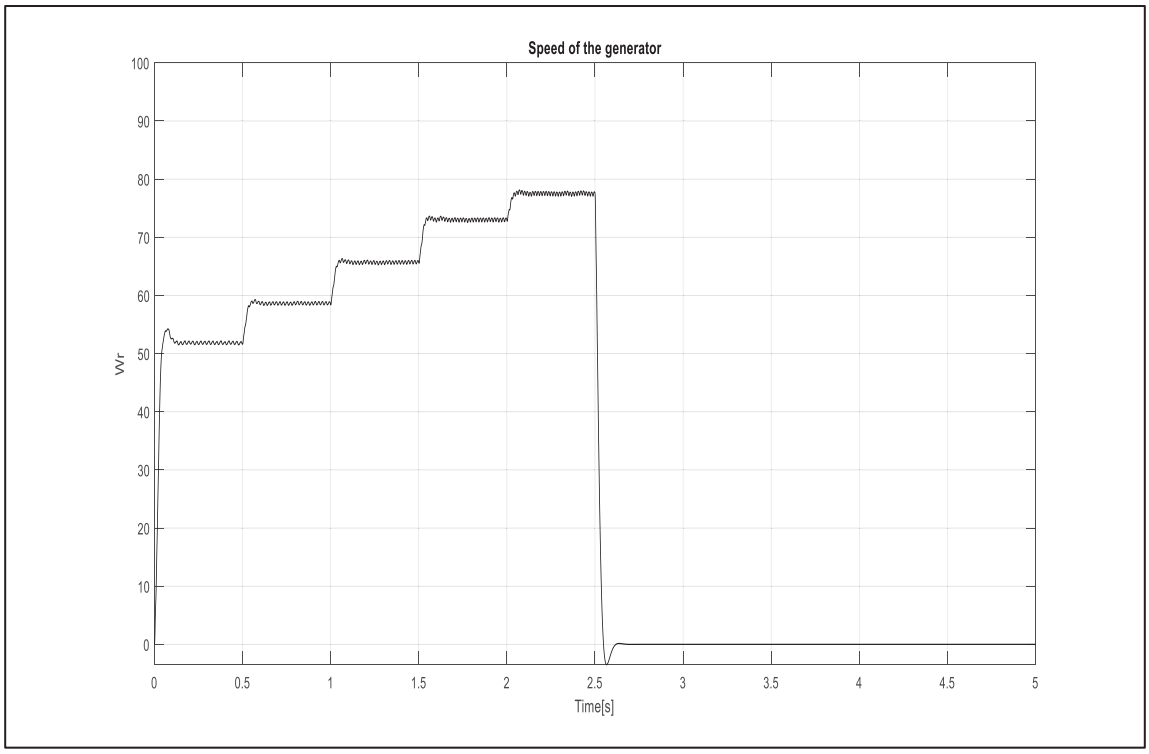

Figure 4.9 Speed of the generator ω_r

In figure 4.10 shows the output voltage of the diode rectifier that is implemented between the generator and the QZSI, also in the figure a zero voltage means that the wind turbine is no longer generating power to the system.

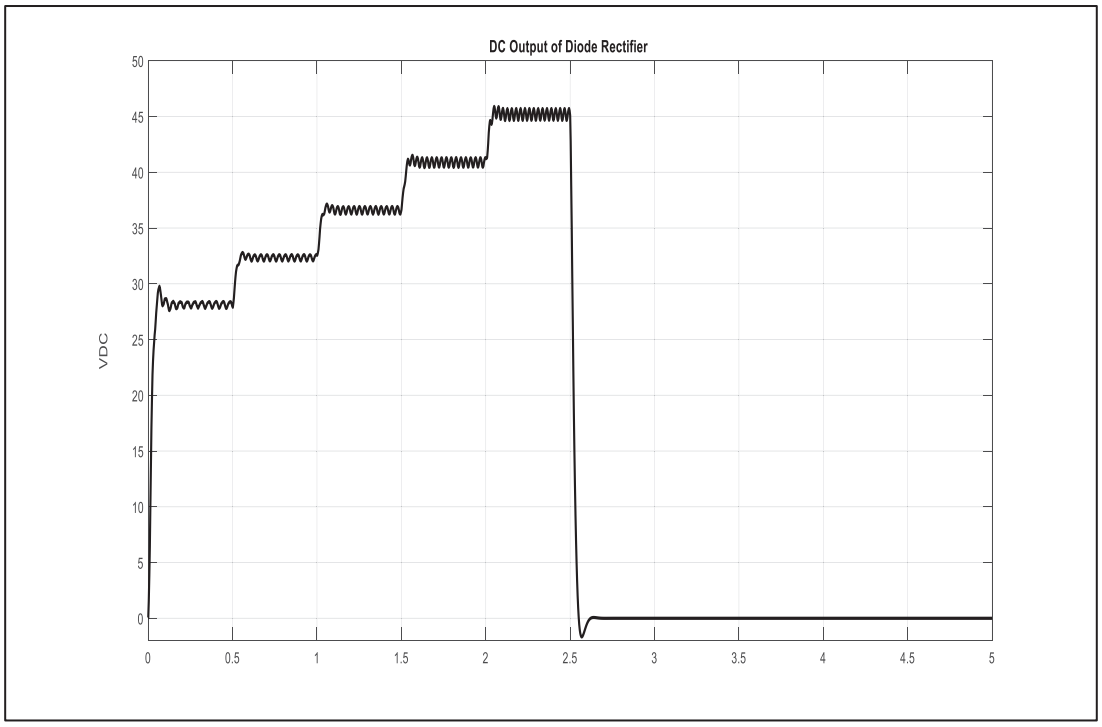

Figure 4.10 Output DC Voltage of the diode rectifier side

In figure 4.11 shows the output of the voltage and current of the stator of the generator that feed our system. In this figure, it shows the stator voltage and stator current are working during the function and variation of the wind speed, then it drops to zero when the WT is not working.

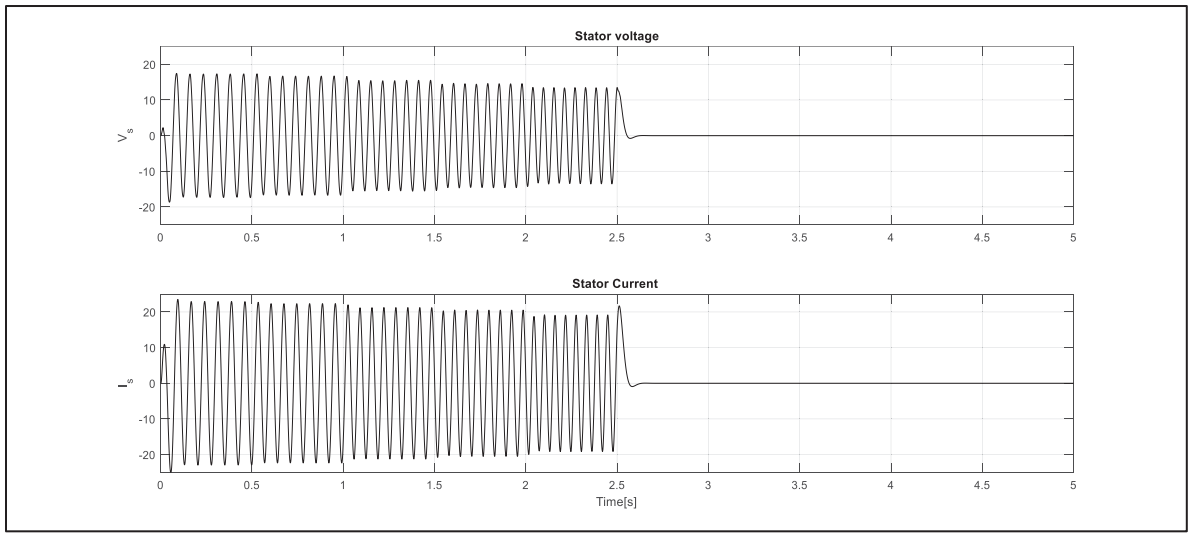

Figure 4.11 Dynamic performance of the stator voltage and current of PMSG

4.2.2 Battery Side

In the figure below, it shows the dynamic performance of the SoC of the battery, as shown in the first graph, the battery starts charging from second 0 to 2.5, during the variation speed of the variable speed generator, after 2.5 seconds the WT is dropped into zero, this means no wind energy, thus as shown the battery starts discharging.

In the second graph it shows the current of the battery, when it's charging the current of the battery in negative, meaning that is charging, while in discharging it shows a positive current of 10A of discharging current. In the last schema, the voltage of the battery shows a higher voltage than the indication of the battery, and it increases when the power of the WT increases, when the WT turned off the voltage drop to the voltage of the battery.

These figures show that the power management of the battery is working, it shows the charging state and the discharging state of the battery during the variable wind speed and during the unfunctional of the WT.

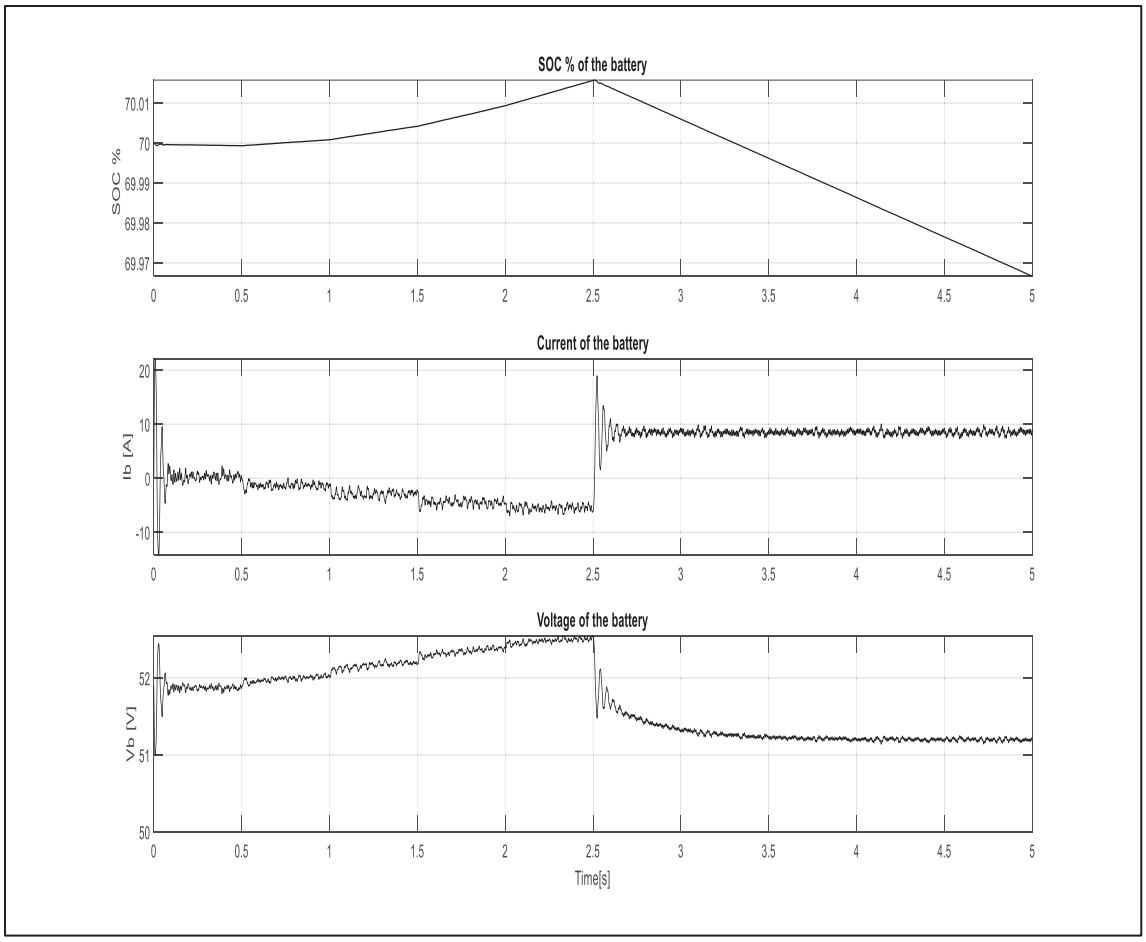

Figure 4.12 Dynamic performance of 1) SoC, 2) the current of the battery, 3) the current of the battery

4.2.3 Quasi-Z Source Converter

The three figures 4.13, 4.14, 4.15 shows the output voltage of the inverter in the first figure, and in second figure shows the V_{DC} of the QZSI. As we can see the effect of the short circuit of the switches of the inverter, and it can show clearly in figure 4.15 where the output DC voltage of QZSI is going between the reference voltage (110V) and zero. This means our proposed control is working in regulating the reference voltage we need, and it controls the duty cycle of the shoot through. As also shown, there is no variation when the wind turbine is OFF, and the battery starts discharging.

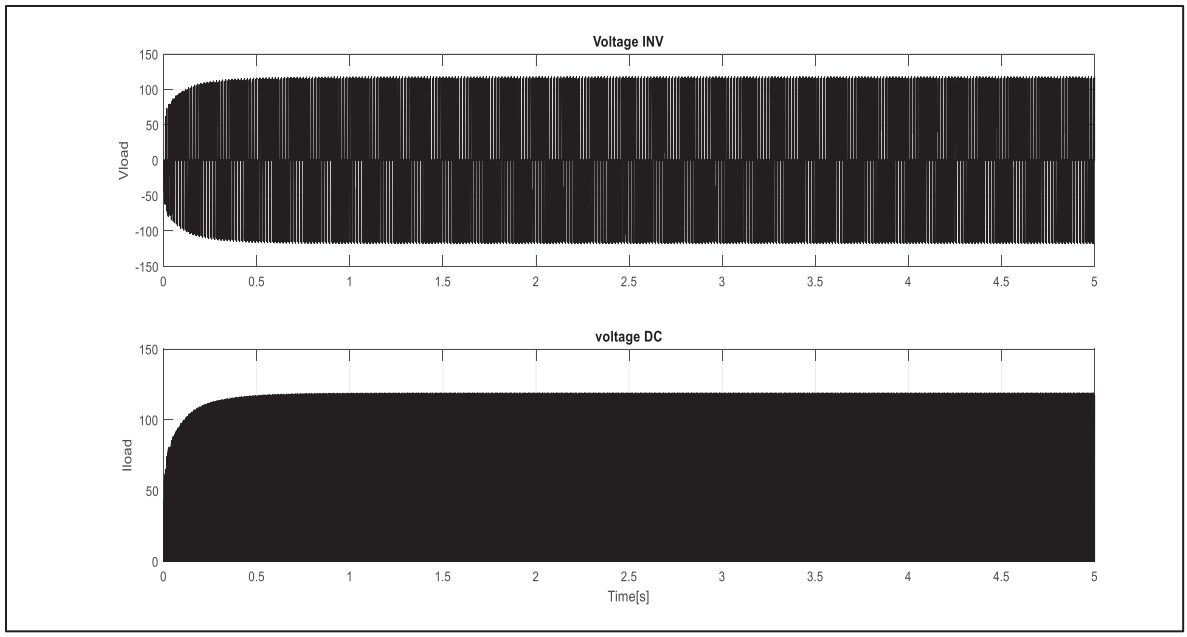

Figure 4.13 The output voltage of QZSI and Voltage Inverter

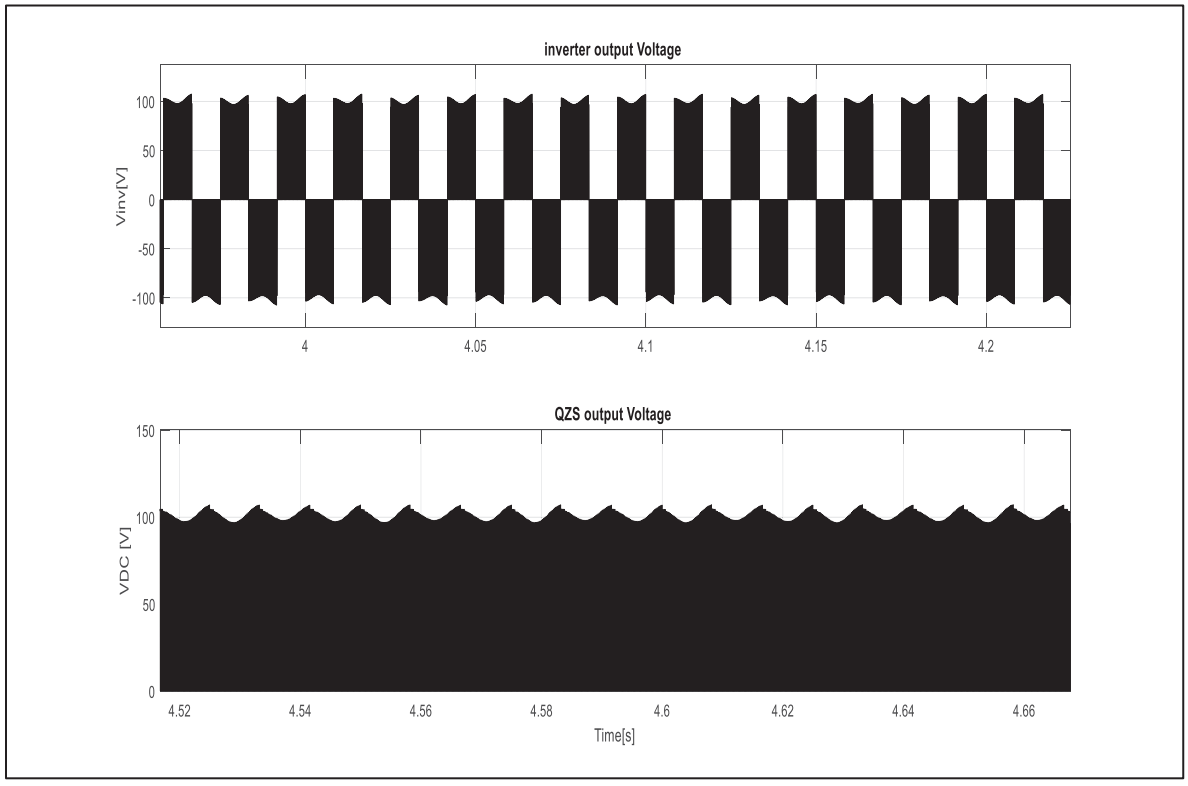

Figure 4.14 The DC voltage of quasi-Z-source and output voltage of the inverter

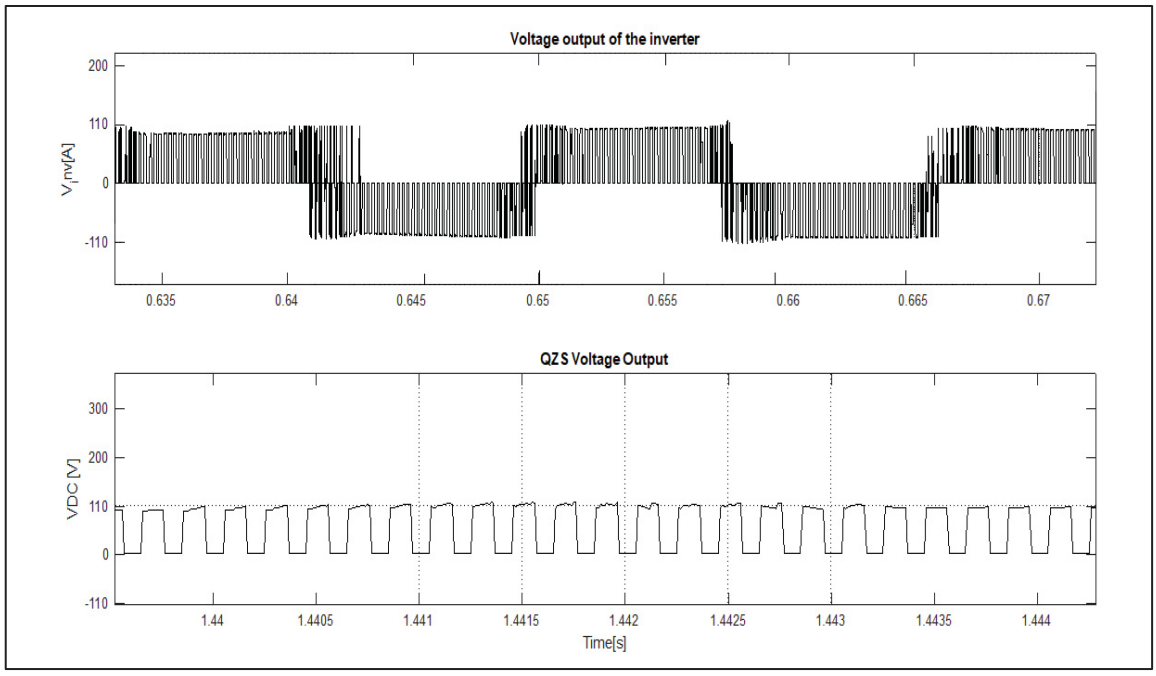

Figure 4.15 The DC voltage of quasi-Z source and output voltage of the inverter

In figure 4.16 shows the output current of the single-phase inverter and the output DC voltage of the quasi-Z source.

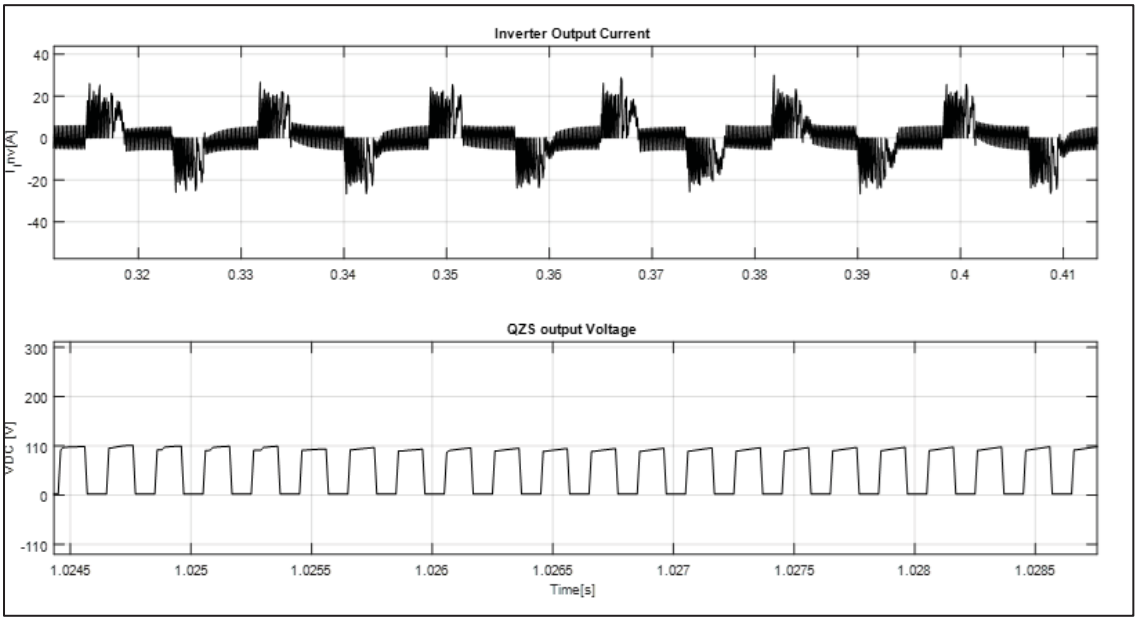

Figure 4.16 The output current of the inverter and output voltage of quasi-Z source

4.2.4 The Switches of the Single-phase Inverter

As said before about in the literature review, and the switches of the single-phase showing the shoot-through state, in 4.18 it shows clearly the shoot-through state in the simulation, where we can see the top and down switches of the inverter are turning on, we add red rectangles on the picture to show the shoot through state.

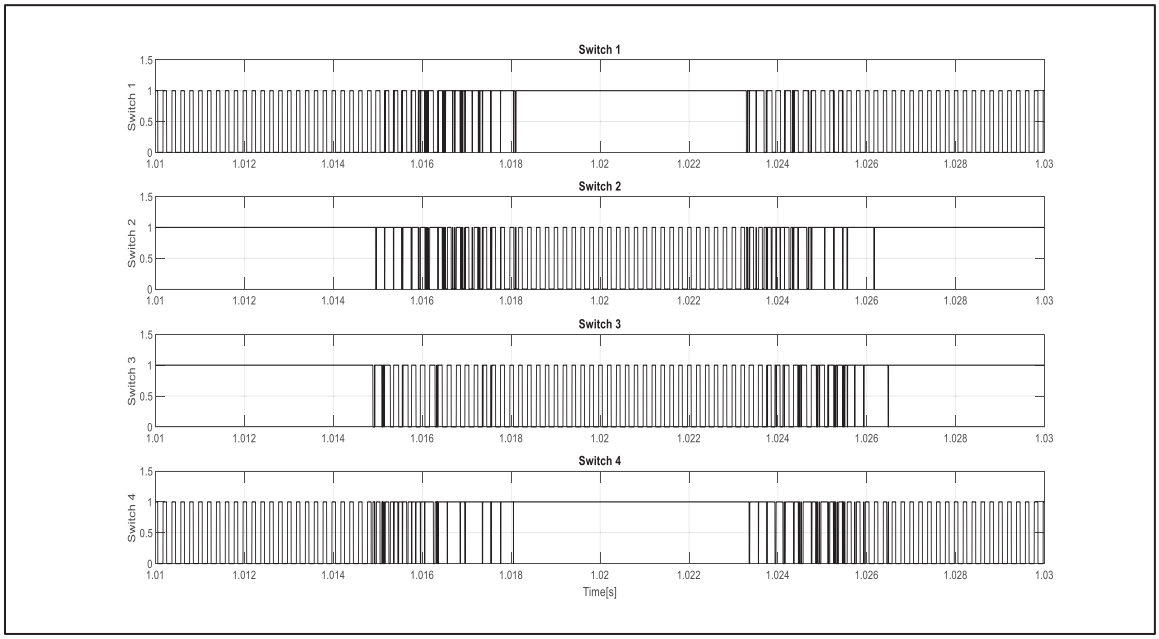

Figure 4.17 The switching of the single-phase half-bridge inverter

Figure 4.18 The switching of the shoot through state

4.2.5 The Output Voltage (V_{load}) and the Output Current (I_{load})

In figures 4.19 and 4.20, the voltage and current at the load works normally, by using the closed loop control, it has been set the voltage to 110V at the output with a frequency of 60 Hz sinusoidal wave, also we can deduce that no variation of the voltage especially with turning OFF the WT.

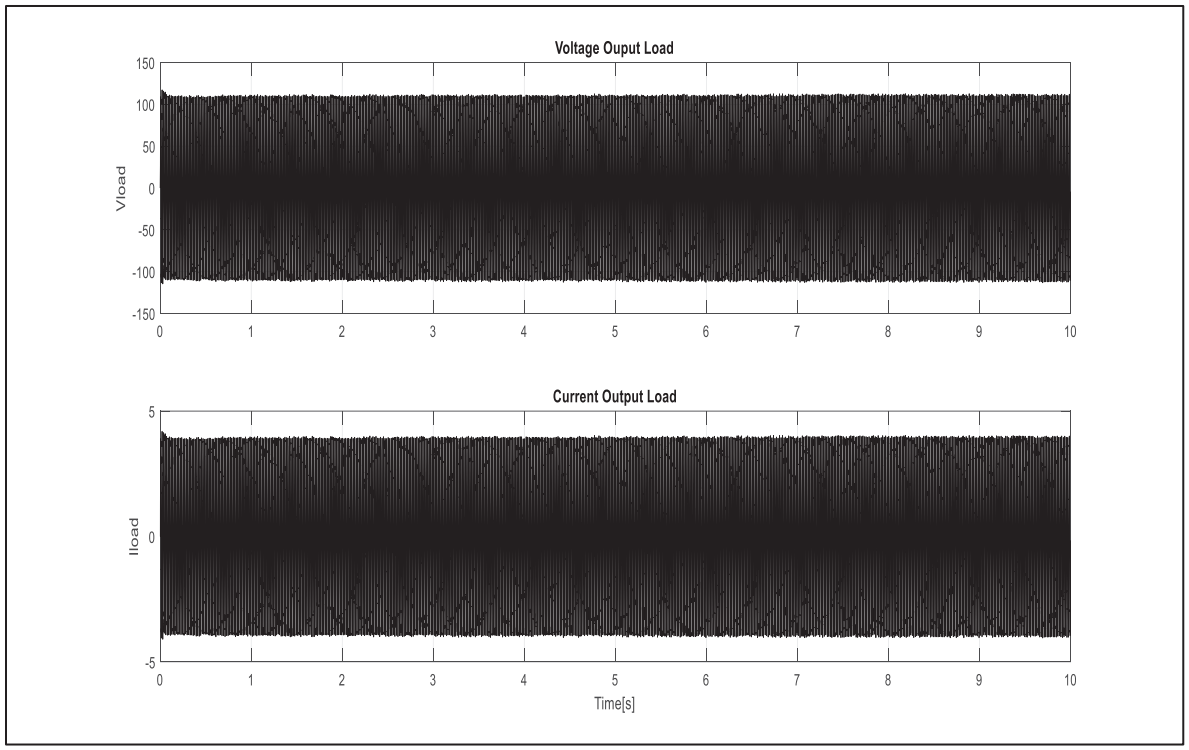

Figure 4.19 The output voltage and output current

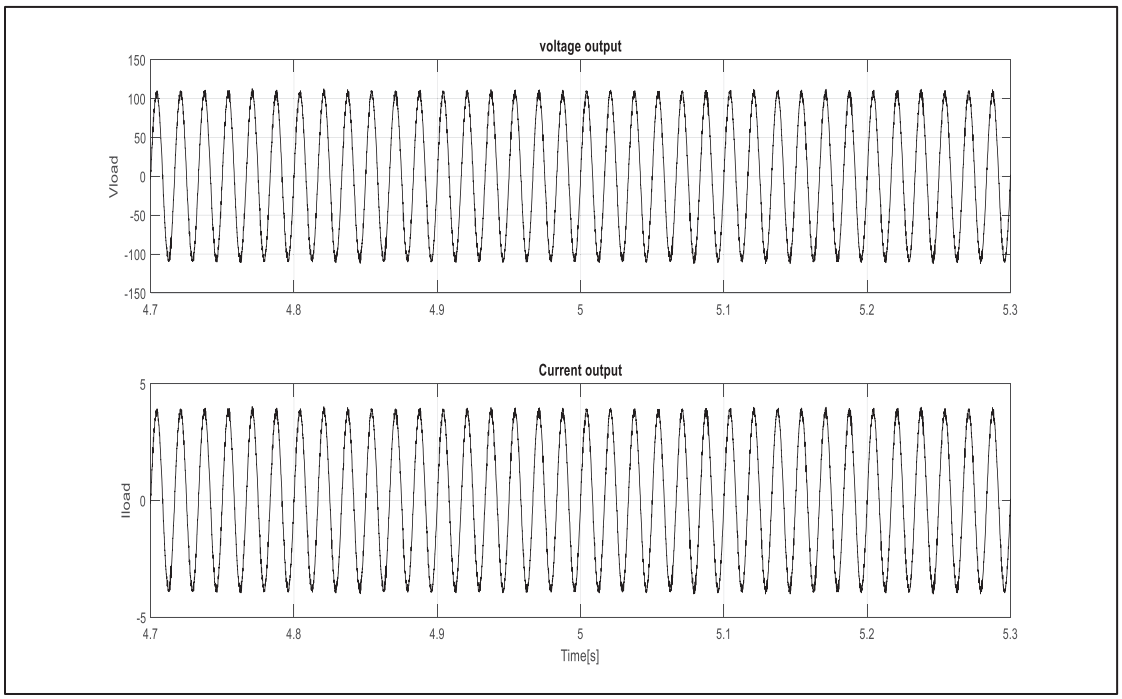

Figure 4.20 The output voltage and output current

In figures 4.21 and 4.22, the voltage and current at the load follow the voltage reference and the current reference created, we try to change the reference voltage from 90V to 110V and see if the control can change the reference voltage needed at the output, and it shows its response of the closed loop control.

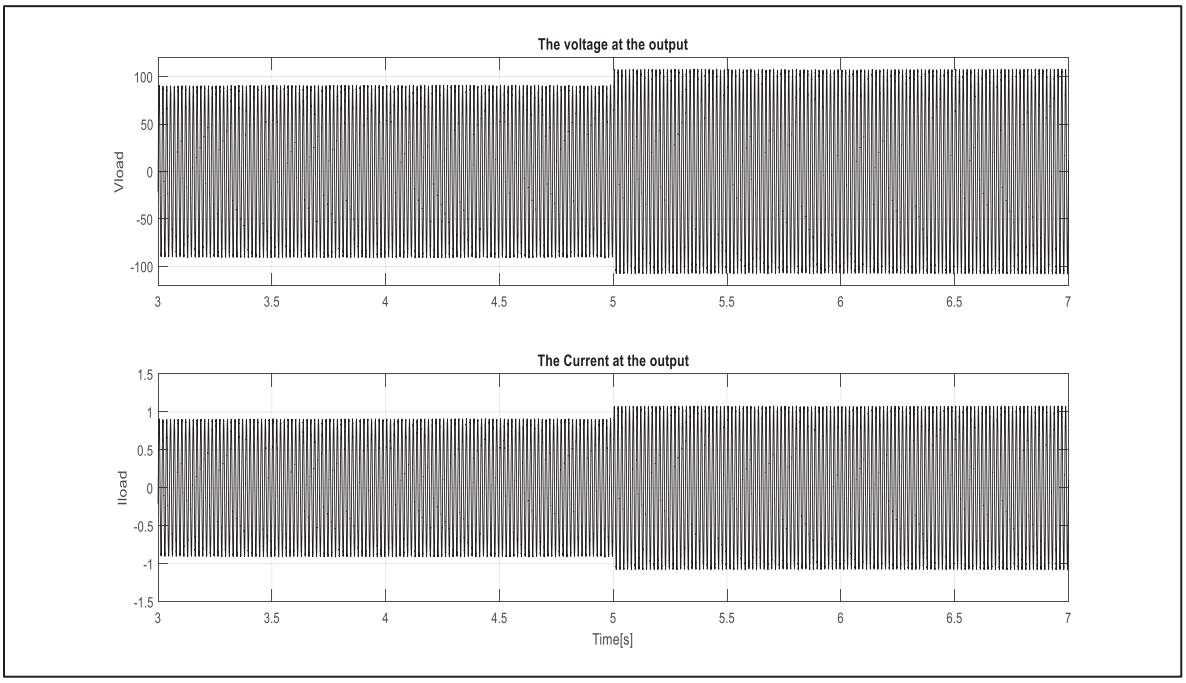

Figure 4.21 The output voltage and output current under the changing the voltage reference

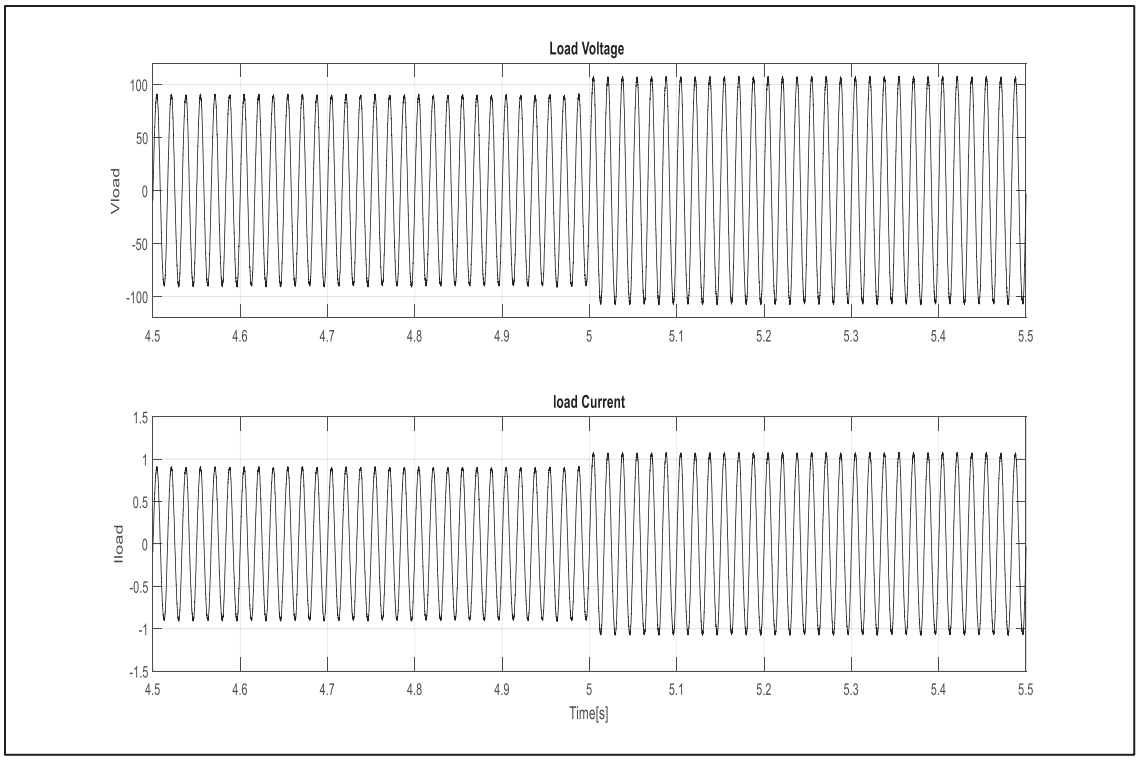

Figure 4.22 The output voltage and output current under the changing the voltage reference

In figure 4.23 and in figure 4.24, shows the voltage and current of the output of the load, when only change the load changes, the voltage remains constant at 110V, this means that the control proposed in the control section is working perfectly, and the voltage remains constant whenever the variation of the load.

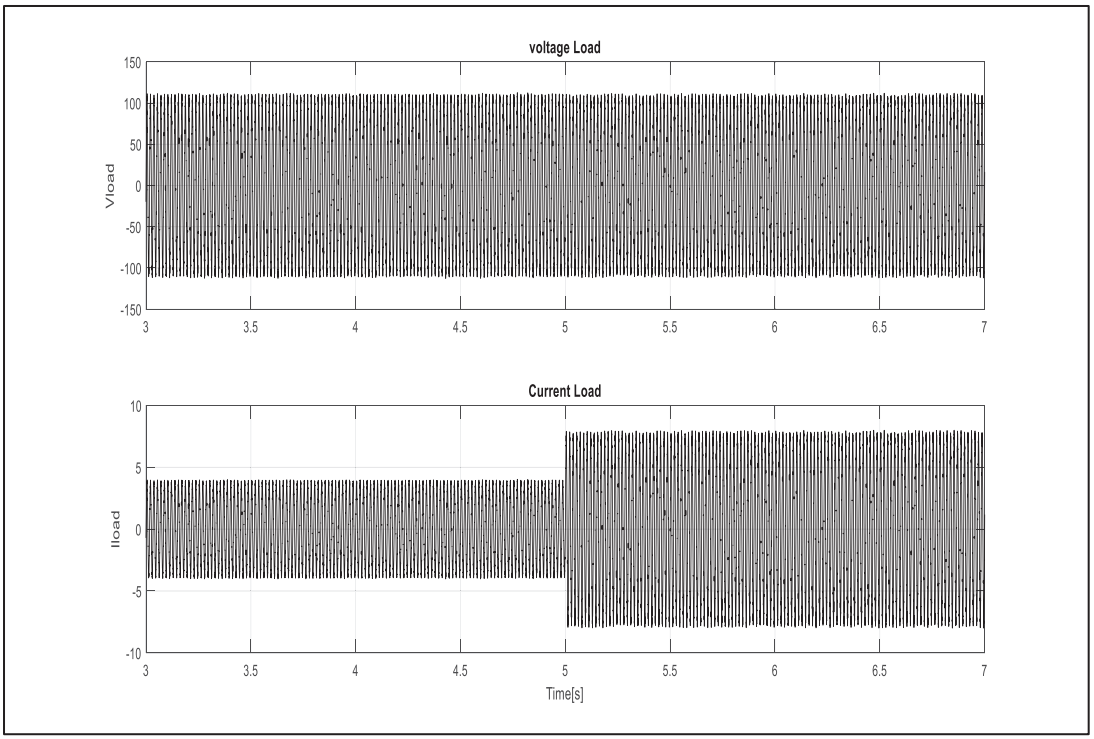

Figure 4.23 The output voltage and output current under the change of load

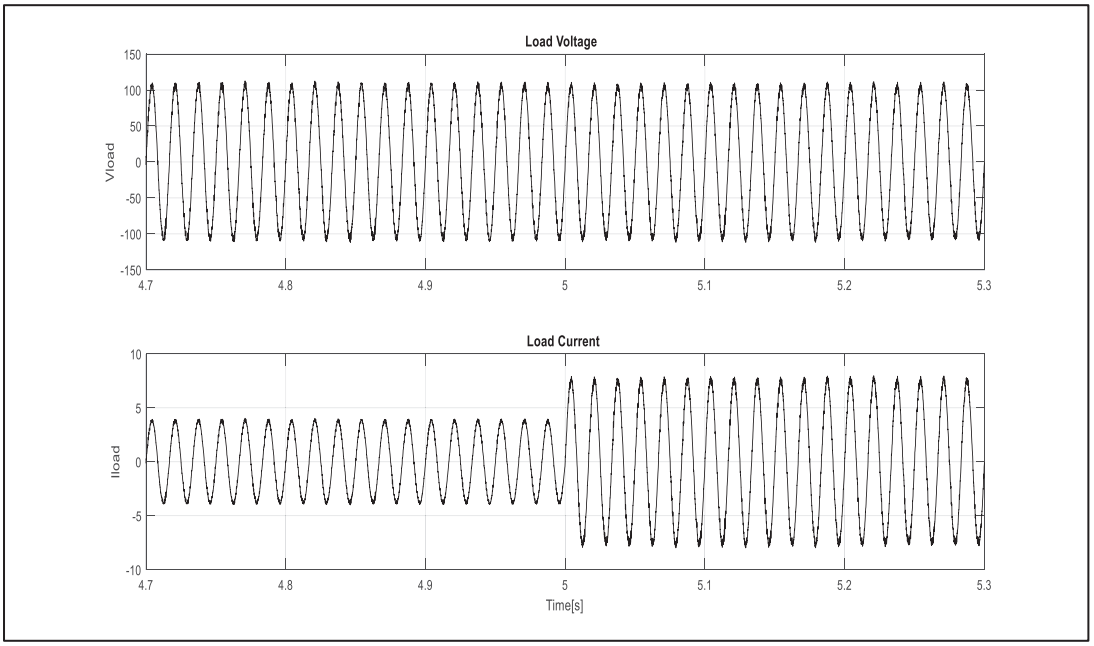

Figure 4.24 The output voltage and output current under the change of load

The efficiency of the converter

At P=450W we get the following data:

$P_{in} = V \times I = 45 \times 10 = 450W.$

Power output $P_{out} = \frac{V^2}{R} = \frac{110^2}{80} = 151.2W.$

Power of Battery calculated: $P_b = P_{in} - P_{out} = 450W - 151.2W = 298.8W.$

Power of battery measured: $P_b = 52.5 \times 6A$= 315.6W.

Efficiency = 298.8/315.6*100=94%.

4.3 Experiment Results

4.3.1 Laboratory Experimental Set-up

An experimental result has been done to improve the results of the design and the simulation of the MATLAB Simulink.

Figure 4.25 shows the implementation of system where number 1 represents the DC voltage source used, number 2 represent the oscilloscope used to collect the results, number 3 represent the QZSI and the inverter (well explained in figure 4.26), number 4 represent the batteries used in the test, number 5 represent the LC filter, number 6 represent the load.

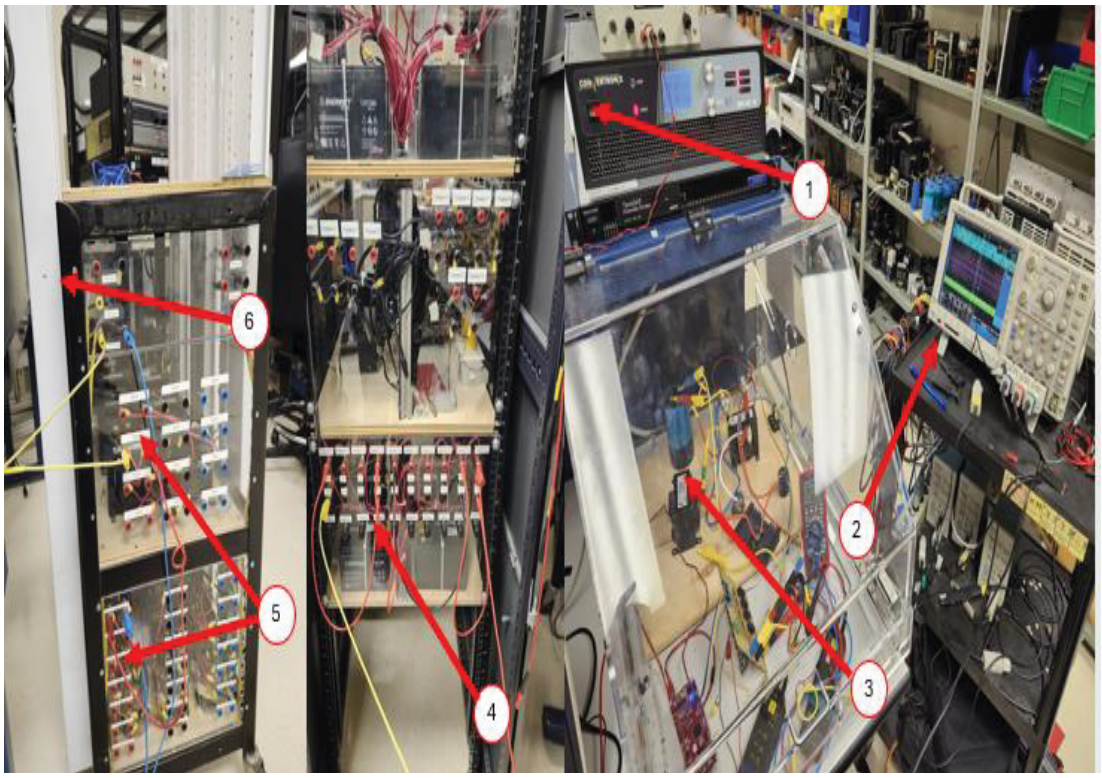

Figure 4.25 The experimental set-up of the system

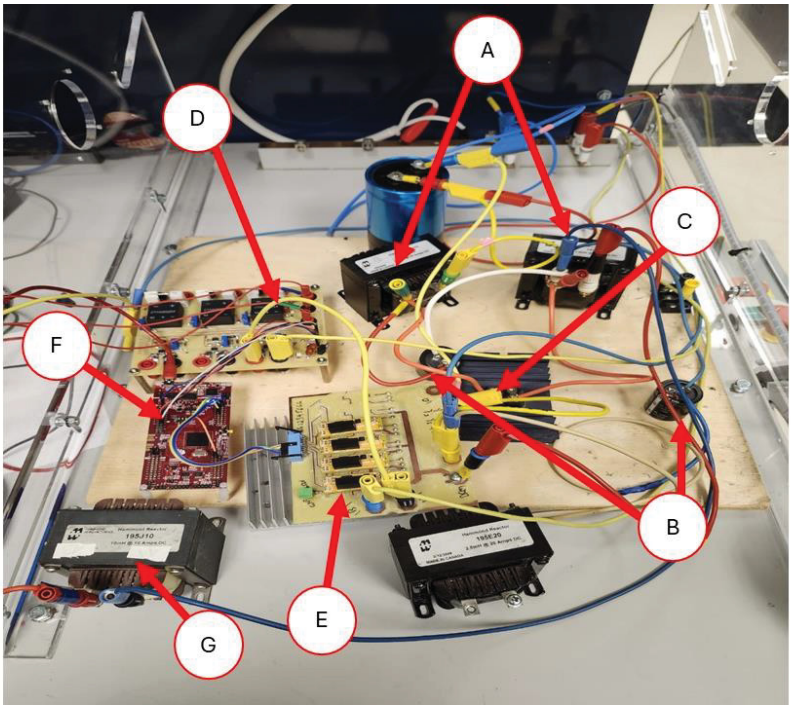

Figure 4.26 The QZSI

.

Figure 4.26 shows the different components of the quasi-Z source that were used. Label A represents the 2 inductances (L_1 and L_2) of the quasi-Z source network, label B represent the 2 capacitors (C_1 and C_2) of the quasi-Z source network, label C represents the diode (D_1) of the quasi-Z source network, coming to label D represents the sensors used, label E represents the single phase inverter used to transform DC voltage to AC voltage. Label F represents the DSP used for the proposed control of the system; label G represents the inductance connected to batteries.

4.3.2 Parameters

The parameters used for the hardware implementation are as follows:

Table 4.1 Parameters of the hardware implementation

Indicator	Value	unit
V_{in}	13	V
$L_1 = L_2$	2.5	mH
$C_1 = C_2$	250	μF
L_3	10	mH
P_{in}	150	W
R_{Load}	80	Ω
C_f	25	μF
L_f	0.5	mH
F_s	5000	Hz
D_{sh}	0.495	

To apply the proposed control into real life we use a DSP manufactured by Texas instrument launchpad F28379D. This DSP takes the code and successfully uploads to it, then a connection made between the sensors and the gate drive used for switching the single-phase inverter.

4.3.3 Experimental Setup

Due to limitation, using a DC source, except using a wind turbine, as an input source for our system is connected to the quasi Z source components, the components are connected as follow L1 connected to Diode D, the diode is connected to C2 and L2, and L2 is connected to C1, C1 is connected to L1, then we connect the single phase inverter to the QZSI, A control circuit is done using a DSP launchpad F28379D to read data from voltage and current

sensors, and to generate a PWM signals for controlling the MOSFETS in the single phase inverter, connect the gate driver circuits to the microcontroller and then to the gates of the transistors. Ensure the gate drivers can provide sufficient voltage to switch the MOSFET on and off. Connect a battery of a rate 48V connected in series to a 10mH, to the C2, then connect the LC filter to the output of the single-phase inverter, finally a resistive load is used, connected to the output of the LC filter.

For the algorithm added to the system and validated using MATLAB Simulink, as I discussed due to the limitations, I used a DC source in front of the PMSG and though the MPPT algorithm cannot be tested, an addition sensor is added to V_{C1} in addition to other sensors on the output voltage of the inverter and output voltage of the load in addition to the output current of the load, they are illustrated and update successfully to the DSP as shown in the following figure.

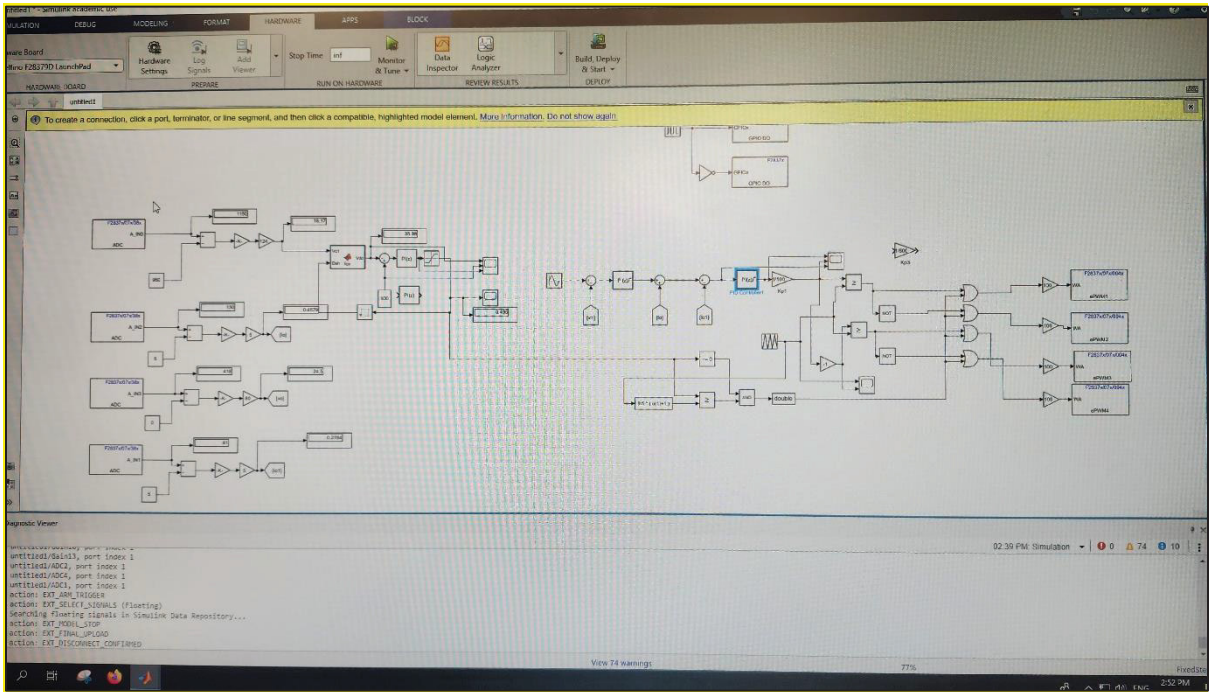

Figure 4.27 The figure up shows the success of upload of algorithm to the DSP

Measurement equipment like an oscilloscope, and multimeter is connected to the experiment, to monitor the voltage and current of the waveforms at various points in the circuit.

For the Battery protection integration, it involved the following steps:

1. **Real-Time Monitoring:** The SoC of the battery is continuously monitored through voltage and current sensors. This data is fed into the control system, which uses it to make real-time decisions regarding power distribution.
2. **Charge Regulation:** When the battery's SoC reaches a predefined upper limit, the control system reduces or halts the charging process to prevent overcharging. This is done by diverting excess energy to the load or reducing the power drawn from the wind turbine.
3. **Discharge Protection:** Similarly, if the SoC drops to a critical level, the control system limits or stops the discharge process, ensuring that the battery does not undergo deep discharge. This helps in prolonging the battery's lifespan.
4. **Algorithmic Control:** The control algorithm adjusts the QZSI's operation based on the SoC. For example, during high wind speeds, the system might boost the output voltage more aggressively to charge the battery faster, while during low wind speeds, the system might prioritize maintaining a stable power supply to the load.

Microcontroller Core Utilization

The microcontroller used in this research had dual cores. Both cores were utilized to optimize the processing load:

- **Core 1** was dedicated to handling the primary control algorithms for the QZSI, including the shoot-through state management, space vector modulation, and voltage regulation.
- **Core 2** managed the battery management system (BMS), handling tasks such as state of charge (SoC) monitoring, charge and discharge control, and protective measures to prevent overcharging and deep discharge.

4.3.4 Experimental Results

The shoot through state has been generated using the DSP F28379D, the code has been uploaded to the DSP and generate the active state and the shoot through state with a frequency of 5 KHz. In figure 4.28 the shoot through state shows clearly where the red rectangle, the S1 and S2 are turned on at the same time, they are shown clearly in the red rectangles.

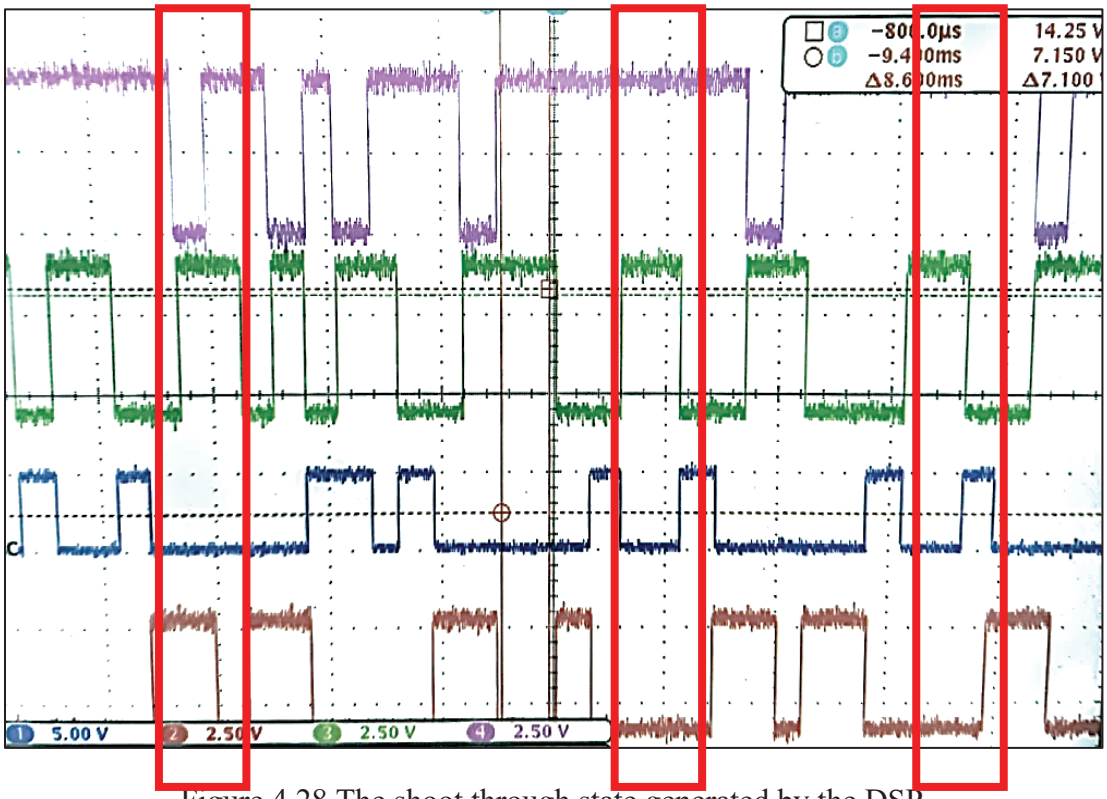

Figure 4.28 The shoot through state generated by the DSP

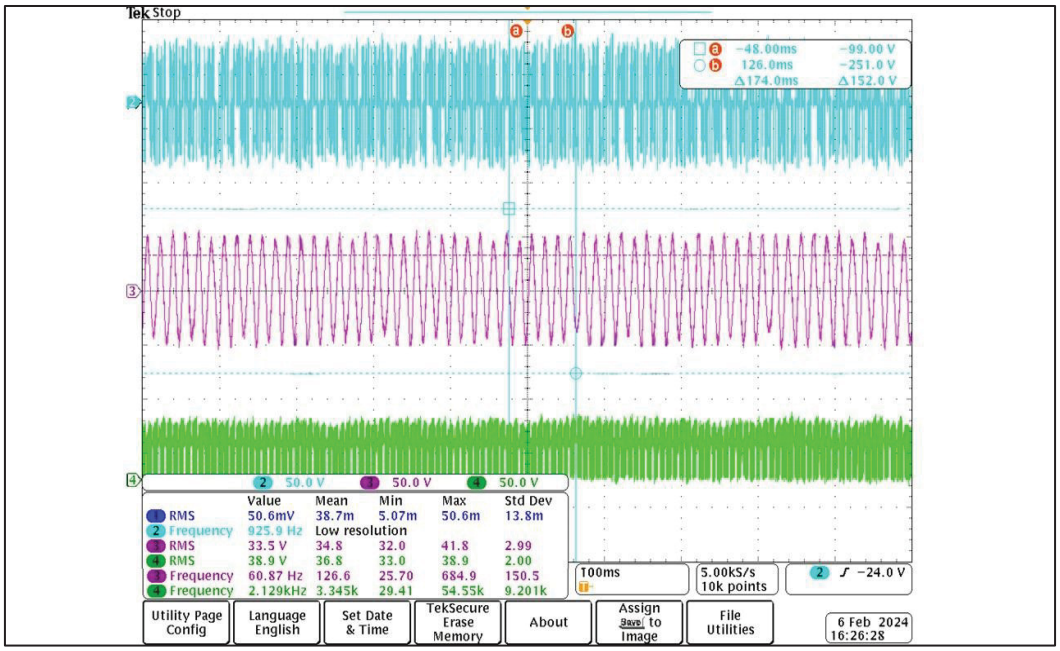

Figure 4.29 The inverter voltage, load voltage and the output voltage of QZSI

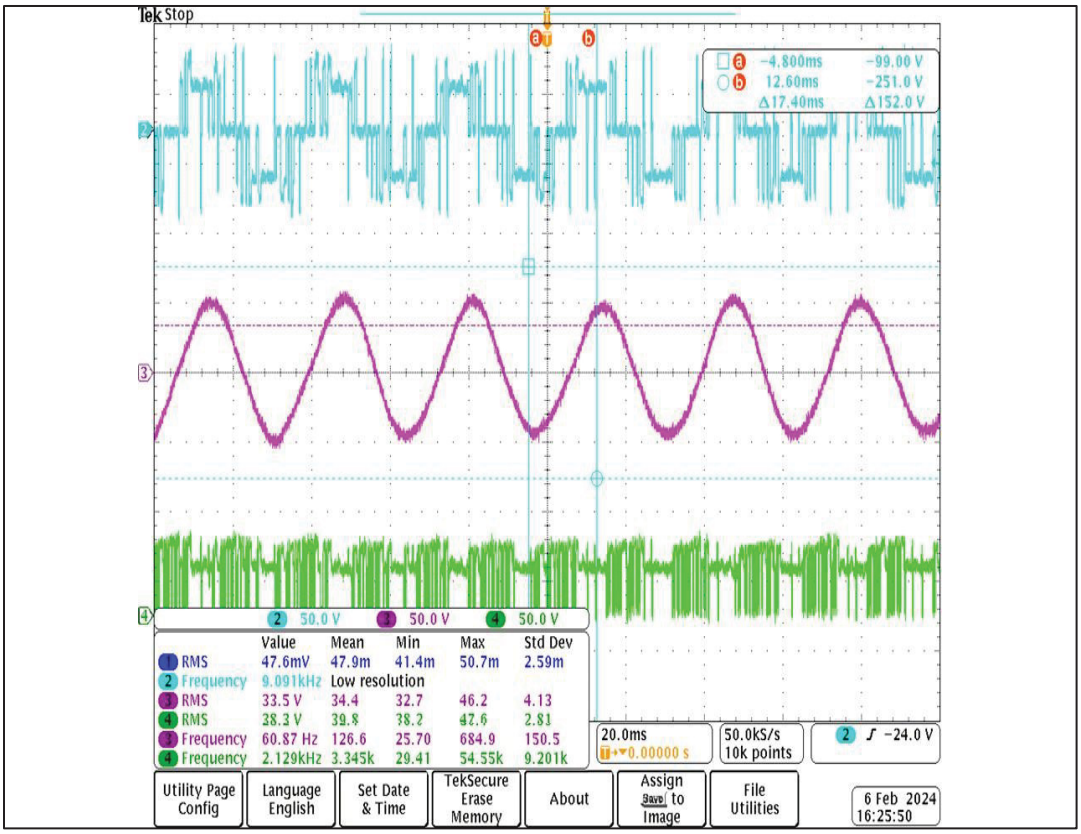

Figure 4.30 The output voltage of the load, the voltage of the load, and the output voltage of the QZSI

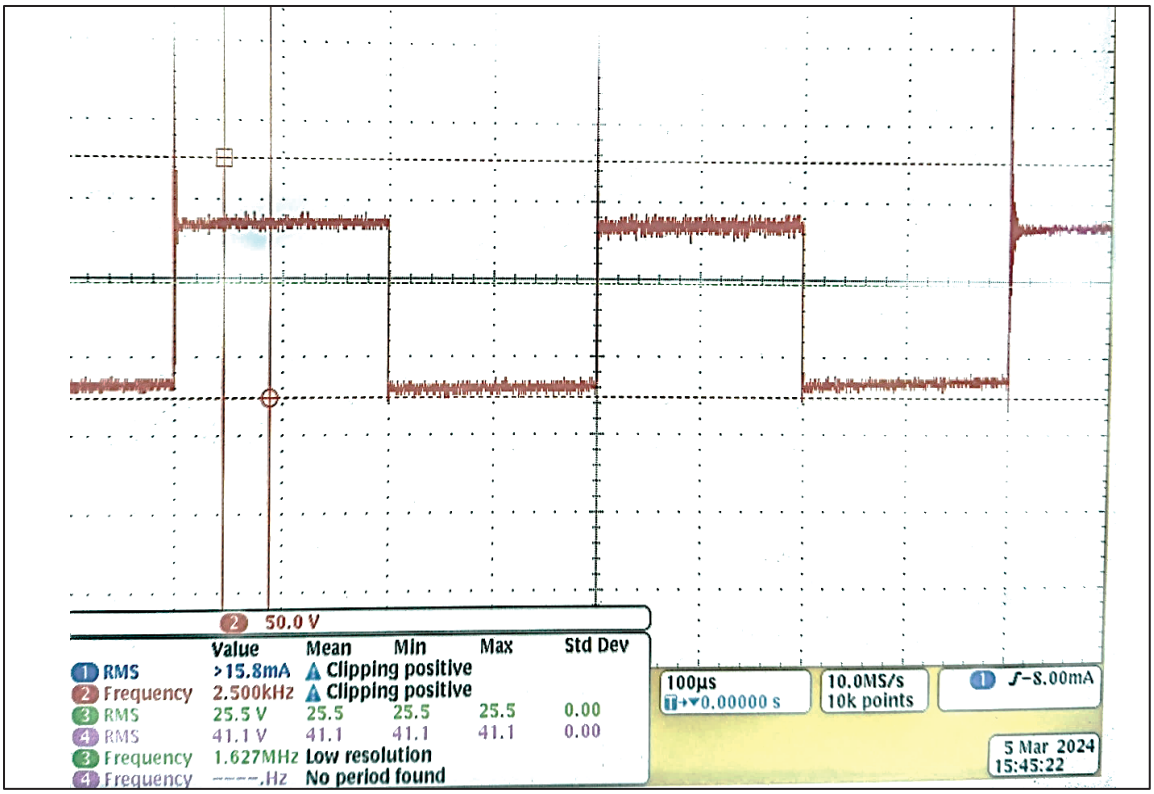

Figure 4.31 The output voltage of the QZSI

4.3.5 Discussion

In figure 4.29 and figure 4.30 it shows the output voltage of the inverter in blue, and the output voltage of the load in pink, and the VDC it shows the output voltage of the QZSI in green. In the two figures it shows clearly the effect of the shoot through especially in the VDC.

In figure 4.31 the VDC reaches 25.5 V and is going between the V_{DC} and zero, knowing that a continuous input voltage is set to 10V with a continuous current of 4A.

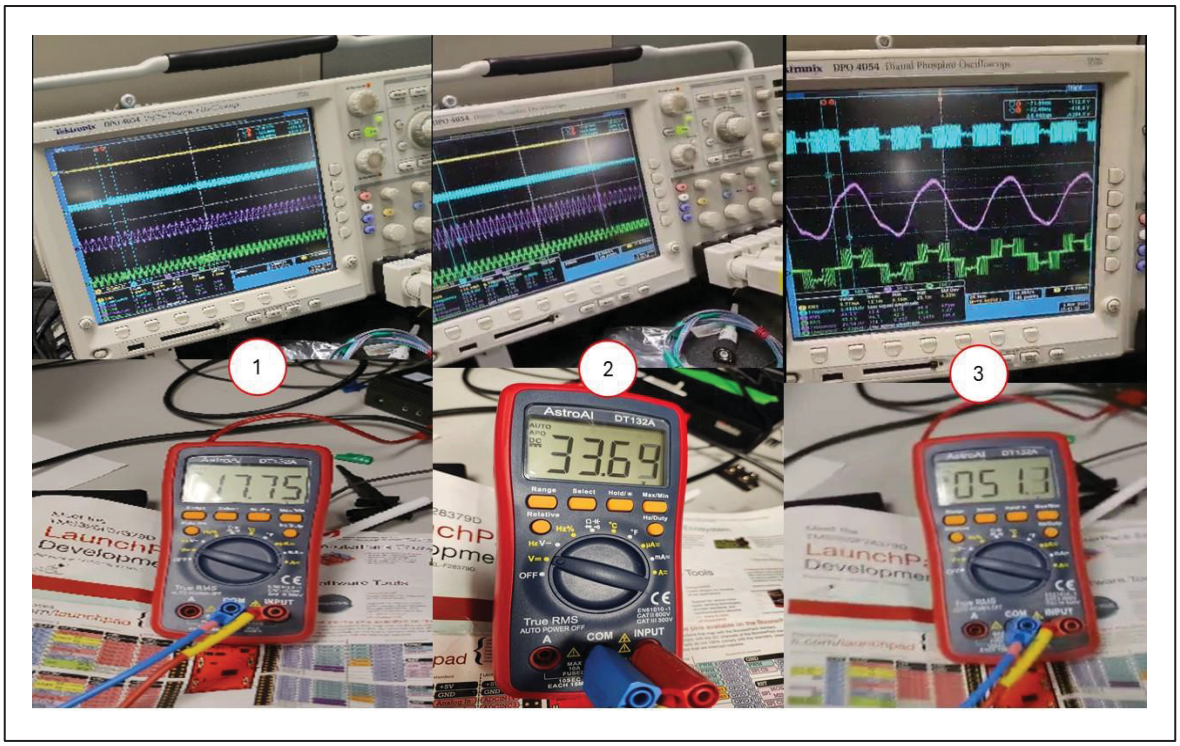

Figure 4.32 Different Tests

In the figure 4.32, the voltage shows the output voltage of the Quasi-Z source, where label one where the input voltage is zero, we get 17.75 V at the output due to the voltage of the battery, then we give a 10 V input voltage we get almost $\times 2.8$ voltage boast, we get a Voltage 33.6V, in the third test we increase the input voltage to 18 we got a 51.1 Volts at the output.

The efficiency of the QZSI in the hardware implementation

In case 1, the battery is discharged for the load R= 80Ω, in case 2 and case 3 the boast is done about 2.8 and a chagrining is done for the battery.

Power input: $P_{in} = V \times I = 18 \times 4.2 = 75.6W$

Power output $P_{out} = \frac{V^2}{R} = \frac{33.5^2}{80} = 14W$

Power of Battery calculated: $P_b = P_{in} - P_{out} = 75.6W - 14W = 61.6W$

Power of battery measured: $P_b = 33 \times 2A$=66W

Efficiency= 61.6/66*100=93%.

CONCLUSION

The designs, control, and real-time implementation of a standalone system based on QZSI integrated with battery storage for residential applications are presented. The challenges of safely integrating variable wind speeds and fluctuating power outputs, which typically hinder the efficiency and reliability of standalone wind systems, are addressed by adopting the QZSI concept. This study demonstrated significant improvements in voltage management and the robustness of the power conversion process, crucial for achieving a high degree of energy sustainability and system autonomy.

The simulation results effectively validated the proposed closed-loop control strategy, showcasing its capability to maintain optimal operation of the wind turbine and the QZSI under varying wind conditions and load demands. The control system adeptly managed the state of charge of the battery, ensuring a continuous and stable power supply while preserving the battery's health. The applied modulation technique proved effective in minimizing power loss and enhancing the overall efficiency of the energy conversion process.

Further validation was provided by the hardware implementation, which corroborated the simulation findings. The practical deployment of the WECS, equipped with the QZSI and the innovative control strategy, demonstrated not only feasibility but also operational reliability and efficiency. This real-world application highlighted the potential of integrating advanced inverter technologies and sophisticated control mechanisms to enhance the performance of renewable energy systems.

This research successfully demonstrated the design, control, and real-time implementation of a standalone system based on the quasi-Z source inverter (QZSI) integrated with battery storage for residential applications. By addressing the challenges of fluctuating wind speeds and variable power outputs, the QZSI proved to be a reliable solution for maintaining

efficiency and stability in standalone wind energy systems. Through simulations and hardware tests, we achieved a boost factor of 2.8 and an overall system efficiency of 94%.

The proposed closed-loop control strategy ensured optimal operation of the wind turbine and the QZSI under varying wind conditions, managing battery charge effectively and ensuring a continuous, stable power supply. Furthermore, the shoot-through control technique reduced power losses and enhanced energy conversion efficiency. The successful hardware implementation validated the system's robustness and operational reliability in real-world conditions.

In conclusion, the successful design, simulation, and implementation of the QZSI within a standalone WECS underscore its superiority over traditional systems, providing a promising pathway toward more sustainable, efficient, and reliable renewable energy solutions. Future work may explore the scalability of this technology, its integration with other renewable sources, and further optimization of the control strategies to enhance the resilience and efficiency of wind energy systems globally.

RECOMMENDATIONS

This thesis presented a comprehensive study on the design and implementation of a quasi-Z source inverter for a variable wind turbine, aiming to enhance the boost voltage at the output of the converter. This section proposes methods to expand the research and identifies potential directions for future work.

Energy Management System (EMS):

Develop a comprehensive energy management system that optimally balances the power flow between the wind turbine, battery, and load to maximize efficiency and extend battery life. Implement real-time monitoring and control to adapt to changing wind conditions and load demands effectively.

Scalability and Modular Design:

Design the system with scalability in mind to accommodate different power levels and applications, from small residential setups to larger commercial installations. Develop a modular design approach that allows for easy expansion and integration of additional renewable energy sources, such as solar PV.

Advanced Control Strategies:

Explore the implementation of more sophisticated control algorithms, such as model predictive control (MPC) or adaptive control, to enhance the dynamic response and robustness of the system. Consider the integration of artificial intelligence (AI) and machine learning (ML) techniques for predictive maintenance and fault detection.

ANNEX I

PRINCIPLES AND IMPLEMENTATION OF SVPWM FOR SINGLE-PHASE QZSI

For controlling the quasi-Z-source, we want to use a specific technique which is the SVPWM (space vector pulse width modulation) , this technique used to extend the voltage vectors with a suitable transformation matrix and to see the basic vectors in new basics(Yu, Zhao, Tseng, Luo, & Zhu, 2015)

This technique usually is used with the three phase quasi-Z-source inverter and it's the same for the voltage source inverters, both have the same voltage vectors.

The aim is to install a SVPWM technique for a single phase for the quasi-Z-source, which is completely different from the three phases that differ in the voltage vector and the basic space vectors.

For designing the technique of the SVPWM of a single phase we must take in consideration the following steps:

1. Presenting the voltage vectors of the single phase of the QZSI with the switching states.
2. Derive the transformation matrix and the coordinate of the new frame
3. Introducing the principle of the shoot out through state.
4. The pattern of the switches for the different selection (shoot out state, active state, zero state).

Usually, for a single-phase QZSI the required output voltage is required to be scalar (not a vector), and the space vector PWM the voltage required is not scalar, it's a vector. To generate the voltage vector needed for the SVPWM, knowing that the line voltage at the output of the QZSI, by the following equations:

$$\begin{bmatrix} V_{ab} \\ V_{ba} \end{bmatrix} = \sqrt{2} V_{\varphi} \begin{bmatrix} sin(wt) \\ sin(wt + \pi) \end{bmatrix} \quad \text{(A I-1)}$$

At every instant t generates a knowing collection of output voltage vector (voltage line to line), defined by $\overrightarrow{V_s} = [V_{ab} \quad V_{ba}]^T$ which can be shown in the following figure:

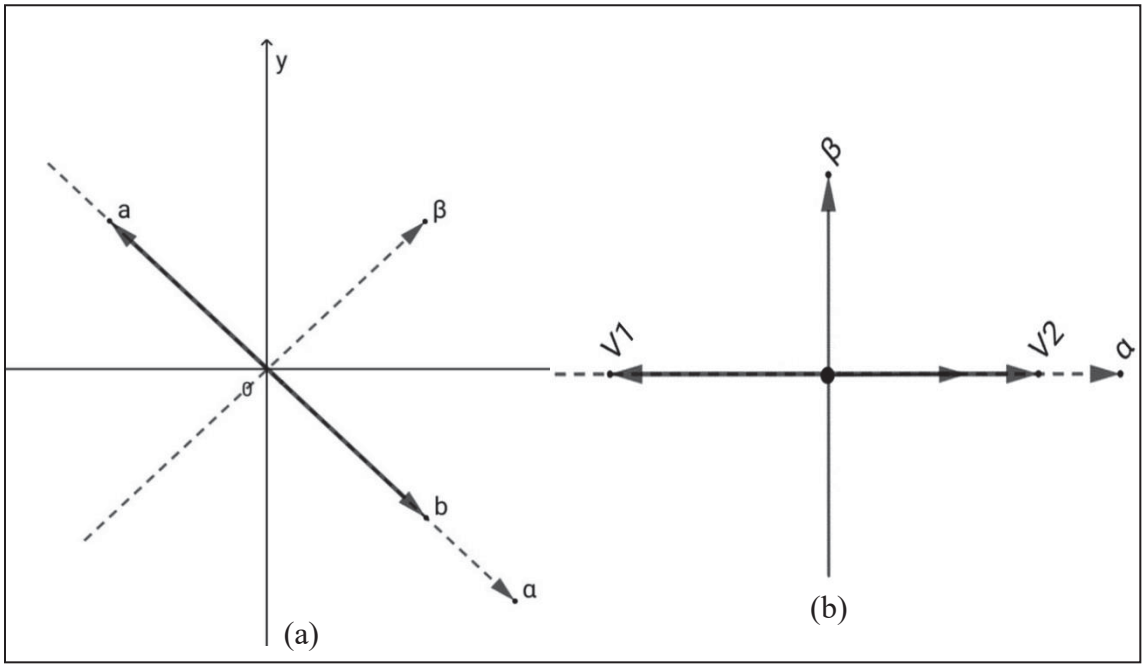

Figure A I-1 SVPWM of single-phase quasi-Z-source inverter. (a) Trajectory of line-to-line voltages of single-phase frame; (b) the basic space vectors of single-phase of a QZSI

By looking for all vectors they lie on a line of equation x+y=0. This line as shown in the figure is named α is chosen with norm of this line and named by β as the new axes of the new system. In addition, we can transfer two-dimensional vector $\overrightarrow{V_s} = [V_{ab} \quad V_{ba}]^T$ in to a one dimensional since the projection of all vectors on the β axis will be zero, from this we can conclude the transformation matrix $T_{ab-\alpha\beta}$ that is corresponding for the transformation in the following equations:

$$T_{ab-\alpha\beta} = \frac{1}{\sqrt{2}}\begin{bmatrix} 1 & -1 \\ 1 & 1 \end{bmatrix} \tag{A I-2}$$

So, the new voltage in the new coordinate plane is as follow:

$$\vec{V_s}' = T_{ab-\alpha\beta}\begin{bmatrix}V_{ab}\\V_{ba}\end{bmatrix} = \begin{bmatrix}V_\alpha\\0\end{bmatrix} = 2V_\varphi\begin{bmatrix}sin(wt)\\0\end{bmatrix} \quad \text{(A I-3)}$$

By calculating all the possible switches state of the quasi-Z-source inverter we can show it in the following table:

Table A I-1 All the possible switches states of the quasi-Z source

	S_a	$S_a{}'$	S_b	$S_b{}'$	V_{ab}	V_{ba}	V_α
V_0	0	1	0	1	0	0	0
V_1	0	1	1	0	$-BU_{DC1}$	BU_{DC1}	$-\sqrt{2}BU_{DC1}$
V_2	1	0	0	1	BU_{DC1}	$-BU_{DC1}$	$\sqrt{2}BU_{DC1}$
V_3	1	0	1	0	0	0	0
V_{sh1}	1	1	0	1	0	0	0
V_{sh2}	1	1	1	0	0	0	0
V_{sh3}	1	0	1	1	0	0	0
V_{sh4}	0	1	1	1	0	0	0
V_{sh5}	1	1	1	1	0	0	0

If we took a look on the table above we can deduce that there is a 9 basic vector space, we can classify these vectors on two three classes, first one the active vectors ($V_1$and V_2), the second one is the zero vectors (V_0 and V_3), and the last one the shoot throughout vectors (V_{sh1}~V_{sh5}).

Now we can write the voltage vectors as mentioned in the following equation:

$$\overrightarrow{V_s} = U_{DC}\begin{bmatrix}1 & -1\\-1 & 1\end{bmatrix}.\begin{bmatrix}a\\b\end{bmatrix} = BU_{DC1}\begin{bmatrix}1 & -1\\-1 & 1\end{bmatrix}.\begin{bmatrix}a\\b\end{bmatrix} \quad \text{(A I-4)}$$

a and b represent the status of the upper switches of the two phases a and b, and we can derive the voltage vector in the new base by multiply by the transformation matrix and it's shown in the following equation:

$$\vec{V}_s' = T_{ab-\alpha\beta} \cdot \overrightarrow{V_S} = \sqrt{2}\, B. U_{DC1} \begin{bmatrix} 1 & -1 \\ 0 & 0 \end{bmatrix} \cdot \begin{bmatrix} a \\ b \end{bmatrix} \quad \text{(A I-5)}$$

Basing on the concept of the vector space, the output voltage of a single phase of quasi-Z-source inverter can be deduced using the linear combination of the active space vector, zero space vector and shoot through space vectors according to the following equations:

$$\vec{V}_{ref} = \frac{T_i}{T}\, \vec{V}_i + \frac{T_z}{T} \left(\vec{V}_0, \vec{V}_3\right) + \frac{T_{sh}}{T} \left(\vec{V}_{sh1} \sim \vec{V}_{sh5}\right) \quad \text{(A I-6)}$$

As we show in figure 1, the choosing the two active vectors V_1 and V_2 rely on the phase angle θ ($\theta = \omega t$). When $0 \leq \theta \leq \pi$, then V_2 is applied; otherwise, the V_1 is selected. To calculate the period of each state the period depending on the equations(Yu et al., 2015):

Case 1:

When θ is between 0 and π ($0 \leq \theta \leq \pi$) we can obtain the following equation derived from figure 1 a:

$$\begin{aligned} T. \left|\vec{V}_{ref}\right| = T_2 \left|\vec{V}_2\right| + T_z \left|\vec{V}_0, \vec{V}_3\right| \\ + T_{sh} \left|\vec{V}_{sh1}, \vec{V}_{sh2}, \vec{V}_{sh3}, \vec{V}_{sh4}, \vec{V}_{sh5}\right| \end{aligned} \quad \text{(A I-7)}$$

As conclude from table 1 that:

$$\left|\vec{V}_{ref}\right| = 2V_{\varphi}. sin\theta = \sqrt{2} B U_{DC1}. M \quad \text{(A I-8)}$$

$$|V_2| = \sqrt{2}.\widehat{U}_{DC} = \sqrt{2}.B.U_{DC1} \tag{A I-9}$$

$$|V_0| = |V_3| = |V_4| = |V_{sh1}| = |V_{sh2}| = |V_{sh3}| = |V_{sh4}| = |V_{sh5}| = 0 \tag{A I-10}$$

By merging the equations, we can calculate the duration of the active state and the zero state:

$$\begin{cases} T_2 = T\,.M\,.sin\,\theta \\ T_z + T_{sh} = T - T_2 \end{cases} \tag{A I-11}$$

Case 2:

When θ is between π and 2π ($\pi \leq \theta \leq 2\pi$) we can obtain the following equation derived from figure 1:

$$\{T.|\vec{V}_{ref}| = T_1|\vec{V}_1| + T_z|\vec{V}_0, \vec{V}_3| + T_{sh}|\vec{V}_{sh1}, \vec{V}_{sh2}, \vec{V}_{sh3}, \vec{V}_{sh4}, \vec{V}_{sh5}| \tag{A I-12}$$

The same calculation done for the case 1 we also obtain the period for the active state T_1 by the following equations:

$$\begin{matrix} T_1 = T\,.M\,.sin(\,\theta - \pi) \\ T_z + T_{sh} = T - T_1 \end{matrix} \tag{A I-13}$$

The pattern of the switches for the different selection

The total period of the zero vectors and the shoot-throughout can be deduced from the above equations when the switching frequency and the index of modulation are stable, then we will get the period of zero vectors T_z and the shoot-throughout vector T_{sh} by the following equation:

$$\begin{cases} T_{sh} = \dfrac{T}{2} - \dfrac{T}{2B} \\ T_z = T_i - T_1 - T_{sh} \end{cases} \quad \text{(A I-14)}$$

As we consider the switching state and output voltage in table 1, all the zero vectors give the same output voltages; so, T_{sh} can be any combination of the shootout through vectors, and T_z can be one of the two null vectors, as shown in the following equations:

$$\begin{cases} T_{sh1} = k_1(wt).T_{sh} \\ T_{sh2} = k_2(wt).T_{sh} \\ T_{sh3} = k_3(wt).T_{sh} \\ T_{sh4} = k_4(wt).T_{sh} \\ T_{sh5} = k_5(wt).T_{sh} \\ k_1(wt) + k_2(wt) + k_3(wt) + k_4(wt) + k_5(wt) = 1 \end{cases} \quad \text{(A I-15)}$$

$$\begin{cases} T_0 = n_0(wt).T_z \\ T_3 = n_3(wt).T_z \\ n_0(wt) + n_3(wt) = 1 \end{cases} \quad \text{(A I-16)}$$

By changing the states of zero states and shoot-through states, we can get a sequence of switching patterns, which we can get the wanted output voltage, for the coefficients $n_i(wt)$ and $k_i(wt)$, we will consider them are constant for simplification of calculations.

Now we will propose all possible transition between the different switching states of the space vector PWM for the quasi-Z-source, every arrow is drawn represent a one switching state.

After we put all the possible transition in the following figure, we can deduce that the transition from an active state to a shootout through state need only one switching action, for example going from V_1(0110, active state) to V_{sh2}(1110, shootout through state), and is if we look the transition from an active state to another zero state it will need for two switching actions.

For getting a typical pattern, let's first take the case 1 where θ is between 0 and π (0≤θ≤π), and according to table 1 we deduce that V_2 is applied (active state use in this case), so there

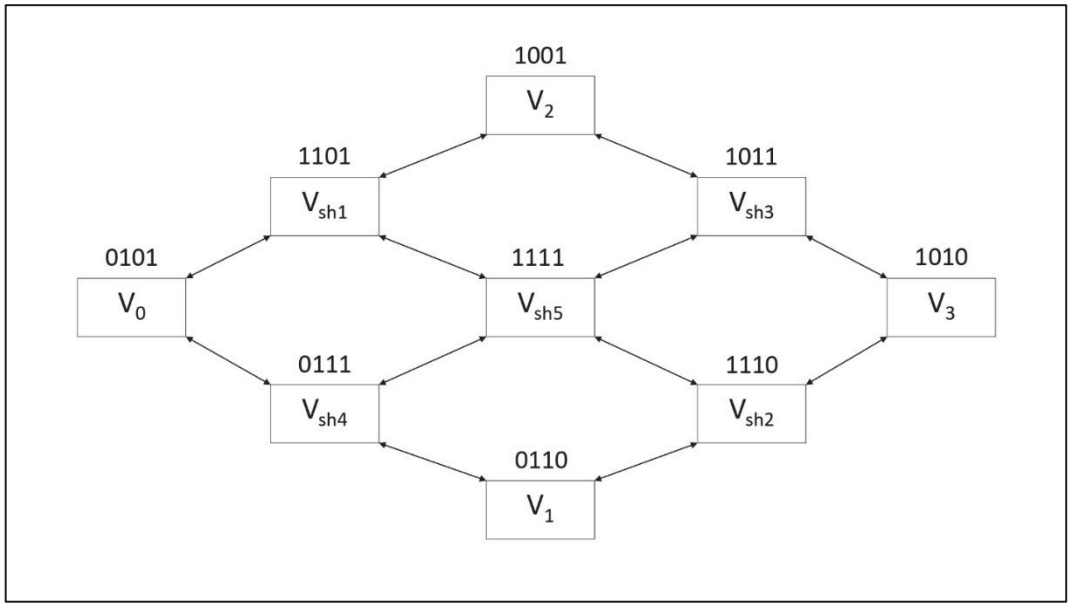

Figure A I-2 Possible transition of the states

is a lot of patterns can be achieved if we are transferring from

the zero state to the active state, as shown in the following tables below:

Table A I-2 The sequence for the shoot-through

V_0	V_{sh1}	V_2	V_{sh1}	V_0
0101	1101	1001	1101	0101
$\frac{T_0}{2}$	$\frac{T_{sh}}{2}$	T_2	$\frac{T_{sh}}{2}$	$\frac{T_0}{2}$

Table A I-3 Another sequence for the shoot-through

V_0	V_{sh1}	V_2	V_{sh3}	V_3	V_{sh3}	V_2	V_{sh1}	V_0
0101	1101	1001	1101	0101	1101	1001	1101	0101
$\frac{T_0}{4}$	$\frac{T_{sh}}{4}$	$\frac{T_2}{2}$	$\frac{T_{sh}}{4}$	$\frac{T_0}{4}$	$\frac{T_{sh}}{4}$	$\frac{T_2}{2}$	$\frac{T_{sh}}{4}$	$\frac{T_0}{4}$

And by taking the second case 2 where θ is between π and 2π ($\pi \leq \theta \leq 2\pi$), $V_1$is applied (the active state used), so there are many patterns can be achieved when transferring from the zero state to active state passing through the shoot through state as can be shown in tables below:

Table A I-4 Passing the shoot through state through active and zero state

V_0	V_{sh4}	V_1	V_{sh4}	V_0
0101	0111	0110	0111	0101
$\frac{T_0}{2}$	$\frac{T_{sh}}{2}$	T_1	$\frac{T_{sh}}{2}$	$\frac{T_0}{2}$

Table A I-5 Passing another way for the shoot through state through active and zero state

V_0	V_{sh4}	V_1	V_{sh2}	V_3	V_{sh2}	V_1	V_{sh4}	V_0
0101	0111	0110	1110	1010	1110	0110	0111	0101
$\frac{T_0}{4}$	$\frac{T_{sh}}{4}$	$\frac{T_1}{2}$	$\frac{T_{sh}}{4}$	$\frac{T_0}{4}$	$\frac{T_{sh}}{4}$	$\frac{T_1}{2}$	$\frac{T_{sh}}{4}$	$\frac{T_0}{4}$

LIST OF BIBLIOGRAPHICAL REFERENCES

2023 - Canada's Energy Future 2023 Energy Supply and Dem.pdf. (s.d.). Repéré à https://www.cer-rec.gc.ca/en/data-analysis/canada-energy-future/2023/canada-energy-futures-2023.pdf

A Fuzzy Logic-based MPPT Technique for PMSG Wind Generation System. (2019). *International Journal of Renewable Energy Research*, (v9i4). https://doi.org/10.20508/ijrer.v9i4.10138.g7778

Abdallah, M. E., Elshafei, A. L., & Arafa, O. M. (2015). Tracking Techniques in WECS.

Anderson, J., & Peng, F. Z. (2008). Four quasi-Z-Source inverters. Dans *2008 IEEE Power Electronics Specialists Conference* (pp. 2743-2749). Rhodes, Greece : IEEE. https://doi.org/10.1109/PESC.2008.4592360

Bajestan, M. M., Madadi, H., & Shamsinejad, M. A. (2019). Control of a new stand-alone wind turbine-based variable speed permanent magnet synchronous generator using quasi-Z-source inverter. *Electric Power Systems Research*, *177*, 106010. https://doi.org/10.1016/j.epsr.2019.106010

Bisenieks, L, Vinnikov, D., & Galkin, I. (s.d.). PMSG based residential wind turbines: possibilities and challenges.

Bisenieks, Lauris, Vinnikov, D., & Galkin, I. (2013). PMSG based residential wind turbines: Possibilities and challenges. *Agronomy Research*, *11*, 295-306.

Bisenieks, Lauris, Vinnikov, D., & Zakis, J. (2011). Analysis of operating modes of the novel isolated interface converter for PMSG based wind turbines. Dans *2011 International Conference on Power Engineering, Energy and Electrical Drives* (pp. 1-8). https://doi.org/10.1109/PowerEng.2011.6036538

Canadian Renewable Energy Association. (s.d.). Repéré à https://renewablesassociation.ca/news-release-new-2023-data-shows-11-2-growth-for-wind-solar-energy-storage/

Fang, Z., Member, S., & Peng, I. (2003). Peng , Z-Source Inverter. *IEEE Transactions on Industry Application*, 2-504.

Fang Zheng Peng. (2003). Z-source inverter. *IEEE Transactions on Industry Applications*, *39*(2), 504-510. https://doi.org/10.1109/TIA.2003.808920

Ge, B., Peng, F. Z., Abu-Rub, H., Ferreira, F. J. T. E., & De Almeida, A. T. (2014). Novel Energy Stored Single-Stage Photovoltaic Power System With Constant DC-Link Peak Voltage. *IEEE Transactions on Sustainable Energy*, *5*(1), 28-36. https://doi.org/10.1109/TSTE.2013.2272437

Gür, T. M. (2018). Review of electrical energy storage technologies, materials and systems: challenges and prospects for large-scale grid storage. *Energy & Environmental Science*, *11*(10), 2696-2767. https://doi.org/10.1039/C8EE01419A

Hussien, A., Taha, M., & Mahgoub, O. A. (2015). Design and control of a quasi-Z-source inverter based for wind power generation using PMSG. Dans *2015 IEEE 15th International Conference on Environment and Electrical Engineering (EEEIC)* (pp. 2050-2055). Rome, Italy : IEEE. https://doi.org/10.1109/EEEIC.2015.7165491

Jegatheeswaran, R., & Rajesh, R. (2015). Variable speed wind energy conversion system using PMSG & Z-Source inverter. Dans *2015 International Conference on Innovations in Information, Embedded and Communication Systems (ICIIECS)* (pp. 1-7). Coimbatore, India : IEEE. https://doi.org/10.1109/ICIIECS.2015.7193004

Kesraoui, M., Korichi, N., & Belkadi, A. (2011). Maximum power point tracker of wind energy conversion system. *Renewable Energy*, *36*(10), 2655-2662. https://doi.org/10.1016/j.renene.2010.04.028

Kosky, P., Balmer, R., Keat, W., & Wise, G. (2013). Green Energy Engineering. Dans *Exploring Engineering* (pp. 339-356). (S.l.) : Elsevier. https://doi.org/10.1016/B978-0-12-415891-7.00016-9

Kroposki, B., Johnson, B., Zhang, Y., Gevorgian, V., Denholm, P., Hodge, B.-M., & Hannegan, B. (2017). Achieving a 100% Renewable Grid: Operating Electric Power Systems with Extremely High Levels of Variable Renewable Energy. *IEEE Power and Energy Magazine*, *15*(2), 61-73. https://doi.org/10.1109/MPE.2016.2637122

Lai, L. L., & Chan, T. F. (2007). *Distributed Generation: Induction and Permanent Magnet Generators* (1re éd.). (S.l.) : Wiley. https://doi.org/10.1002/9780470511824

Liu, Y., Abu-Rub, H., Ge, B., Blaabjerg, F., Ellabban, O., & Loh, P. C. (2016). *Impedance Source Power Electronic Converters* (1re éd.). (S.l.) : Wiley. https://doi.org/10.1002/9781119037088

Liu, Y., Ge, B., Abu-Rub, H., & Peng, F. Z. (2013). Control System Design of Battery-Assisted Quasi-Z-Source Inverter for Grid-Tie Photovoltaic Power Generation. *IEEE Transactions on Sustainable Energy*, *4*(4), 994-1001. https://doi.org/10.1109/TSTE.2013.2263202

Liu, Y., Ge, B., Abu-Rub, H., & Peng, F. Z. (2014). Modelling and controller design of quasi-Z-source inverter with battery-based photovoltaic power system. *IET Power Electronics*, *7*(7), 1665-1674. https://doi.org/10.1049/iet-pel.2013.0389

Liu, Y., Ge, B., Abu-Rub, H., & Peng, F. Z. (2014). Modelling and controller design of quasi-Z-source inverter with battery-based photovoltaic power system. *IET Power Electronics*, *7*(7), 1665-1674. https://doi.org/10.1049/iet-pel.2013.0389

Nguyen, M.-K., Lim, Y.-C., Choi, J.-H., & Cho, G.-B. (2016a). Isolated High Step-Up DC–DC Converter Based on Quasi-Switched-Boost Network. *IEEE Transactions on Industrial Electronics*, *63*(12), 7553-7562. https://doi.org/10.1109/TIE.2016.2586679

Nguyen, M.-K., Lim, Y.-C., Choi, J.-H., & Cho, G.-B. (2016b). Isolated High Step-Up DC–DC Converter Based on Quasi-Switched-Boost Network. *IEEE Transactions on Industrial Electronics*, *63*(12), 7553-7562. https://doi.org/10.1109/TIE.2016.2586679

Olabi, A. G., & Abdelkareem, M. A. (2022). Renewable energy and climate change. *Renewable and Sustainable Energy Reviews*, *158*, 112111. https://doi.org/10.1016/j.rser.2022.112111

Raghavendra, K. V. G., Zeb, K., Muthusamy, A., Krishna, T. N. V., Kumar, S. V. S. V. P., Kim, D.-H., … Kim, H.-J. (2019). A Comprehensive Review of DC–DC Converter Topologies and Modulation Strategies with Recent Advances in Solar Photovoltaic Systems. *Electronics*, *9*(1), 31. https://doi.org/10.3390/electronics9010031

Raja Nayak, M., Tulasi, V. V. K., Divya Teja, K., Koushic, K., & Suresh Naik, B. (2023). Implementation of quasi Z-source inverter for renewable energy applications. *Materials Today: Proceedings*, *80*, 2458-2463. https://doi.org/10.1016/j.matpr.2021.06.383

Renewable Energy. (s.d.). *Center for Climate and Energy Solutions*. Repéré à https://www.c2es.org/content/renewable-energy/

Samadian, A., Hosseini, S. H., Sabahi, M., & Maalandish, M. (2020a). A New Coupled Inductor Nonisolated High Step-Up Quasi Z-Source DC–DC Converter. *IEEE Transactions on Industrial Electronics*, *67*(7), 5389-5397. https://doi.org/10.1109/TIE.2019.2934067

Samadian, A., Hosseini, S. H., Sabahi, M., & Maalandish, M. (2020b). A New Coupled Inductor Nonisolated High Step-Up Quasi Z-Source DC–DC Converter. *IEEE Transactions on Industrial Electronics*, *67*(7), 5389-5397. https://doi.org/10.1109/TIE.2019.2934067

Sánchez, A., Zhang, Q., Martín, M., & Vega, P. (2022). Towards a new renewable power system using energy storage: An economic and social analysis. *Energy Conversion and Management*, *252*, 115056. https://doi.org/10.1016/j.enconman.2021.115056

Shamouei-Milan, M., Asgarniya, R., Marangalu, M. G., Islam, Md. R., & Mehrizi-Sani, A. (2023). A Single-Phase High Gain Active-Switched Quasi Z-Source NNPC Inverter. Dans *2023 IEEE IAS Global Conference on Renewable Energy and Hydrogen Technologies (GlobConHT)* (pp. 1-6). Male, Maldives : IEEE. https://doi.org/10.1109/GlobConHT56829.2023.10087432

Shekar, T. C., & Veerachary, M. (2009). Multi-loop control of Z-source inverter for single-phase power conditioning systems. Dans *INTELEC 2009 - 31st International Telecommunications Energy Conference* (pp. 1-6). Incheon, South Korea : IEEE. https://doi.org/10.1109/INTLEC.2009.5351780

Shrivastava, A., Karkar, H. M., & Singh, S. (2016). Quasi-Z-source inverter based pmsg wind generation system with pitch angle control. Dans *2016 International Conference on Electrical Power and Energy Systems (ICEPES)* (pp. 46-51). Bhopal, India : IEEE. https://doi.org/10.1109/ICEPES.2016.7915904

Siwakoti, Y. P., Peng, F. Z., Blaabjerg, F., Loh, P. C., & Town, G. E. (2015). Impedance-Source Networks for Electric Power Conversion Part I: A Topological Review. *IEEE Transactions on Power Electronics*, *30*(2), 699-716. https://doi.org/10.1109/TPEL.2014.2313746

Soares-Ramos, E. P. P., De Oliveira-Assis, L., Sarrias-Mena, R., Garcia-Trivino, P., Garcia-Vazquez, C. A., & Fernandez-Ramirez, L. M. (2021). Averaged Dynamic Modeling and Control of a Quasi-Z-Source Inverter for Wind Power Applications. *IEEE Access*, *9*, 114348-114358. https://doi.org/10.1109/ACCESS.2021.3104797

Sonar, S., & Maity, T. (2013). Wind power conversion based on quasi-z source inverter. Dans *2013 International Conference on Control, Automation, Robotics and Embedded Systems (CARE)* (pp. 1-6). Jabalpur, India : IEEE. https://doi.org/10.1109/CARE.2013.6733733

Stiebler, M. (2008). *Wind energy systems for electric power generation*. Berlin : Springer.

Sue, D.-C. (2011). High Efficiency Double–Fed Induction Generator Applied to Wind Power Generator Technical Analyses. *Energy and Power Engineering*, *03*(03), 253-261. https://doi.org/10.4236/epe.2011.33032

Tiwari, R., & Babu, N. R. (2016). Recent developments of control strategies for wind energy conversion system. *Renewable and Sustainable Energy Reviews*, *66*, 268-285. https://doi.org/10.1016/j.rser.2016.08.005

Vinnikov, D., & Roasto, I. (2011a). Quasi-Z-Source-Based Isolated DC/DC Converters for Distributed Power Generation. *IEEE Transactions on Industrial Electronics*, *58*(1), 192-201. https://doi.org/10.1109/TIE.2009.2039460

Vinnikov, D., & Roasto, I. (2011b). Quasi-Z-Source-Based Isolated DC/DC Converters for Distributed Power Generation. *IEEE Transactions on Industrial Electronics*, *58*(1), 192-201. https://doi.org/10.1109/TIE.2009.2039460

Vinnikov, D., & Roasto, I. (2011c). Quasi-Z-Source-Based Isolated DC/DC Converters for Distributed Power Generation. *IEEE Transactions on Industrial Electronics*, *58*(1), 192-201. https://doi.org/10.1109/TIE.2009.2039460

Wong, Y.-S., Chen, J.-F., Liu, K.-B., & Hsieh, Y.-P. (2017). A Novel High Step-Up DC-DC Converter with Coupled Inductor and Switched Clamp Capacitor Techniques for Photovoltaic Systems. *Energies*, *10*(3), 378. https://doi.org/10.3390/en10030378

Yang, S., Peng, F. Z., Lei, Q., Inoshita, R., & Qian, Z. (2011). Current-Fed Quasi-Z-Source Inverter With Voltage Buck. *IEEE Transactions on Industry Applications*, *47*(2), 882-892. https://doi.org/10.1109/TIA.2010.2102995

Yu, K., Zhao, J., Tseng, K. J., Luo, F. L., & Zhu, M. (2015). Space vector pulse-width modulation for single-phase full-bridge Z-source inverter: SVPWM FOR SINGLE-PHASE ZSI. *International Journal of Circuit Theory and Applications*, *43*(3), 374-389. https://doi.org/10.1002/cta.1946